

Electronic Thesis and Dissertation Repository

10-14-2014 12:00 AM

A Surface Chemistry Study of the Effects of Zinc Sulphate on Sphalerite During Flotation Separation at the Laronde Mine

Dennis M. Laliberty, *The University of Western Ontario*

Supervisor: Dr. Brian Hart, *The University of Western Ontario*

A thesis submitted in partial fulfillment of the requirements for the Master of Science degree in Geology

© Dennis M. Laliberty 2014

Follow this and additional works at: <https://ir.lib.uwo.ca/etd>

 Part of the [Geochemistry Commons](#)

Recommended Citation

Laliberty, Dennis M., "A Surface Chemistry Study of the Effects of Zinc Sulphate on Sphalerite During Flotation Separation at the Laronde Mine" (2014). *Electronic Thesis and Dissertation Repository*. 2481. <https://ir.lib.uwo.ca/etd/2481>

This Dissertation/Thesis is brought to you for free and open access by Scholarship@Western. It has been accepted for inclusion in Electronic Thesis and Dissertation Repository by an authorized administrator of Scholarship@Western. For more information, please contact wlsadmin@uwo.ca.

A SURFACE CHEMISTRY STUDY OF THE EFFECTS OF ZINC SULPHATE ON
SPHALERITE DURING FLOTATION SEPARATION AT THE LARONDE MINE

Monograph

by

Dennis Michael Laliberty

Graduate Program in Earth Sciences

A thesis submitted in partial fulfillment
of the requirements for the degree of
Master of Science

The School of Graduate and Postdoctoral Studies
The University of Western Ontario
London, Ontario, Canada

© Dennis Michael Laliberty 2014

Abstract

The LaRonde mine is a gold-rich VMS deposit in the Abitibi Greenstone Belt of Canada. Like many polymetallic ore deposits, loss of sphalerite occurs during the Cu circuit of flotation separation at the mill. Zinc sulphate was tested as a sphalerite depressant. XRD, TOF-SIMS and XPS were used to examine the mineralogy and surface chemistry of ore samples collected at select stages of the milling process in the mill and in the laboratory. Data analyses showed that $ZnSO_4$ likely promotes sulphoxyl and hydroxide adsorption to the sphalerite surface inhibiting Cu activation. Addition of $ZnSO_4$ in the LaRonde mill has reduced the amount of sphalerite recovered in the Cu concentrate by one third.

Keywords

LaRonde, VMS deposits, sphalerite, flotation separation, inadvertent copper activation, zinc sulphate, sphalerite depression, XRD, XPS, TOF-SIMS.

Acknowledgments

The author would like to thank: Dr. Brian Hart for his knowledge, support and most of all patience; Dr. Norm Duke; Dr. Mark Biesinger, Dr. Saeed Chelgani and the rest of the staff at Surface Science Western; Caroline Olsen and the staff at Corem; Dr. Alan Pratt; and finally, the person without whom, none of this would have been possible, my incredible wife, Jennifer.

Table of Contents

Table of Contents

Abstract.....	ii
Acknowledgments.....	iii
Table of Contents	iv
List of Tables	vii
List of Figures	viii
Preface.....	xi
Chapter 1	1
1 Introduction.....	1
1.1 Archean Greenstone Belts.....	1
1.2 Abitibi Greenstone Belt	2
1.3 Volcanogenic Massive Sulphide (VMS) Deposits	5
1.4 LaRonde Au-Rich VMS Deposit.....	6
1.5 Flotation Separation.....	8
1.6 Electrochemistry	12
1.7 Sphalerite Activation	16
1.8 ZnSO ₄	21
1.9 Objectives of the Study.....	23
Chapter 2.....	24
2 Sample Collection and Methodology.....	24
2.1 Sample Collection.....	24
2.1.1 Copper flotation circuit at LaRonde	24
2.1.2 Duplication of plant operational parameters in the laboratory	25
2.1.3 ZnSO ₄ bench tests	28

2.2 Analytical techniques	28
2.2.1 XRD	28
2.2.2 TOF-SIMS	29
2.2.3 XPS	31
Chapter 3.....	33
3 Results and Discussion.....	33
3.1 XRD results.....	33
3.1.1 XRD results discussion.....	36
3.2 TOF-SIMS results: LaRonde Mill Samples.....	37
3.2.1 TOF-SIMS results: LaRonde Mill Samples: Discussion.....	41
3.3 TOF-SIMS results: Instrumented Mill Tests	41
3.3.1 TOF-SIMS results: Instrumented Mill Tests: Discussion.....	45
3.4 ZnSO ₄ bench tests: XPS results	46
3.4.1 ZnSO ₄ bench tests: Discussion	54
Chapter 4.....	58
4 Final discussion.....	58
4.1 Flotation Laboratory Test	58
4.2 Instrumented Mill.....	60
4.3 Bench Tests.....	61
4.4 Plant Implementation	65
5 Conclusions	66
References.....	67
Appendices.....	82
1 Appendix A – LaRonde Mill Test.....	82
1.1 XRD Plots for LaRonde Mill Samples	82
1.2 Vertical Box Plots of TOF-SIMS Data for LaRonde Mill Samples.	87

2	Appendix B – Instrumented Mill Test	93
2.1	Vertical Box Plots of TOF-SIMS Data.....	93
3	Appendix C – Bench Tests.....	99
3.1	XPS Survey Spectra.....	99
3.2	XPS High Resolution Spectra.....	106
4	Curriculum Vitae.....	113

List of Tables

Table 2-1 LaRonde Cu/Pb and Zn flotation circuit sample locations and descriptions.....	25
Table 2-2 Received samples, sample locations, test parameters and analysis performed and reported on in the thesis.	27
Table 3-1 Semi-quantitative XRD analysis of selected samples from the LaRonde Cu flotation circuit.....	34
Table 3-2 Sample legend showing equivalent sample nomenclature from the LaRonde Mill and that used in the vertical box plots.....	37
Table 3-3 Range, median and average concentration of Cu as measured on the surface of sphalerite grains by XPS.....	47
Table 3-4 Relative proportion in % of S species identified from the S2p spectra on the surface of sphalerite grains from the various bench tests.	56
Table 4-1 Flotation testing conditions	59

List of Figures

Figure 1-1 Approximate outline of the Abitibi Greenstone Belt overlain on a Google Earth image showing the location of the LaRonde Mine.	3
Figure 1-2 Summary cross-section of a typical Noranda type VMS deposit. Py: pyrite; Sp: sphalerite; Cp: chalcopyrite; Po: pyrrhotite; Mt: magnetite. Modified from Franklin 1995. ...	6
Figure 1-3 Geologic setting and hydrothermal alteration associated with gold-rich volcanogenic massive sulphide deposits (taken from Dubé et al., 2007).	7
Figure 1-4 The general mineral recovery process (class notes – Hart 2010).....	9
Figure 1-5 The general mineral recovery process (class notes – Hart 2010).....	10
Figure 1-6 A schematic of particle/bubble attachment during the froth flotation process (class notes – Hart 2010).....	11
Figure 1-7 On the left is the sodium xanthate molecule (potassium xanthate is also used). On the right is the dixanthogen molecule which is an oxidation product created during the anodic process (Eq. 1.4).	14
Figure 2-1 Flowsheet of the copper flotation circuit at LaRonde with sample collection locations.	24
Figure 2-2 Example of the “Denver” flotation equipment used in the testing.....	26
Figure 2-3 Flotation scheme and parameters for the instrumented mill/flotation test. The red X marks the sampling locations.....	27
Figure 2-4 (Clockwise starting top left) TOF-SIMS Zn map showing a region of interest (ROI), spectra showing the mass positions for Cu and Zn isotopes in the region of 64.5-66.5 amu, spectra showing Cu on the surface of sphalerite, and a vertical box plot comparing Cu and collector 3418A on the surface of sphalerite in the concentrate and tail.	30
Figure 3-1 Stacked XRD spectra of samples from the LaRonde Cu flotation circuit.	35

Figure 3-2 Histogram showing the percent sphalerite identified in the listed samples from the LaRonde flotation circuit.	37
Figure 3-3 Vertical box plot of copper intensities on the surface of sphalerite grains. For sample location abbreviations refer to Table 3-2.	38
Figure 3-4 Vertical box plots of copper on sphalerite grains in the Cu/Pb circuit. For sample location abbreviations refer to Table 3-2.	39
Figure 3-5 Vertical box plot of lead intensities on the surface of sphalerite grains. For sample location abbreviations refer to Table 3-2.	40
Figure 3-6 Vertical box plots of lead on sphalerite grains in the Cu/Pb circuit. For sample location abbreviations refer to Table 3-2.	40
Figure 3-7 Vertical box plot of Cu on sphalerite grains from the instrumented mill test samples.	42
Figure 3-8 Vertical box plot of ZnOH on sphalerite grains from the instrumented mill test samples.	43
Figure 3-9 Vertical box plot of SO ₃ on sphalerite grains from the instrumented mill test samples.	44
Figure 3-10 Vertical box plot of the collector 3418A on sphalerite grains from the instrumented mill test samples.	45
Figure 3-11 XPS survey spectrum of vacuum-fractured sphalerite surfaces.	46
Figure 3-12 XPS high resolution S 2p peak of vacuum-fractured sphalerite surfaces.	47
Figure 3-13 XPS survey spectra of sphalerite surfaces in de-ionized water.	48
Figure 3-14 XPS high resolution S 2p peak of sphalerite surfaces in de-ionized water.	48
Figure 3-15 XPS survey spectra of sphalerite surfaces in de-ionized water with 5 ppm CuSO ₄	49

Figure 3-16 XPS high resolution S 2p spectra of sphalerite surfaces in de-ionized water with 5 ppm of CuSO ₄	50
Figure 3-17 XPS survey spectra of sphalerite surfaces in de-ionized water with 25 ppm of ZnSO ₄	51
Figure 3-18 XPS high resolution S 2p peak of sphalerite surfaces in de-ionized water with 25 ppm of ZnSO ₄	52
Figure 3-19 XPS survey spectra of sphalerite in de-ionized water with 5 ppm CuSO ₄ and 25 ppm ZnSO ₄	53
Figure 3-20 XPS high resolution S 2p of sphalerite in de-ionized water with 5 ppm CuSO ₄ and 25 ppm ZnSO ₄	54
Figure 3-21 The variability in dominant S species as identified on sphalerite grains by XPS in the bench test samples. Fracture: freshly fractured; SPH: in DIW; CuSO ₄ : DIW + CuSO ₄ ; ZnSO ₄ : DIW + ZnSO ₄ ; CuSO ₄ + ZnSO ₄ : DIW + CuSO ₄ + ZnSO ₄	55
Figure 3-22 Average Zn:S ratio as determined by XPS analyses for sphalerite grains from the 5 bench tests.	57
Figure 4-1 Effect of zinc sulphate on ZnS in Cu rougher flotation tests, with and without Cu ²⁺	60
Figure 4-2 High resolution XPS spectrum of the Cu 2p _{3/2} peak with no “shake-up” peak. ...	62
Figure 4-3 High resolution XPS spectrum of S 2p _{3/2} peaks on sphalerite in de-ionized water.	63
Figure 4-4 High resolution spectrum of S 2p _{3/2} peaks on sphalerite in 25ppm ZnSO ₄ and 5ppm CuSO ₄ solution.	64
Figure 4-5 Monthly mean Zn recovery in the Cu flotation circuit at LaRonde (2009).	65

Preface

Complex polysulphide ores are usually difficult to process without incurring inadvertent activation of unwanted minerals, in particular sphalerite in a copper and PM (precious metal) flotation circuit (Aslan, 2010). It is well established that inadvertent sphalerite activation is linked to the dissolution of lead and copper sulphides (yielding Cu^{2+} and Pb^{2+}) and their transfer via solution to the sphalerite surface (Ralston, 1980; Chen, 2010; Mehrabini, 2010; Pulido, 2011). Ore grinding can influence changes in mineral surface properties that occur during grinding and flotation can modify the stream partitioning behavior of minerals (Biesinger et al, 2007; Chen, 2010; Peng, 2010; Ye, 2010; Simpson, 2011). Experience has shown that process improvement scenarios solely based on laboratory-identified solutions often fall short of expectations. Therefore the key to providing relevant improvement strategies is to perform testing scenarios based on the duplication of plant operational parameters with conditions that allow for the monitoring and testing of process outcomes in response to changes in the predefined operational parameters.

During the last decade, the understanding of flotation systems has been greatly enhanced by the use of surface characterization techniques like TOF-SIMS and XPS. Knowledge of the surface composition allows establishing a correlation between mineral surface chemistry and flotation response. (Piantadosi et al, 2000; Smart et al, 2003; Hart et al, 2006; Abreu, 2011; Peng, 2011; Smart et al, 2013). Unfortunately, the action mechanism of depressants, in particular the addition of zinc sulphate, remains partly unknown because of the complexity of sulphide mineralogy and the availability of surface chemistry techniques. This work examined the surface chemical effects on sphalerite in response to zinc sulphate addition in flotation testing scenarios designed to evaluate changes in zinc recovery. The laboratory test results were compared to surface chemical data collected from plant samples toward potentially identifying the mechanism of sphalerite depression.

Samples used in this study were from the LaRonde Division of Agnico-Eagle Mines Limited located ~45km east of Rouyn-Noranda, Quebec. The ore is a polymetallic VMS deposit hosted in the Blake River Group of the Archean Abitibi Greenstone Belt. Samples from the LaRonde concentrator were collected from various locations in the copper flotation circuit.

Samples for the laboratory testing were collected from the same ore and crushed to 1.7 mm, homogenized, split, sealed and frozen to prevent oxidation prior to use.

A simple beaker test was also carried out using pristine samples of chalcopyrite, pyrite and sphalerite in order to determine the effect of zinc sulphate addition during the flotation process for comparison to the samples taken from the mill.

Chapter 1

1 Introduction

The following section gives the geological background of the LaRonde deposit as well as the separation flotation processes of the mill.

1.1 Archean Greenstone Belts

Archean greenstone belts represent one of the earliest records of Earth's lithospheric history (de Wit & Ashwal, 1995). The term greenstone comes from the green colour of many of the low grade (most commonly greenschist facies) mafic and ultramafic volcanic minerals present, such as serpentine, chlorite, actinolite and epidote (de Wit & Ashwal, 1995). Granite greenstone terranes are comprised of granitic plutons intruding extrusive mafic to ultramafic igneous rocks, felsic volcanics, and either inter-flow or cover sedimentary rocks (Cengage, 2003). Greenstone belts separate domical granitoids and gneisses (Rollinson, 2007). Common features in the volcanics of greenstone belts are pillow structures which indicate that the lava that formed them was extruded under water (Stanley, 2009).

Several models have been proposed for the origins of greenstone belts and a single tectonic setting for the origin and evolution of all greenstone belts does not exist (de Wit & Ashwal, 1995). It is generally believed that in Archean times the Earth's mantle would have been far hotter. However, de Wit & Hynes (1995) propose that Archean magmatism and tectonism represent a more volatile-rich mantle and not necessarily a hotter mantle. It is generally accepted that magmatic and tectonic processes were different than present day and that there are no exact modern analogues to greenstone belts (Cengage, 2003).

Opponents to Archean plate tectonics contend that greenstone belts commonly represent a laterally continuous volcanic sedimentary sequence. These opponents suggest an autochthonous model whereby younger greenstone units erupt through and accumulate in place upon older units (Thurston, 2002; Thurston et al., 2008) with the sedimentary sequences marking periods of volcanic inactivity. This scenario is dominated by mantle

plumes and is analogous to the tectonics of Venus (little to no plate movement). Greenstone belts are therefore interpreted as oceanic plateaus generated by mantle plumes, similar to those found in the southern Caribbean (Cengage, 2003).

The contrary view is that present day tectonic processes were operative during the Late Archean, and possibly earlier. In this case, greenstone belts may have formed as volcanic arcs or inter-arc or back-arc basins. In allochthonous models, greenstone belts are interpreted to represent the accretion of differing lithological assemblages from a variety of tectonic settings (Thurston, 2002; Rollinson, 2007; Thurston et al., 2008) and record crustal evolutionary histories that vary from 50 to 500My (de Wit & Ashwal, 1995).

1.2 Abitibi Greenstone Belt

The Abitibi Greenstone Belt (AGB) cuts a 300 X 700 km swath across northwestern Quebec and northeastern Ontario (Figure 1–1) and is home to many world class Archean volcanogenic massive sulphide (VMS) deposits. The AGB represents the collision of ocean arcs over a span of approximately 65 million years that date between 2735-2700 Ma (Meuller et al., 2009).

Years of geological and geophysical mapping, age dating, lithological correlation, and mineral deposit distribution have painted a clear stratigraphic picture of the Abitibi Subprovince. The subprovince is comprised of an array of “lozenge”-shaped blocks, longer in their east-west than in their north-south dimensions and framed by anastomosed and intersecting ductile shear zones and in many cases, by narrow belts of metasedimentary rocks (Norman, 1946; Kalliokoski, 1968; Ludden et al., 1986). The AGB is underlain by low to medium grade Archean metavolcanic and metasedimentary rocks (Goodwin & Ridler, 1970; Card, 1990). The metavolcanic sequences of the southern Abitibi are typically composed of several volcanic cycles (Ayer et al., 2002) each of which is commonly composed of a lower ultramafic to mafic portion and an upper felsic volcanic to sedimentary portion (Dimroth et al., 1982). Chemical analyses and consequent identification of mineral compositions suggest that the former are products of eruption of laterally extensive flows on subaqueous lava plains or emergent volcanic islands (Dimroth et al., 1985; Ludden et al., 1986). Occurrences of komatiite

may provide evidence indicating involvement of mantle plumes (Goodwin, 1982; Wyman et al., 2002).

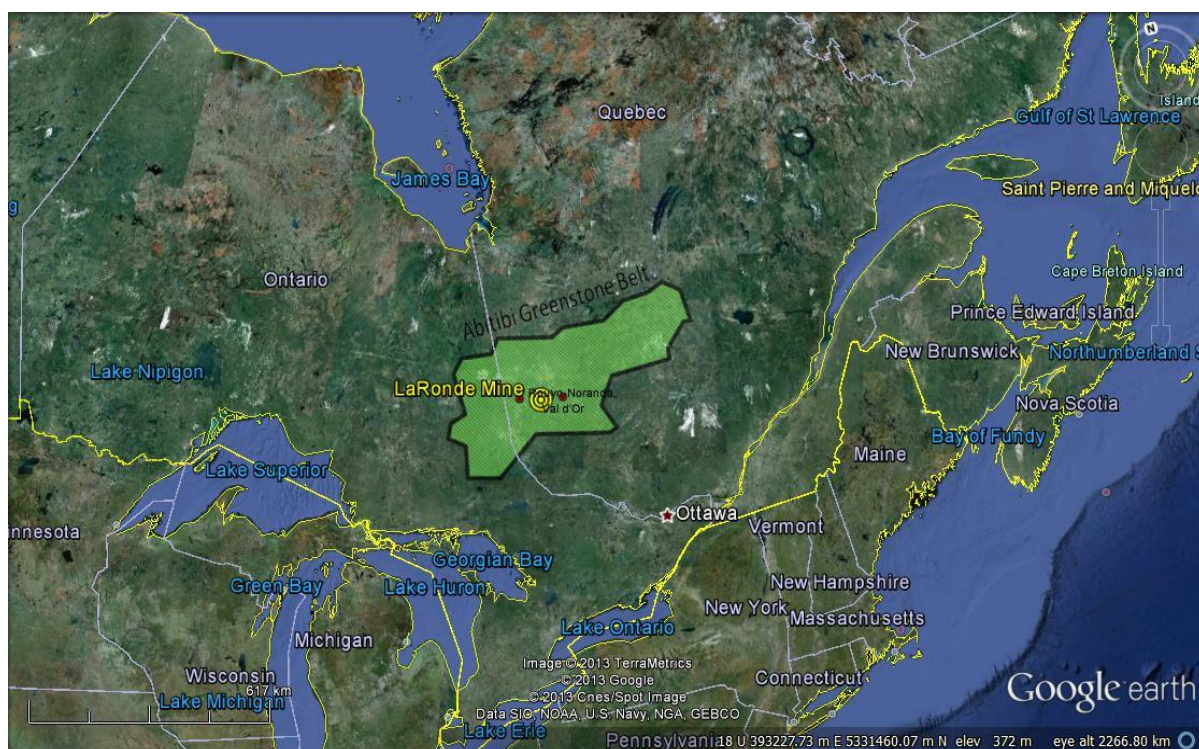


Figure 1-1 Approximate outline of the Abitibi Greenstone Belt overlain on a Google Earth image showing the location of the LaRonde Mine.

Clastic metasedimentary rocks, representing subaerial to deep-water facies (Ojakangas, 1985; Mueller & Donaldson, 1992), are generally composed of turbiditic greywacke with local conglomerate and are regarded to have formed in submarine fans and channels (Hyde, 1980; Dimroth et al., 1982; Mueller & Donaldson, 1992).

Plutonic rocks of the AGB consist of large older sodic intrusions such as the Kamiskotia Complex, the Flavrian Granite and the Bourlamaque Batholith where tonalite and quartz diorite are common (Sutcliffe et al., 1993). Younger, smaller granitoid intrusions are granodiorite to syenite in composition (Mortensen & Card, 1993).

The rocks of the AGB are metamorphosed to assemblages indicative of prehnite-pumpellyite to amphibolite facies developed at low to medium pressure. Throughout the

region most metamorphic rocks, particularly near major fault zones, contain penetrative foliation and lineation formed during the Kenoran Orogeny (Jolly, 1978). Despite weak metamorphic and deformational overprinting, the rocks of the Abitibi show exceptional preservation of primary volcanic, sedimentary and plutonic features at most localities.

Chronostratigraphic studies have shown that most rocks and mineral deposits of the southern Abitibi belt formed between 2740 to 2650 Ma (Mortensen & Card, 1993; Corfu, 1993; Ayer et al., 2002; Davis, 2002). Most of the notable deformation, plutonism and metamorphism occurred towards the end of this interval and constitute the Kenoran Orogeny (Stockwell, 1982).

The primary tectonic grain in the Abitibi Subprovince is the predominance of E-W trending structures. Most of the volcanic, sedimentary and early plutonic rocks have been heterogeneously strained to produce folds, foliations and lineations conforming to an overall E-W trend, with local dispersion around folds hinges and oval domes. The first order faults tend to be parallel with stratigraphic contacts and comprise 20 to 200 m wide zones of metasomatic phyllonite and gouge resulting from localized intensification of regional metamorphic fabric (Robert, 1989). The most important of these are the E-W striking Larder Lake-Cadillac and the Porcupine-Destor faults. The presence of steep lineations within and adjacent to these faults, as well as their concordant map view orientation with respect to stratigraphic units, has led most workers to regard them as steep thrusts (Dimroth et al., 1983). At some localities minor dextral or sinistral movements have been suggested (Dimroth et al., 1983; Robert, 1989; Wilkinson et al., 1999) and may result from local strike-slip reactivation of these faults (Powell & Hodgson, 1992; Powell et al., 1995a).

Gold deposits in the southern Abitibi region are mainly distributed along the two major structural corridors defined in part by the Destor-Porcupine and Larder Lake-Cadillac faults. Major districts include Timmins, Harker-Holloway, Kirkland Lake, Larder Lake, Rouyn-Noranda, Bousquet, Malartic and Val d'Or.

1.3 Volcanogenic Massive Sulphide (VMS) Deposits

Volcanogenic Massive Sulphide (VMS) deposits are stratiform accumulations of sulphide minerals which formed on or near the sea floor by precipitation near the discharge site of submarine hydrothermal fluids. VMS deposits are major sources of Zn, Cu, Pb, Ag, and Au. The ores characteristically consist of >60% sulphide most of which is pyrite and/or pyrrhotite plus variable amounts of sphalerite, chalcopyrite and galena (Franklin et al., 1981). The massive ore lenses may be underlain by Cu-rich veins and disseminated sulphides, forming stringer zones or stockworks within intensely altered rocks of the discharge pipe. This alteration pipe is where the complex interaction of the host rock, the ore-forming hydrothermal fluid and locally circulating hot sea water takes place. Lower alteration zones represent source zones for the bulk of metals and reduced sulphur. The VMS deposits are characterized by internal metal zoning located above the feeder pipes (Figure 1–2). In distal cases the ore bodies are tabular with or without underlying stringer zones (Franklin et al., 1981).

The source of metal in VMS deposits is a result of incompatible elements, metals and sulphur being leached from the underlying rocks in the sub-seafloor hydrothermal alteration zone by hydrothermal circulation. The hydrothermal circulation is driven by igneous heat in the crust, often related to deep-seated synvolcanic granite intrusions or gabbroic magma chambers. Cool ocean water is drawn into the hydrothermal zone and is heated by the hot volcanic rocks. It is then expelled into the ocean, usually through a series of fractures and faults. When the hydrothermal fluids are expelled into the ocean, they cool and precipitate sulphide minerals as stratiform sulphide ore. Some deposits show evidence of sulphide replacement of altered volcano-sedimentary rocks. There may also be invasion of sulphur-rich brines into unconsolidated sediments. The major source of sulphur in this type of deposit is from the reduction of seawater sulphate to sulphide during fluid-rock interaction prior to venting (Robb, 2005).

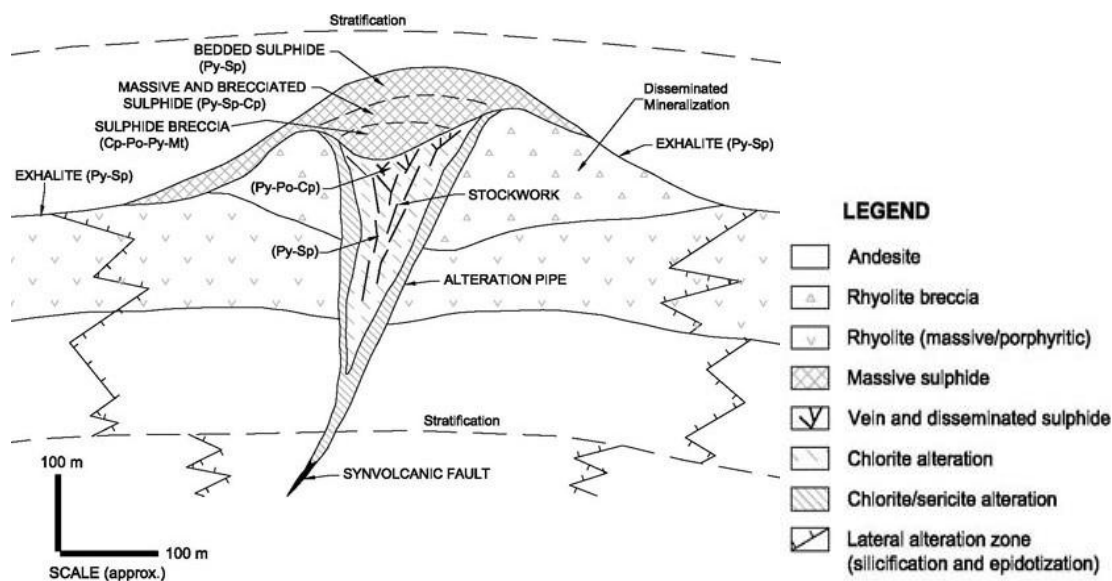


Figure 1-2 Summary cross-section of a typical Noranda type VMS deposit. Py: pyrite; Sp: sphalerite; Cp: chalcopyrite; Po: pyrrhotite; Mt: magnetite. Modified from Franklin 1995.

VMS deposits can be found throughout geological history starting at around 3.4 Ga to actively forming deposits on the modern sea floor. Deposits are formed in a variety of tectonic settings such as oceanic ridges, thickened oceanic crust, sediment-covered oceanic ridges and rifted continental margins. Deposits are generally associated with volcanism in extensional settings, mostly in rifted settings within arcs and back-arcs. Modern examples of VMS deposits are formed by black smokers at oceanic ridges but the vast majority of this mid-ocean ridge lithosphere is subducted due to negative buoyancy (it is more dense). This is why Archean to Cenozoic VMS deposits preserved in the geological record are more likely to be from convergent margin settings (Groves & Bierlein, 2007). Modern examples of convergent margin VMS deposits are formed in back arc basins.

1.4 LaRonde Au-Rich VMS Deposit

Gold-rich volcanogenic massive sulphide (Au-rich VMS) deposits (Figure 1–3) form a subtype of both volcanogenic massive sulphide (VMS) and lode-Au deposits (Poulsen &

Hannington, 1996; Hannington et al., 1999; Huston, 2000; Poulsen et al., 2000). The distinguishing characteristic of the Au-rich VMS deposit is that the average Au content (g/t) is more economical than the Cu, Pb and Zn grades (weight %) combined (Poulsen et al., 2000).

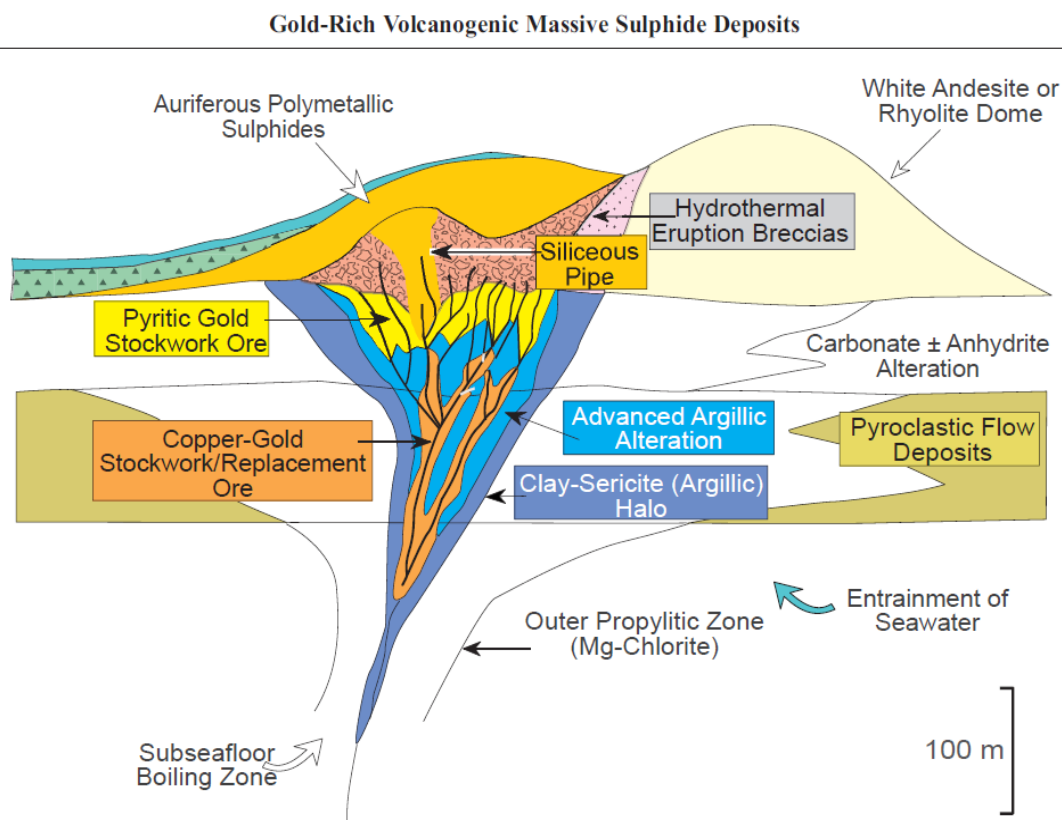


Figure 1-3 Geologic setting and hydrothermal alteration associated with gold-rich volcanogenic massive sulphide deposits (taken from Dubé et al., 2007).

The typical morphology of Au-rich VMS deposits consists of a lenticular massive sulphide body with associated underlying discordant stockwork-stringer feeders and replacement zones. Some deposits, such as LaRonde, contain stacked massive sulphide lenses. The orebodies are commonly tabular and stratabound to discordant and in most cases have been deformed and tilted parallel to foliation. In turn, the stockwork-stringer zones may be transformed to foliation-parallel sulphide veinlets in schistose, altered rocks with quartz, white mica, and sometimes aluminous silicates (Dubé et al., 2007).

The LaRonde deposit lies between Rouyn-Noranda and Val d'Or, within the Blake River Group (2704-2696 Ma), immediately north of the Larder Lake-Cadillac fault zone. The deposit occurs in the southern portion of a narrow volcanic belt, which contains both mafic, and felsic volcanoclastic rocks and mafic flows. These volcanic rocks strike east, dip steeply south and are bound to the north and south, by clastic sedimentary rocks of the Kewagama and Cadillac Groups (<2687 Ma) respectively. (Savoie et al., 1991; Lafrance et al., 2005; McNicoll et al., 2014). The Dumagami high strain zone, exhibits an intense penetrative S_2 foliation, which overprints these rocks (Trudel et al., 1992).

There are three main types of orebodies: (i) massive sulphide lenses, (ii) zones of sulphide-rich (>25% sulphides veins, typically <20cm thick) with intervening disseminated pyrite, and (iii) zones of 5-20% disseminated pyrite (Dubé et al., 2007).

A variety of genetic models have been proposed for the LaRonde deposits. Synvolcanic models propose that gold was introduced together with the sulphides during felsic volcanism and associated plutonism either by sub-seafloor, or possibly shallow-marine exhalative, hydrothermal processes (Valliant & Hutchinson, 1982; Stone, 1990; Tourigny et al., 1993). This would involve the remobilization of the sulphides and gold during later deformation and metamorphism events. Multistage models also have massive sulphide lenses forming during volcanism, but propose that the gold and sulphide-rich veins were introduced during deformation by fluids of metamorphic origin (Marquis et al., 1990a). Still others believe that the gold and sulphide introduction were synchronous with deformation and metamorphism (Savoie et al., 1990).

1.5 Flotation Separation

Mineral separation involves several processes (Figure 1–4) to reduce the raw ore to the final metal end product. Flotation separation is a complex physical and chemical process that occurs at the surface of mineral particles and air bubbles in the flotation pulp. The basis of froth flotation is related to the difference in surface wettabilities of the different minerals; those that are easily wettable by water are hydrophilic, those that are water-

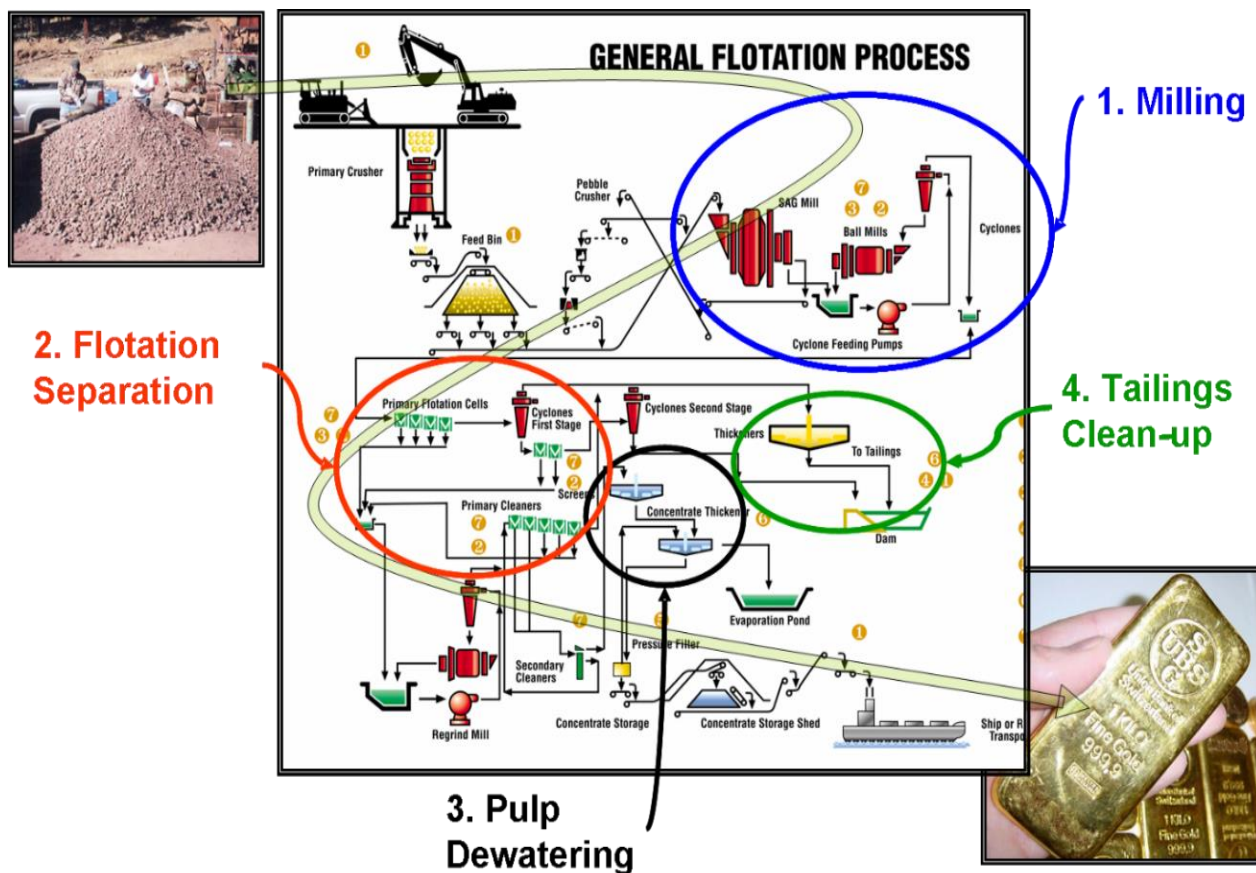


Figure 1-4 The general mineral recovery process (class notes – Hart 2010).

repellent are hydrophobic. The process involves collisions between particles and their interaction with air bubbles in the pulp. When air is bubbled through a mixture of hydrophobic and hydrophilic particles suspended in water, the hydrophobic particles will tend to attach to the air bubbles and float to the surface. The froth layer on the surface of the flotation cell either overflows the lip of the cell or is removed by a froth scraper. The hydrophilic particles which are less inclined to attach to air bubbles remain in suspension and are ultimately removed from the flotation cell in the tail (Rao & Leja, 2004; Bulatovic, 2007; Wills, 2010). A schematic of the process is included in Figure 1–5.

It is often necessary to enhance or induce the hydrophobicity of one or more desired mineral phases in the ore while promoting the hydrophilic character of the remaining phases. Mineral surface hydrophobicity is promoted by the attachment of collector molecules.

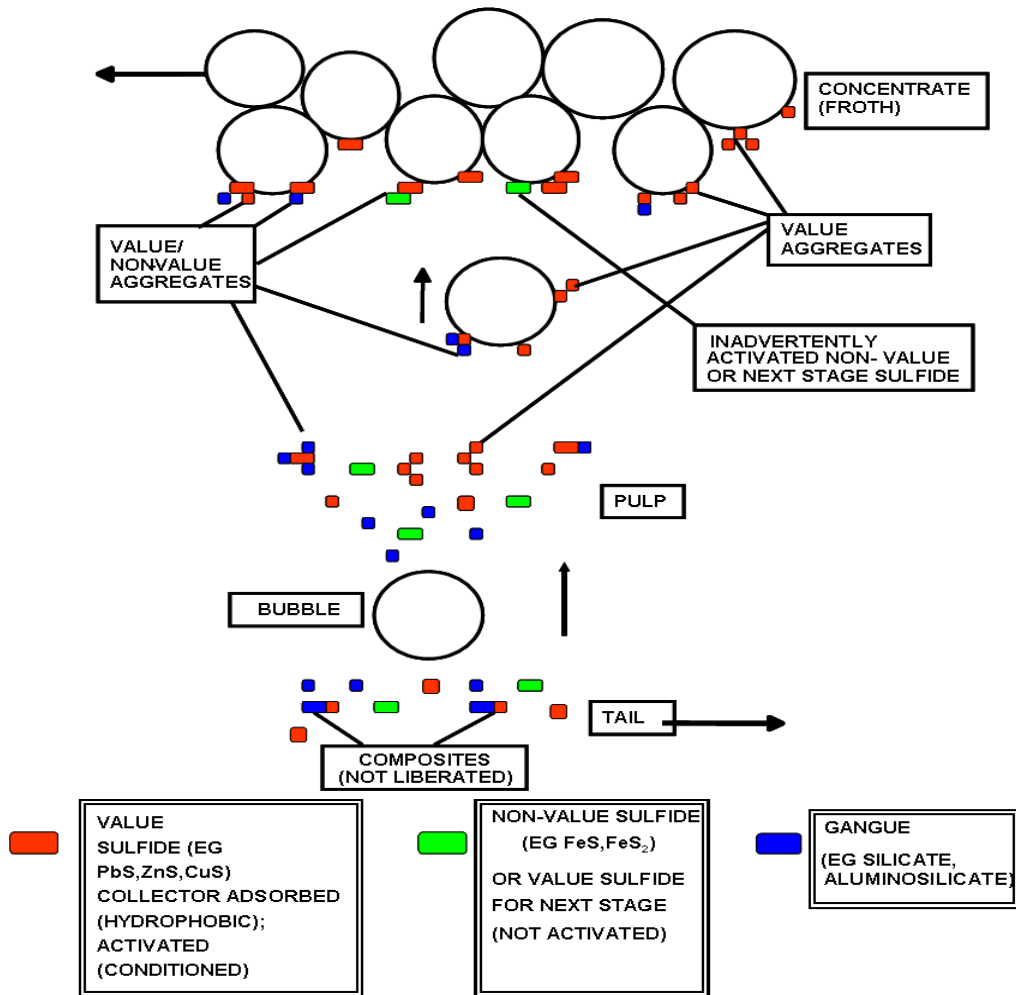


Figure 1-5 The general mineral recovery process (class notes – Hart 2010).

Collectors generally have a polar end with an ionic group that attaches to the particle surface and a long non-polar (hydrophobic) tail that attaches to the bubbles (Figure 1–6). The selectivity of the collector for the desired mineral is partially controlled by the type of ionic group attached to the non-polar tail. (Hu et al, 2009). Selective flotation is strongly dependent on the degree of collector adsorption on the mineral’s surface. Even a 10-20% coverage of hydrophobic layer can be enough to make a mineral floatable (Ruonala et al., 1997). Collector attachment to a particle surface can be through physical adsorption where there is no transfer of electrons or chemisorption; a transfer or sharing of electrons (partial covalent bonding). The mechanism is dependent upon the surface charge of the mineral, the type of collector and the pulp condition in which the flotation

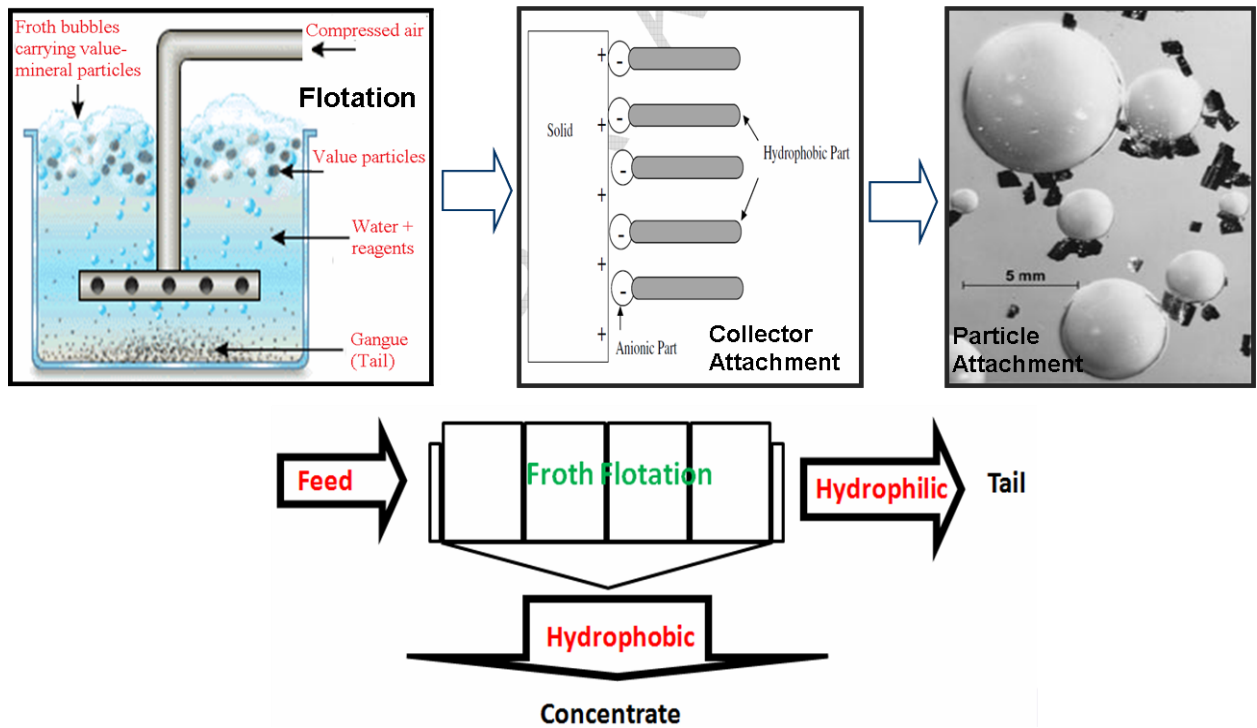


Figure 1-6 A schematic of particle/bubble attachment during the froth flotation process (class notes – Hart 2010).

is performed. The addition of collectors and development of hydrophobic surfaces is accomplished throughout various stages of the recovery process. Once the collector is adsorbed to the particle surface, they move to the bubble surface where attachment and subsequent flotation may occur. Particle bubble attachment is not a straightforward process and involves a number of factors in order to be successful. Some of these include; i) bubble and particle size – it is important that particle size matches bubble size in order to ensure and maintain attachment; ii) bubble velocity – the bubbles need time to interact with the particles; iii) induction time – the time required for the actual attachment which involves removal of the water layer between the particle and bubble (Rao, 2004).

Along with collectors, other chemicals called modifiers are added to the solution to increase the recovery of the target particles. Modifiers include: activators, depressants, dispersants and pH regulators. Activators chemically change the surface of the target particles to aid in the attachment of the collectors. A depressant is a reagent which inhibits the adsorption of a collector on a given mineral or is adsorbed on the mineral to

make the surface hydrophilic. Some of these include inorganic depressants such as lime, sodium cyanide, sulphur dioxide, zinc sulphate, sodium sulphite etc., and organic depressants such as acetic acid, oxalic acid and polyacrylamide polymers containing various functional groups etc. (Hu et al, 2009). Dispersants work to break up agglomerated particles into smaller units that can more readily interact with the collectors and bubbles. The pH of the flotation system is controlled using pH regulators to optimize the conditions for the promotion of collector attachment to the target particles.

Once the target mineral has been removed to acceptable recovery standards the remaining solution (tailings) can be disposed of or sent through another separation circuit to remove a different mineral. Because of the complexity of flotation processes, the utilization of process knowledge requires careful combination of different factors affecting the process. The success or failure of flotation separation is dependent upon the ability to manipulate the chemistry of the system through careful process planning (Ruonala et al., 1997).

1.6 Electrochemistry

The sulphide flotation process depends on chemical reactions that are both electrochemical and surface chemical in nature. Under certain conditions self-oxidation and the generation of elemental sulphur on the mineral surface renders it hydrophobic, but for the most part, sulphide minerals do not exhibit natural floatability. The chemistry of the flotation pulp is highly dependent upon the type and proportion of minerals present, galvanic reactions (due to different energy states of the minerals) and the ensuing oxidation/reduction reactions occurring at mineral surfaces, introduced chemicals and the generation of dissolved ions in the process (Ruonala et al., 1997). Therefore, development of flotation processes remains a trial and error method despite attempts to apply theoretical principles and measuring techniques in practice. In the laboratory, on a smaller scale, electrochemical methods using mineral electrodes offer effective techniques for the process design, study and control to ascertain the optimized process conditions. However, scaling up of laboratory or pilot testing results to true operations

where the quantity and quality of the components affecting the chemical reactions are often underestimated, is not always successful (Ruonala et al., 1997).

The mineralogy of the ore entering the system may vary dramatically from one ore body to another (from the same mine), or even within the same ore body, affecting several process variables. Thus the concentrations of activators, collectors, depressants, dispersants and pH regulators have to be monitored and adjusted accordingly. The grindability of the ore is also dependent on the mineralogy. Selective excavation or mixing ores are common ways to control ore type variation (Ruonala et al., 1997).

Traditionally, metal sulphide orebodies consist of unoxidized primary sulphides and in the flotation processes there may be some degree of mineral oxidation required to achieve proper economic results. It is likely that oxidation begins even before conditioning while the sulphide minerals are stockpiled at the mine, where the ore is crushed and conveyed to heaps which are in contact with air and moisture/rain. After exposure to air or aqueous solution during grinding and conditioning, metal sulphide minerals may exhibit oxide and hydroxide species on the surface (Eq. 1.1) (Smart et al., 1998). Conditioning time, pH, Eh and the gas atmosphere above the sample all affect the surface oxidation mechanisms (Smart et al., 1998).



Where MS is a metal sulphide.

The mechanisms of oxidation are more complex than those of the above general reaction due to factors such as; the chemical nature of the $M_{1-x}S$ product, the spatial distribution of the oxidation products on the mineral surface, dissolved and reprecipitated species, higher oxidation products and interactions with other dissolved species (Smart et al., 1998). These mechanisms result in surface oxidation products such as: metal deficient (sulphur-rich) oxide surfaces, polysulphides and elemental sulphur; oxidized fine particles attached to larger sulphide particle surfaces; colloidal metal hydroxide particles and flocs (flocculations that come out of suspension but are not precipitated); continuous surface layers (oxide/hydroxide) of varying depth; formation of sulphate and carbonate

species; and non-uniform spatial distribution due to differing oxidation rates (Smart et al., 1998).

After conditioning, the flotation of sulphide minerals is accomplished by the interaction with surface modifiers and collectors. Some common sulphide collectors include; xanthate (Figure 1-7), dialkyl dithiophosphates, dialkyl dithiophinates (DTP) and dialkyl dithiocarbamates. These collectors form a hydrophobic layer by adsorption to the mineral surface or oxidation product.

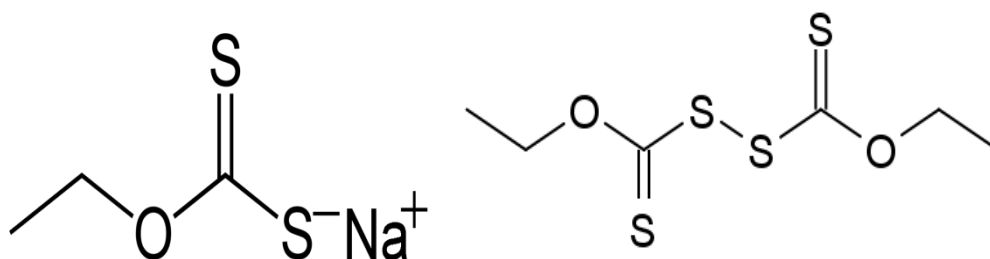
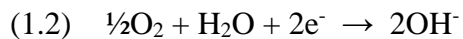
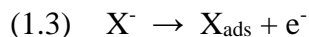


Figure 1-7 On the left is the sodium xanthate molecule (potassium xanthate is also used). On the right is the dixanthogen molecule which is an oxidation product created during the anodic process (Eq. 1.4).

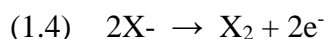
For sulphides the mixed potential theory suggests that there is an anodic oxidation reaction involving the collector which transfers electrons to the mineral which are then returned to the solution phase by the cathodic reduction of oxygen (Fuerstenau et al., 1968; Woods, 1971; Allison, 1972; Goold, 1972; Richardson, 1976; Trahar, 1984; Hu et al., 2000; Yu et al 2004b, c). The International Union of Pure and Applied Chemistry (IUPAC) defines mixed potential as the potential of an electrode (against a suitable reference electrode, often the standard hydrogen electrode) when appreciable fraction to the anodic or cathodic current arises from species of two or more different redox couples, but when the total current on the electrode is zero. In other words, any electrochemical reaction can be divided into two or more separate oxidation and reduction reactions with no net accumulation of electric charge or net current during that electrochemical reaction. The cathodic reduction of oxygen that takes place between thio-collector and sulphide mineral is shown in Eq. (1.2):



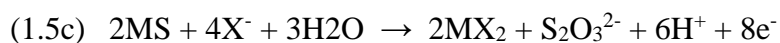
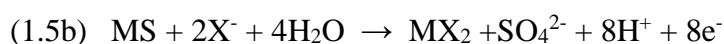
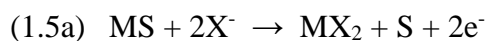
In the anodic process, the collector can transfer electrons to the mineral in different ways: the adsorption of the thio-collector ion (xanthate) in Eq. (1.3);



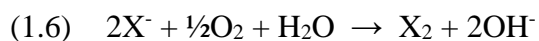
the oxidation of the thio-collector to its dithiolate (dixanthogen) in Eq. (1.4);



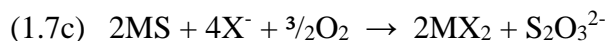
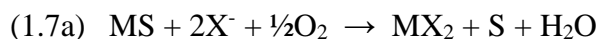
or the chemisorption reaction mechanism in Eqs. (1.5);



Where X^- represents a thio ion and MS represents a sulphide mineral. The overall reactions then become:



Or:

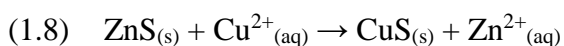


(Hu et al., 2009).

These equations reflect the reactions for sulphides in general, however activation of sphalerite will be looked at in more detail in the next section.

1.7 Sphalerite Activation

Sphalerite does not respond well to short chain thiol collectors (Leppinen, 1990; Wills, 1997; Kartio et al., 1998) due to the relative instability of zinc xanthate and hence requires the use of activators (Cu^{2+} in the form of a sulphate or nitrate is the most commonly used activator) to enhance the adsorption between collector molecules and the sphalerite surface (Leppinen, 1990; Wills, 1997). Separation of sphalerite through copper activation becomes problematic when other minerals within the pulp are inadvertently activated along with the sphalerite (Chandra & Gerson, 2009). Copper activation of sphalerite is due to ~1:1 ion exchange (uptake of Cu^{2+} and release of Zn^{2+} into solution) (Sutherland & Wark, 1955; Popov & Vucivic, 1990; Finkelstein, 1997; Gerson et al., 1999) as seen in equation (1.8):

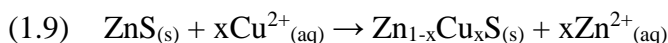


Cu^{2+} on the sphalerite surface is reduced to Cu^{1+} resulting in the oxidation of the sulphide surface. Collector molecules then attach to the copper sulphide species (Cu^{1+} -xanthate is most common surface product formed especially at low pH) (Popov & Vucivic, 1990) increasing hydrophobicity and thus increasing the flotation response (Patrick et al., 1999). Copper uptake depends on impurities, such as iron in the sphalerite, surface oxidation, copper and xanthate concentration, activation time, oxygen concentration in solution (pulp potential), and most importantly pH (Chandra & Gerson, 2009). In mildly acidic solutions hydrophobic species (polysulphides and elemental sulphur) predominate, due to oxidation of metal-deficient sulphide on the sphalerite surface. Collectorless flotation can occur at low pH due to diffusion of impurities such as copper and iron from the bulk to the surface after zinc dissolution (Buckley et al., 1989). In these situations collectorless flotation of the sphalerite is facilitated by the development of elemental sulphur on the sphalerite surface. Hydrophilic species (zinc hydroxide and copper hydroxide) along with some sulphite/sulphate occurs at higher pH (Popov & Vucinic, 1990; Prestidge et al., 1997; Fornasiero & Ralston, 2006) and reduce flotation recovery.

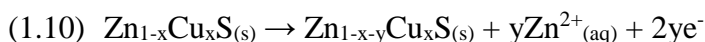
When copper activation is carried out in open circuit conditions, a covellite-like (CuS) activation product forms, while activation conducted at lower potentials produces a

chalcocite-like (Cu_2S) product. Also activation conducted under slightly oxidising conditions produce hydrophobic species on the surface (e.g. Copper polysulphides) (Chen & Yoon, 2000).

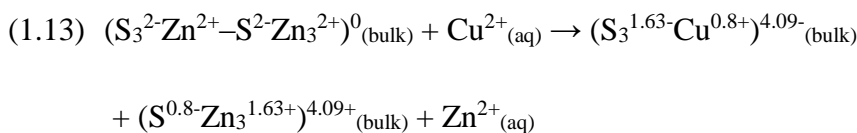
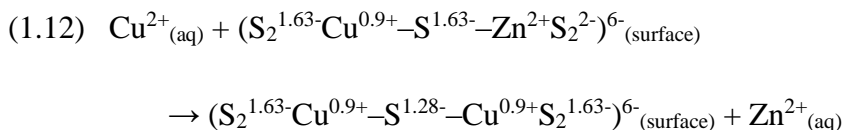
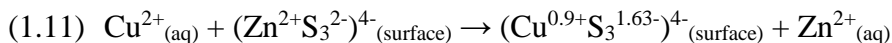
Buckley et al. described the activated sphalerite surface as a copper-substituted sphalerite lattice with the formation of a metal-deficient sulphide (sulphur-rich) surface layer in both acidic and alkaline media. This, according to them, is better represented by equation (1.9), than by equation (1.8) where the product is metastable.



Shorter Cu-S bonds (compared to the Zn-S bonds) create a slightly pushed-up and outward, distorted trigonal planar structure (Cu-S_3) on the sphalerite surface which elongates the attaching Zn-S bonds (Gerson et al., 2008). It has also been suggested that unsubstituted (by copper) oxidative losses of zinc (Eq. 1.10) from the sphalerite lattice leads to the development of enhanced sulphur regions (Buckley et al., 2007).



Variable XPS S 2p binding energies suggest that sulphur is present in different oxidation states (non-integer) depending on the extent of copper activation (more copper activation – less negative sulphur oxidation state)(Gerson et al., 1999). The reaction mechanism for surface substitution involves an initial then second copper substitution (Eqs. 1.11 & 1.12) and then a bulk substitution of zinc with copper (Eq. 1.13).

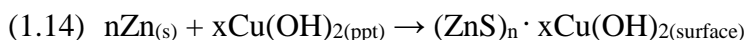


This mechanism results in the formation of the distorted trigonal planar geometry with Cu bonded to three sulphur atoms of differing oxidation states (Chandra & Gerson, 2009).

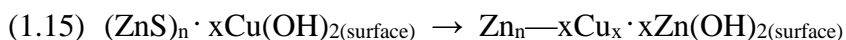
Activation of sphalerite (a natural insulator) by Cu^{2+} reduces the band gap (of the valence orbitals from 3.5eV to 1.1eV) (Kartio et al., 1998; Fornasiero & Ralston, 2006) increasing the conductivity and allowing the thiol collectors to form an insoluble collector complex on the sphalerite surface through mixed potential electrochemical reactions (Buckley et al., 1989; Kartio et al., 1998).

Initial uptake of copper is very fast within the first 10-15 min (Solecki et al., 1979, Popov & Vucinic, 1990; Kartio et al., 1998) of the activation process (the rate is controlled by diffusion through the solution phase) (Finkelstein, 1997) but slows and shows logarithmic time dependency (Kartio et al., 1998) (which reflects the copper diffusion into the bulk sphalerite lattice) (Buckley & Woods, 1987; Finkelstein, 1997). On the surface, copper replaces three Zn-S with three Cu-S bonds which requires a low activation energy (Gerson et al., 1999). However in the lattice, four Zn-S bonds are replaced by only three Cu-S bonds requiring higher activation energy (Chandra & Gerson, 2009). Longer activation times reduce the formation of surface Cu^{1+} -xanthate (especially in dilute acid solutions) (Popov & Vucinic, 1990). However, studies do not show a correspondingly significant reduction in sphalerite recovery (Lascelles et al., 2001; Chandra & Gerson, 2009).

Prestidge et al. explain that equation (1.9) is more representative of copper activation in an acidic medium where the activating species is only Cu^{2+} . At high pH (≥ 9) and high copper concentrations the sphalerite surface becomes heavily coated with colloidal copper hydroxide (equation 1.14) (Prestidge et al., 1997; Gerson et al., 1999; Fornasiero & Ralston, 2006; Beisinger et al., 2007) which may have a depressing effect on sphalerite flotation (Popov & Vucinic, 1990).



The copper from the hydroxide can then exchange with the zinc of the sulphide as seen in equation (1.15) (Prestidge et al., 1997).



The surface zinc hydroxide then dissolves and/or disperses to varying degrees which in turn affects the surface hydrophobicity (Prestidge et al., 1997; Fornasiero & Ralston, 2006). The Cu^{2+} sulphide is then reduced to Cu^{1+} and may then combine with xanthate upon collector addition (Patrick et al., 1999).

Some researchers believe that the surface copper hydroxide directly interacts with the xanthate (OH^- exchanges with xanthate) and the resulting product then decomposes to form Cu^{1+} -xanthate and dixanthogen on the surface (Leppinen, 1990; Popov & Vucinic, 1990).

The copper concentration needed to give maximum flotation response differs depending on the activation conditions, origin of the mineral sample and available surface area for activation. In the absence of collector, increased Cu^{2+} concentration has the effect of continuously decreasing the flotation of sphalerite with maximum reduction seen at pH 8.5-10; presumably due to the formation of $\text{Cu}(\text{OH})_2$ precipitates. Above pH 12 the stable species is $\text{Cu}(\text{OH})_3^-$ and below pH 5 Cu^{2+} is stable (Fornasiero & Ralston, 2006). High copper concentrations may also interact with xanthate collectors in the pulp preventing adsorption onto the activated sphalerite surfaces (Popov & Vucinic, 1990). In these circumstances the collectors act as chelators fixing the copper in solution nullifying its ability to react with the sphalerite surface. In order to maintain the effectiveness of copper and the reagent due to this side reaction, Cu^{2+} , followed by collector and then lime are added in sequence (Finch et al., 2007). Increase in activation time increases the copper uptake (and release of Zn^{2+}) (Kartio et al., 1998) by allowing the copper from the $\text{Cu}(\text{OH})_x$ on the surface to migrate into the bulk of the sphalerite (Prestidge et al., 1997). However, surface Cu^{1+} -xanthate decreases with extended activation time as the Cu^{1+} moves into the bulk (Popov & Vucinic, 1990). Increased time delays between Cu^{2+} addition and collector addition decreased the amount of collector adsorbed onto the sphalerite surface at high pH (9.2) but not at neutral or mildly acidic pH (Lascelles et al.,

2001). At high pH copper hydroxide colloids can adsorb onto the sphalerite surface (Prestidge et al., 1997) which can be lost to solution if the delay between Cu^{2+} addition and collector addition is too great, which in turn decreases surface xanthate adsorption. However, flotation recovery of sphalerite was greater for samples activated for prolonged periods and/or with increased copper concentration and there was no decrease in flotation with reduced surface xanthate (probably due to collectorless flotation but early addition of xanthate is recommended) (Lascelles et al., 2001).

Natural sphalerite normally contains iron, (along with other minor impurities substituted for zinc) (Harmer et al., 2007) the amount of which depends on the temperature and chemistry of the crystallization environment (Dana et al., 1977; Wenk & Bulakh, 2004). Sphalerite is a wide band gap (the distance between the valence band and the conduction band) semiconductor with a band gap of 3.5-3.9 eV (Harmer et al., 2008). The presence of iron in sphalerite decreases the band gap and increases its reactivity which in turn may influence activation and subsequent flotation (Harmer et al., 2008). Using synthetic sphalerite with iron contents ranging up to 40 wt% it has been shown that Cu^{2+} adsorption decreases with an increase in iron concentration (Solecki et al., 1979). Furthermore there is also a decrease in xanthate attachment to copper-activated sphalerite, due to reduced copper on the surface of the higher iron sphalerite (Szczypta et al., 1980). It was also seen that increased iron content reduced the rate of copper-activated sphalerite flotation which is believed to be related to the presence of iron in the sphalerite lattice which reduces the zinc exchange sites for Cu^{2+} (Boulton et al., 2005). However, others have shown that in natural sphalerite, the iron-rich samples adsorbed more xanthate onto the surface (Gigowski et al., 1991; Harmer et al., 2008). Impurities such as iron create defects due to bond rotation as well as reconstruction at cleavage steps, necessary to lower surface free energy (Harmer et al., 2008). However, these defects and steps are still of a higher energy and tend to be sites of increased reactivity. As iron content increases, the number of defects increases which allows for more rapid oxidation and thus increased Cu^{2+} adsorption in the iron-rich samples compared to lower iron samples (Harmer et al., 2008). XPS studies showed that the iron $2p_{3/2}$ intensity decreased compared to that of zinc indicating that the Cu^{2+} replaced iron preferentially

over zinc which enhances copper activation and thus collector attachment to sphalerite (Harmer et al., 2008).

Sphalerite with high iron content generally has a higher lead content and the presence of Pb^{2+} in the sphalerite lattice or adsorbed on the surface from solution can activate sphalerite and promote flotation by reacting with xanthate (Basilio et al., 1996; Sui et al., 1999; Morey et al., 2001; Rashchi et al., 2002). It has been suggested that lead can substitute for zinc (and react with xanthate) in the sphalerite lattice only under acidic conditions and that from pH 7-10 lead forms a $Zn-O-Pb^+$ species on the surface through adsorption of $Pb(OH)^+$ which also reacts with the xanthate. Above pH 10 lead hydroxide precipitates dominate, rendering the surface hydrophilic thus depressing flotation (Rashchi et al., 2002). The mechanism of lead activation of sphalerite remains poorly understood (Chandra & Gerson, 2009).

Gangue minerals may also be affected by the quantities of copper and xanthate present and misreport to the concentrate. Silicate gangue minerals primarily misreport through entrainment (when no reagents are present) and a combination of entrainment and aggregation (with sphalerite particles) when copper and xanthate are added (Duarte & Grano, 2007). In an unpublished report, Hart & Dimov (2011), investigated a significant increase in gangue recovery in the Highland Valley copper concentrator. Using the TOF-SIMS, they identified significantly higher copper contents (and collector) on the surface of silicate grains reporting to the concentrate relative to the tails. In this operation gangue silicates float in response to copper activation and collector attachment.

1.8 $ZnSO_4$

The flotation separation of polymetallic (lead-zinc, copper-zinc and copper-lead-zinc) ores generally involves several steps. The first step, generally a copper/lead float, recovers copper and lead sulphide minerals into a bulk concentrate from an alkaline pulp. The zinc sulphides (typically sphalerite) which report to the tails, are then recovered from the remaining gangue phases in a second downstream flotation circuit.

In froth flotation there are two mechanisms which may contribute to grain department into the froth phase; genuine flotation and mechanical entrainment (Cao & Liu, 2006). During grinding and the copper/lead flotation process, dissolution and/or oxidation of chalcopyrite and galena can contribute to the presence of copper and lead ions in the pulp. The copper and lead ions can be transferred to the surface of sphalerite resulting in inadvertent activation, promoting collector attachment and flotation recovery (Finkelstein, 1997; Seke & Pistorius, 2005). In order to inhibit recovery of the sphalerite to the copper/lead concentrates, reagents are added to the pulp to depress (inhibit) sphalerite recovery.

Zinc sulphate is a well-known selective depressant for sphalerite during the flotation of complex Cu-Pb-Zn sulphide ores (Clarke et al., 1995; El-Shall et al., 2000; Pearse, 2005; Cao & Liu, 2006; Bulatovic, 2007). Zinc sulphate inhibits sphalerite flotation by replacing zinc for the attached activating copper ions. The depression mechanism is believed to be related to the development of hydrophilic coatings of zinc hydroxyl species on sphalerite surfaces (Fuerstenau, 1985; Cao & Liu, 2006; Bulatovic, 2007). The best depression results are seen in pulps of pH 8-10. In this pH range zinc cations undergo hydrolysis reactions forming zinc hydroxyl and zinc hydroxide species (Cao & Liu, 2006). These species are very surface active and either adsorb (zinc hydroxyl) or precipitate (zinc hydroxide) on the sphalerite surface (Fuerstenau & Palmer, 1976; Laskowski et al., 1997).

If the particles are sufficiently small they can still enter the froth phase by mechanical entrainment. However, Cao & Liu, (2006) observed that zinc sulphate (in the absence of xanthate) induced coagulation of fine sphalerite particles and such coagulation significantly reduced the mechanical entrainment of the fine sphalerite.

Cao & Liu, (2006) have termed zinc sulphate a “dual function” selective flotation depressant due to its ability to make mineral surface hydrophilic, which reduces genuine flotation, as well as its ability to coagulate the mineral, which reduces mechanical entrainment (Cao & Liu, 2006).

1.9 Objectives of the Study

This work will examine the surface chemical effects on sphalerite in response to zinc sulphate addition in flotation testing scenarios designed to evaluate changes in zinc recovery. The laboratory test results will be compared to surface chemical data collected from plant samples toward potentially identifying the mechanism of sphalerite depression. Bench test results will examine the effect of copper sulphate and copper sulphate plus zinc sulphate on the surface of sphalerite to better understand what is taking place during flotation separation. The following analytical techniques will be employed;

- XRD will be used to determine the mineralogy of the samples.
- TOF-SIMS will be used to compare the surface chemistry of sphalerite grains collected from the LaRonde copper/lead and zinc concentrator circuit and laboratory flotation tests performed with the LaRonde ore and at the same conditions as those identified in the concentrator.
- XPS analyses of sphalerite grains from a series of simple bench conditioning tests will be used to examine the effect of zinc sulphate on sphalerite surfaces in a mineral pulp. Combining TOF-SIMS and XPS analyses will potentially provide insight into the sphalerite depression mechanism.

Chapter 2

2 Sample Collection and Methodology

The following section outlines the method of sample collection and the techniques used for sample analyses.

2.1 Sample Collection

2.1.1 Copper flotation circuit at LaRonde

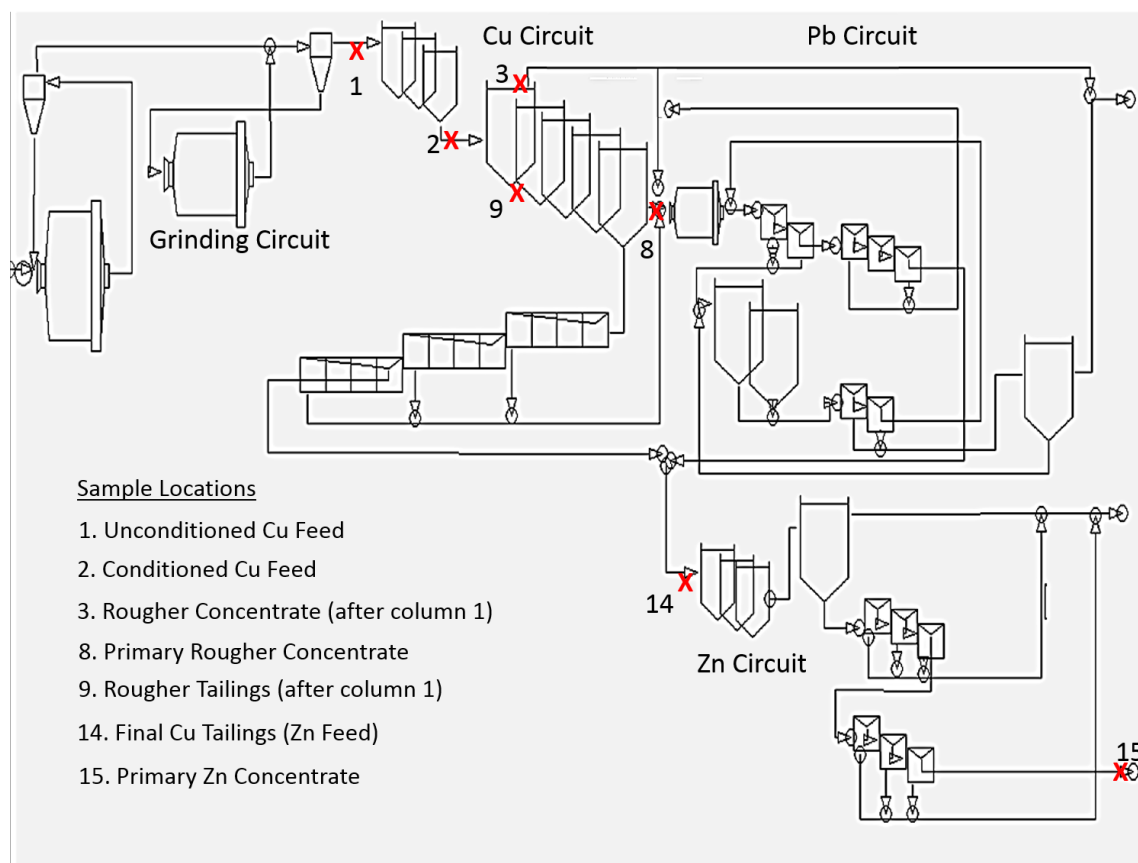


Figure 2-1 Flowsheet of the copper flotation circuit at LaRonde with sample collection locations.

Fifteen samples were collected from the LaRonde mill but only seven were used for this study (Figure 2–1 and Table 2–1). Sample 1 is the baseline for comparison with the other samples. Sample 2 was used to observe the result of the conditioning phase of the process. Samples 3 and 9 were analyzed to compare the con and tail after the first

flotation column of the copper circuit. Sample 8 was chosen because it allows for the comparison of initial flotation column to the cumulative copper flotation concentrate. Samples 14 and 15 were selected to demonstrate the changes that take place during the zinc circuit.

Table 2-1 LaRonde Cu/Pb and Zn flotation circuit sample locations and descriptions.

Collection Points	Description	Circuit	ToF Analysis
LR1	Ball mill discharge	Cu/Pb	Yes
LR2	Conditioning discharge	Cu/Pb	Yes
LR3	Rougher concentrate 1	Cu/Pb	Yes
LR4	Rougher concentrate 2	Cu/Pb	No
LR5	Rougher concentrate 3	Cu/Pb	No
LR6	Rougher concentrate 4	Cu/Pb	No
LR7	Rougher concentrate 5	Cu/Pb	No
LR8	Rougher combined concentrate (2-4)	Cu/Pb	Yes
LR9	Rougher concentrate 1 tail	Cu/Pb	Yes
LR10	Global rougher tail reject	Cu/Pb	No
LR11	did not collect due to regrind maintenance	Cu/Pb	No
LR12	did not collect due to regrind maintenance	Cu/Pb	No
LR13	Final Cu/Pb con	Cu/Pb	No
LR14	Final Reject Cu/Pb (Tail); Feed to Zn circuit	Cu/Pb	Yes
LR15	Primary Zinc Con	Zn	Yes

2.1.2 Duplication of plant operational parameters in the laboratory

For the instrumented mill test, approximately ½ tonne of feed ore from the LaRonde mill was collected during the sampling campaign as discussed above. The feed ore from the mill was homogenized and split into 50 kg lots, sealed and frozen. From a single lot, 2.8 kg charges were separated for the instrumented mill laboratory study. Before the ore was added, the ball mill and the steel balls were cleaned by running the mill with silica sand and water for thirty minutes. Once the ore (2.8 kg) and demineralized water (2.8 L) were added to the clean ball mill, the pH is adjusted to 9.8-10 by adding sodium hydroxide. Dissolved oxygen was kept low by manually adjusting nitrogen gas flow throughout the

process. The temperature is maintained at $\sim 32^{\circ}\text{C}$. Following milling the samples were conditioned for six minutes during which all reagents were added including MIBC (methyl isobutyl carbinol), 3418A (sodium di-isobutyl dithiophosphate), copper sulphate and zinc sulphate.

Samples were periodically collected at 0, 10, 20 and 30 min (ball mill discharge or final grind) from the ball mill via an exit hose. The hose was rinsed with demineralized water to prevent contamination of the next sample. The samples were collected in 50 mL Falcon tubes, sealed and frozen using dry ice to minimized oxidation of the sample surface.



Figure 2-2 Example of the “Denver” flotation equipment used in the testing.

After grinding, the remaining mill sample was transferred to the flotation unit (Figure 2–2) where it was aerated and conditioned for 6 minutes using various (test dependent) reagents listed in Table 2–2. Samples were taken at this point. The pH was measured using a pH meter and maintained at 9.8-10 throughout the process using sodium hydroxide. The frother used for all tests was 0.1% solution of MIBC. Samples (concentrates – Con) were then taken by manually skimming the froth from the surface of the flotation unit into a collection tray and transferred to 50 mL Falcon tubes which were then frozen in dry ice (to prevent oxidation). The collection tray was rinsed with

demineralized water between samples. Flotation times for Con 1 and Con 2 were 30 seconds each. Con 3 and Con 4 were both floated for 1 minute and Con 5 for 3 minutes. Between flotation tails C3/C4 and C5 the streams were conditioned for 1 minute. The flotation scheme including sampling locations is given in Figure 2–3.

Table 2-2 Received samples, sample locations, test parameters and analysis performed and reported on in the thesis.

Run	Sample	Test sample	TOF-SIMS
F-194-B	Ball Mill Discharge	Std with 3418A	Yes
F-194-B	C1-2	Std with 3418A	Yes
F-194-B	C3-5	Std with 3418A	No
F-194-B	REJECT	Std with 3418A	Yes
F-195-B	Ball Mill Discharge	Std + Cu ²⁺ @ 5 ppm	No
F-195-B	C1-2	Std + Cu ²⁺ @ 5 ppm	Yes
F-195-B	C3-5	Std + Cu ²⁺ @ 5 ppm	No
F-195-B	REJECT	Std + Cu ²⁺ @ 5 ppm	Yes
F-196-B	Ball Mill Discharge	Std + ZnSO ₄ 25g/t + Cu ²⁺ @ 5 ppm	No
F-196-B	C1-2	Std + ZnSO ₄ 25g/t + Cu ²⁺ @ 5 ppm	Yes
F-196-B	C3-5	Std + ZnSO ₄ 25g/t + Cu ²⁺ @ 5 ppm	No
F-196-B	REJECT	Std + ZnSO ₄ 25g/t + Cu ²⁺ @ 5 ppm	Yes

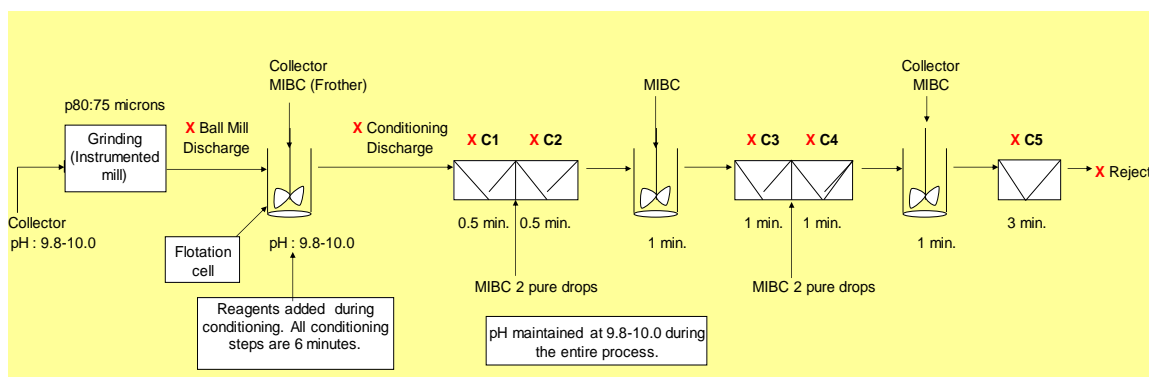


Figure 2-3 Flotation scheme and parameters for the instrumented mill/flotation test. The red X marks the sampling locations.

2.1.3 ZnSO₄ bench tests

Pristine samples of (low iron) sphalerite (from Balmat, N.Y.), chalcopyrite (unknown origin) and pyrite (from Zacatecas, Mexico) were ground and sieved to a grain size of 180-300 μ m. Two grams of each mineral were mixed (~six grams total) in four separate flasks. Reagents used for conditioning were as follows: i) de-ionized water; ii) 5ppm solution of CuSO₄ in de-ionized water (mill concentration); iii) 5ppm solution of CuSO₄ with 25mg/L of ZnSO₄ in de-ionized water (mill concentration); iv) 25mg/L solution of ZnSO₄ in de-ionized water (mill concentration). The reagent pH was adjusted to pH 9.8-10 using CaOH. Reagents were then added to the mineral samples and conditioned for 15 minutes on a shaker table. After the conditioning, each sample was split (~ in half) and frozen by immersion in liquid nitrogen (to prevent oxidation). One split of each sample was analyzed using XPS. The results from this experiment were compared to the data from the first two data sets.

2.2 Analytical techniques

2.2.1 XRD

Seven LaRonde ore samples were ground to a fine powder using a mortar and pestle. Each sample was then made into a paste using ethanol to be more easily mounted on a clean XRD slide. The analyses were performed on a Rigaku rotating-anode X-Ray Diffractometer. The diffractometer employs CoK α radiation, and monochromation is achieved using a curved crystal, diffracted beam, graphite monochromator. The instrument was operated at 45kV and 160mA, using the normal scan rate of 10 $^{\circ}$ 2 θ per minute (equivalent to 0.5 $^{\circ}$ 2 θ on conventional diffractometers). X-rays were collimated using 1 $^{\circ}$ divergent and scatter slits, and a 0.15mm receiving slit. Sample scans were completed from 2 to 82 $^{\circ}$ 2 θ , at a rate of 10 $^{\circ}$ per minute. EVA software (version 16.0) (Bruker-AXS 1996-2010) was utilized for phase identification and peak analysis. Approximate percentages of each mineral present are calculated by summing the most intense diffraction peak for each mineral and dividing by the total intensity. These approximate percentages are included on each plot (See Appendix A) to show an increase or decrease relative to the other minerals with progression through the milling process.

XRD is a versatile, non-destructive technique that reveals detailed information about the mineral phases present and crystallographic structure of natural and manufactured materials by measuring the average distance between layers or rows of atoms called d-spacings. When a monochromatic X-ray beam with wavelength (λ) is projected onto a powdered crystalline material at an angle (θ_1), and certain conditions are met to satisfy Bragg's Law ($n\lambda=2d\sin\theta$) diffracted rays are detected at another angle (θ_2). Since $\theta_1+\theta_2=2\theta$, by varying the angle (θ_1), the Bragg's Law conditions are satisfied by different d-spacings in polycrystalline materials at a different diffracted angle (θ_2) maintaining the 2θ . The resulting diffraction patterns are characteristic and can be used to identify the crystalline materials (Klein 2002).

2.2.2 TOF-SIMS

The instrument used in this work is an ION-TOF, TOF SIMS IVTM secondary ion mass spectrometer. This technique allows for the analysis of the outermost 1-3 atomic layers of a surface by mass spectrometry. A $^{209}\text{Bi}_3^+$ (Bismuth) primary ion beam is rastered across an area of interest on the sample surface. The raster size used was ~300 microns with an acquisition time of 125 scans. The bombardment of the surface with the bismuth primary ion beam induces the emission of positively and negatively charged secondary ions from the sample surface. These secondary ions are extracted from the sample surface and mass analysed using a time-of-flight mass spectrometer. A plot of secondary ion intensity *versus* mass produces a mass spectrum, with an ideal resolution of 4000 above 200 atomic mass units (amu) for these types of samples. TOF-SIMS can detect species with concentrations in the ppm-ppb range. The data were recorded with full mass spectra in 256x256 pixel format using a high current bunched mode $^{209}\text{Bi}_3^+$ cluster ion beam and the following beam conditions for mass and spatial resolution:

- Ion source: 25 keV, ion beam; cluster of 3 Bi^+ ions
- Current: ~0.3 pA
- Pulse: 1 ns
- Beam spot size: ~ 1 μm
- Raster area: generally 300 x 300 μm (variable)
- Mass range: 1-850 amu
- Mass resolution: 4,000

Sample charging was neutralized with an electron flood gun

Mineral recognition technique, essential to the statistical analyses is illustrated in Figure 2–4. The figure shows a typical spectrum in the region of 62.5 to 66.5 amu identifying the peaks for Cu and Zn (both isotopes). Individual phase recognition in a multi-mineral mixture is accomplished by scanning for regions of high ion yield peculiar to a selected mineral phase; a map for Zn identifying sphalerite is given in the inset of Figure 2–4. Regions of interest (ROI) identified by the particular element or specie of interest are then mapped and mass spectra collected for ROI's representing each mineral phase. Statistical analysis is performed on phase specific spectra after normalization to total ion yield and area. The technique used in this manner is not quantifiable however comparative species analyses between ROI's can provide valuable information regarding factors driving grain partitioning.

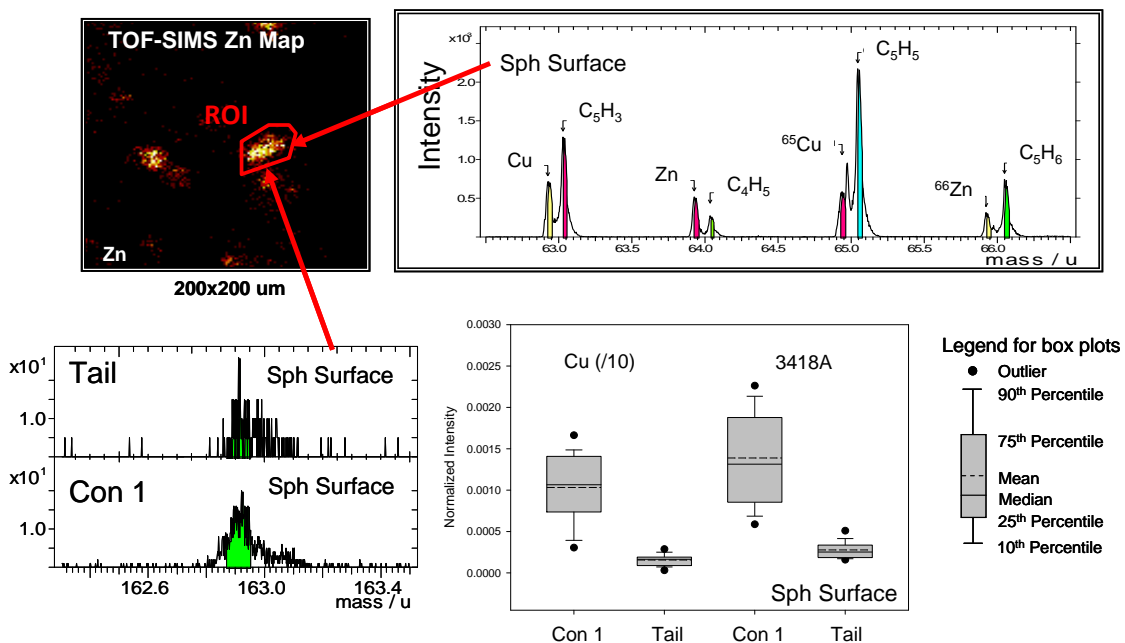


Figure 2-4 (Clockwise starting top left) TOF-SIMS Zn map showing a region of interest (ROI), spectra showing the mass positions for Cu and Zn isotopes in the region of 64.5-66.5 amu, spectra showing Cu on the surface of sphalerite, and a

vertical box plot comparing Cu and collector 3418A on the surface of sphalerite in the concentrate and tail.

For the TOF-SIMS analyses, a minimum of 30 ROI's, each representing an individual grain of the grains of interest, were examined for each of the samples. All TOF-SIMS data presented (counts) are normalized by the total ion intensity (counts of the recorded total mass spectrum) for the region of interest. The normalization technique accounts for variability in the ROI size and allows for cross grain comparison. For the comparative analysis the normalized intensity data are plotted in vertical box plots and illustrate relative changes in surface specie abundance for the mineral grain examined in the sample. The discussion refers to a relative increase or decrease in measured specie intensity between grains in the samples. Relative differences are based on the **median values** indicated in the figures. In the vertical box plots, the median is plotted as the solid line across the box whereas the mean is plotted as the dashed line. An illustration of a box plot showing the various components is given above (Figure 2- 4).

2.2.3 XPS

The methodology used for this work follows that of Biesinger et al (2007). Each bench test sample was thawed, pressed into indium foil and transferred to the introduction chamber of the X-Ray Photoelectron Spectrometer (XPS) with the mineral surfaces still wet, to prevent contact with air. Excess solution was removed by contact with the edge of a tissue. The remaining surface liquid was then pumped away in the vacuum. This wet introduction method helps to minimize surface contamination and in particular, it reduces adventitious carbon deposition by exposure to air. For the analyses of a pristine sphalerite grain a single grain of sphalerite was placed into a special sample holder, introduced into the instrument and fractured while under vacuum. The XPS analyses were carried out with a Kratos Axis Nova spectrometer using a monochromatic Al K α source (15 mA, 14 kV). The instrument work function was calibrated to give a binding energy (BE) of 83.96 eV for the Au 4f $_{7/2}$ line for metallic gold and the spectrometer dispersion was adjusted to give a BE of 932.62 eV for the Cu 2p $_{3/2}$ line of metallic copper. Binding energy accuracy is ± 0.025 eV. The Kratos charge neutralizer system was used on all specimens. Survey spectra were collected with a pass energy of 160 eV and an analysis area of ~ 300

by 700 μm . High-resolution spectra were obtained using either a 20 eV or 40 eV pass energy and an analysis area of ~ 300 by 700 μm . Spectra were analysed using CasaXPS software (version 2.3.14) (Fairley, 1999–2005) using relative sensitivity factors (R.S.F.) derived for the Kratos Axis Ultra and Kratos Axis Nova at Surface Science Western. Peak fitting parameters used to interpret the spectra were derived from X-ray Photoelectron Spectroscopy (XPS) Reference Pages by M. Biesinger (www.xpsfitting.com) along with the listed references and those provided in the literature.

The XPS probes the near-surface of solids and has the ability to obtain the elemental composition of a mineral surface, as well as determine the oxidation states and bonding partners of the constituent elements. This makes the technique very powerful in the study surface reactivity of minerals. Applied carefully, surface reactant species, intermediate and final products of reactions at mineral surfaces can be identified and their abundances and oxidation states determined.

Chapter 3

3 Results and Discussion

The following section provides the results from a particular analytical technique and a discussion regarding their interpretation of the data in the context of the testing scenario; either laboratory or mill sample analyses.

3.1 XRD results

The following discusses the results from the XRD analyses of selected samples collected from the LaRonde Cu/Pb and Zn flotation circuits (Figure 2–1). The XRD patterns are included in Appendix A. Figure 3–1 shows several stacked patterns from selected samples. The relevant mineralogical data provided by the XRD analyses are included in Table 3–1 which shows the semi-quantitative percentages of the raw data and the data normalized to 100% for each phase in each sample. The percentages of each mineral present are included to show the relative increase or decrease in the various samples.

The XRD analysis provides some information regarding the partitioning of the minerals to the various stream components of the flotation process. The information reflects the efficiency of the process and was used in conjunction with the surface chemical analyses to discuss the factors promoting the mineral partitioning. It should be pointed out that the proportion (%) of the mineral only reflects the proportion relative to the minerals identified in the XRD trace and is not equal to the actual percentage recovery of that phase in that particular sampling location.

The proportion of pyrite identified in the samples from the copper/lead flotation circuit (LR2-LR9) is relatively consistent ranging from 27-31%. The highest proportion was identified in the mill discharge sample (LR1) and the lowest in the primary zinc concentrate from the zinc flotation circuit (LR15). The proportion of chalcopyrite is relatively consistent ranging from 2-3% in the samples from the copper/lead circuit with the exception of sample LR8 (the primary rougher concentrate) where the proportion of chalcopyrite increases dramatically to 26%.

Table 3-1 Semi-quantitative XRD analysis of selected samples from the LaRonde Cu flotation circuit.

Sample	Pyrite (%)		Chalcopyrite (%)		Galena (%)		Sphalerite (%)		Quartz(%)		Anorthite (%)	
	Raw	Normalized	Raw	Normalized	Raw	Normalized	Raw	Normalized	Raw	Normalized	Raw	Normalized
LR1	60	36	5	3	4	3	15	9	76	46	6	4
LR2	31	29	4	3	2	2	12	11	52	49	6	6
LR3	49	31	4	3	3	2	18	12	74	47	9	6
LR8	59	30	52	26	25	13	23	12	35	18	3	2
LR9	48	27	4	2	5	3	37	21	77	43	8	5
LR14	51	28	3	2	3	2	33	18	85	47	7	4
LR15	15	16	3	3	1	1	62	67	9	10	2	2

The proportion of chalcopyrite in the mill discharge sample is 3% as well as in the primary zinc concentrate sample. The trend in the proportion of galena identified in the copper/lead circuit samples is identical to that of copper. The range is from 2-3% with the highest proportion, 13%, in sample LR8. The proportion of galena in the mill discharge sample is 3% and in the primary zinc concentrate sample is 1%. For the sulphides, the overall proportion of sphalerite is significantly higher in all samples with the exception of sample LR8. For the copper/lead circuit samples, the sphalerite proportion varied from 11-21% with the higher proportion found in the rougher concentrate tails and the feed to the zinc circuit (samples LR9 and LR14). The proportion of sphalerite in the mill discharge sample is 9% and in the primary zinc concentrate sample is 67%. Quartz, the dominant gangue phase identified shows variable recovery. The proportion of quartz in the discharge samples, LR2, LR3, LR9 and LR14 varies from 42-48%. Low proportions were identified in the combined rougher concentrate (LR8) and the final zinc concentrate (LR15). The proportion of anorthite (a minor gangue phase) ranges from 2-6%. The XRD data from the feed ore (sample LR1) identify the target metal sulphides chalcopyrite, pyrite, galena, sphalerite, along with dominant gangue minerals quartz and anorthite.

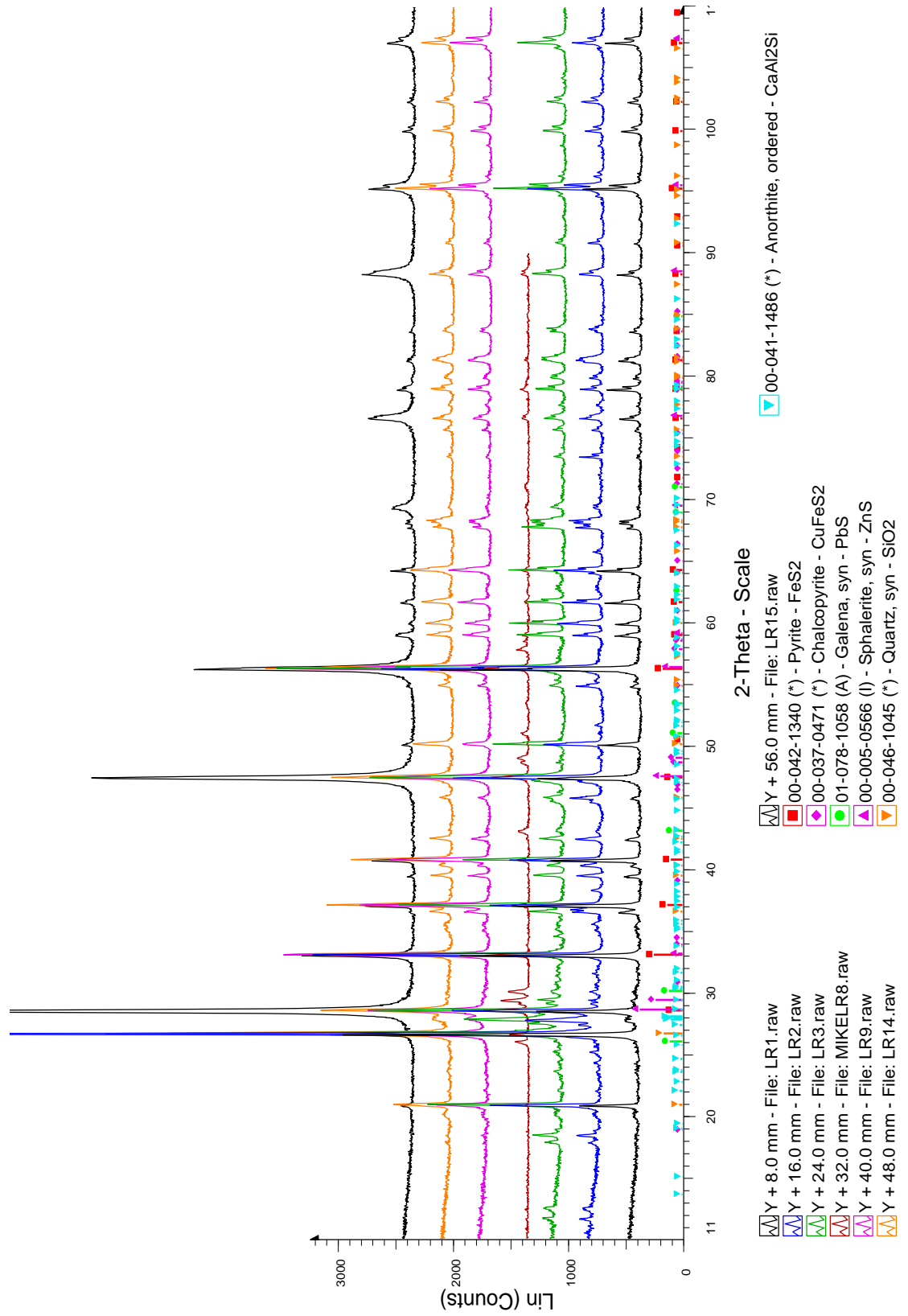


Figure 3-1 Stacked XRD spectra of samples from the LaRonde Cu flotation circuit.

The minerals willemite (Zn_2SiO_4), gibbsite ($\text{Al}(\text{OH})_3$) and/or wollastonite ($\text{Ca}_2\text{Si}_2\text{O}_6$) were potentially identified (weak intensities and overlapping peaks could not give 100% certainty of the presence of these minerals) in samples LR2 and LR3. However, their presence has been confirmed in the ore body and their inclusion in these samples is likely through entrainment.

3.1.1 XRD results discussion

Sample LR1 (baseline), LR2 (baseline after conditioning) and sample LR3 (rougher concentrate) have virtually identical proportions of chalcopyrite, galena and sphalerite which goes against the anticipated increase in chalcopyrite and galena accompanied by a decrease in sphalerite after rougher column 1 (Figure 3–2). This indicates that the flotation kinetics of chalcopyrite and galena, as well as the concurrent separation of sphalerite in the early part of the Cu circuit is slow.

The data indicate that sphalerite recovery early in the process (LR3), and later to the general concentrate (LR8), may be accomplished by inadvertent activation. The results for sample LR9 demonstrate that most of the sphalerite is being separated into the tailings accompanied by a very low percentage of chalcopyrite and galena. The presence of chalcopyrite and galena grains in the tail could be due to poor liberation; recovery is hampered by attachment to gangue phases. The results from samples LR14 (Zn Feed) and LR15 (Zn Con) verify that concentration of sphalerite is taking place.

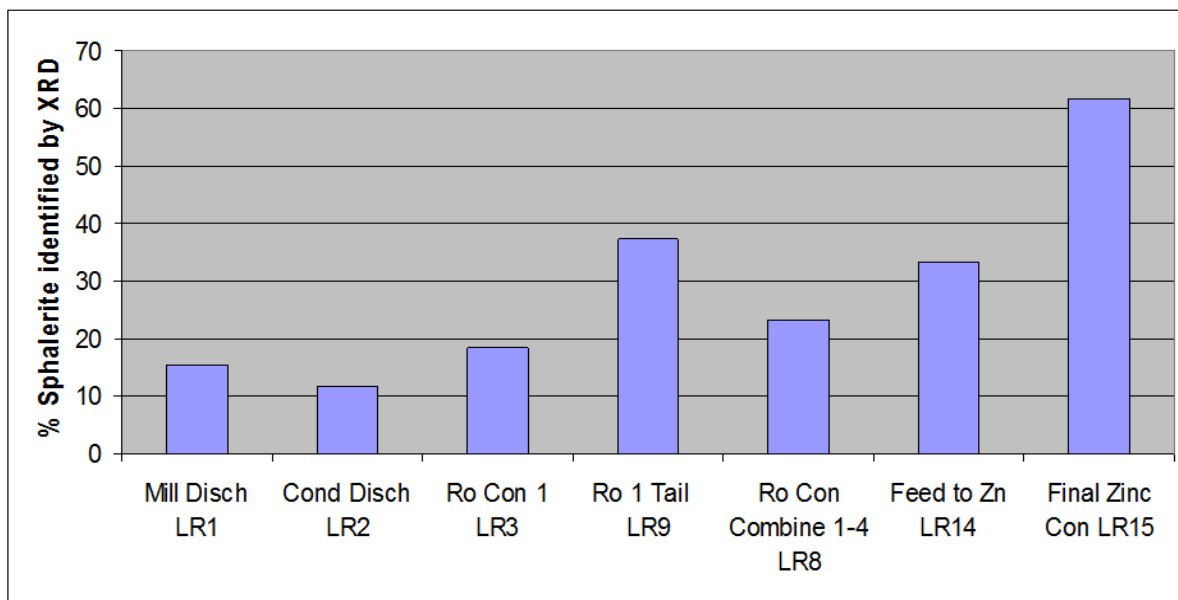


Figure 3-2 Histogram showing the percent sphalerite identified in the listed samples from the LaRonde flotation circuit.

3.2 TOF-SIMS results: LaRonde Mill Samples

The following discussion refers to the intensity variability of indicated elements as measured on the surface of sphalerite grains. The discussion uses the median value (solid line in the box plots – see legend in Figure 3–3) as a measure for comparison between samples. It should be noted that the box plots for Sample LR2 (CD) and Sample LR3 (CON 1) may not be statistically representative due to the limited number of sphalerite grains confidently identified and examined.

Table 3-2 Sample legend showing equivalent sample nomenclature from the LaRonde Mill and that used in the vertical box plots.

LaRonde Mill Sample	Sample Location	Box Plot Name
LR1	Ball mill discharge (Feed) before conditioning	FD
LR2	Conditioning Discharge	CD
LR3	Rougher concentrate from column 1	CON 1
LR8	Primary rougher concentrate	Gen Con
LR9	Rougher tail from column 1	Col 1 Tail
LR14	Cu/Pb circuit tail- feed for Zn circuit	Gen Tail
LR15	Primary Zn concentration	Zn Con

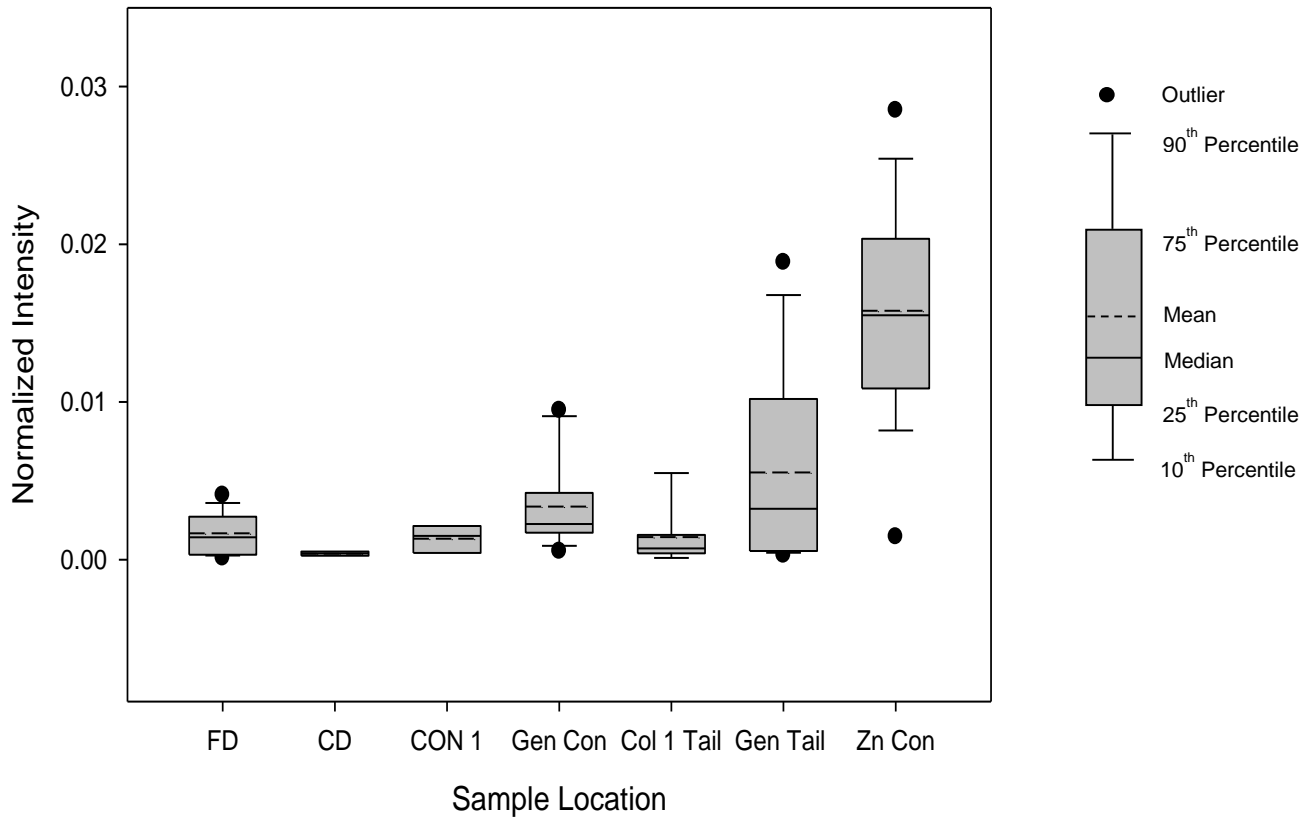


Figure 3-3 Vertical box plot of copper intensities on the surface of sphalerite grains. For sample location abbreviations refer to Table 3–2.

Copper values on the sphalerite surface are highest in the Gen Con (LR8), Gen Tail (LR14) and Zn Con (LR15) samples (Figure 3–3) and lowest in the CD (LR2) and Col 1 Tail (LR9). Copper intensities are discriminatory between con and tail samples from the copper/lead circuit (Figure 3–4).

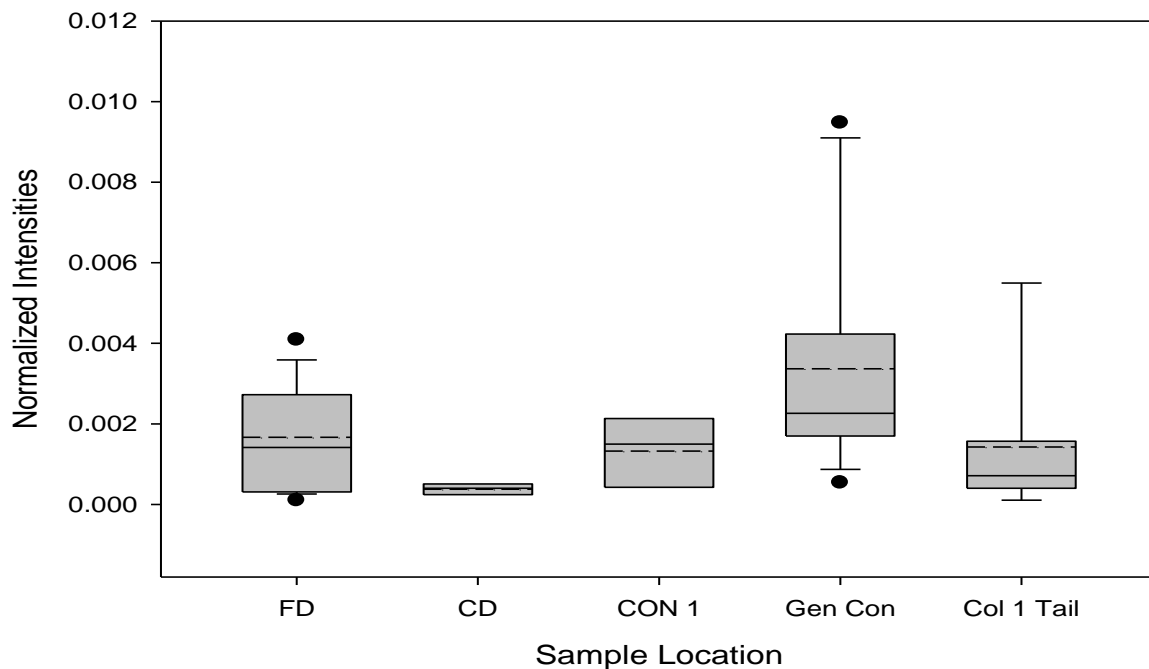


Figure 3-4 Vertical box plots of copper on sphalerite grains in the Cu/Pb circuit. For sample location abbreviations refer to Table 3–2.

Lead values on the sphalerite surface are highest immediately after grinding, in the Gen Con (LR8) and Zn Con (LR15) samples (Figure 3–5).

Lead intensities on the surface of sphalerite grains are not discriminatory between the Con 1 (LR3) and Col 1 Tail (LR9) samples (Figure 3–6). The lead intensity on the sphalerite grains in the Gen Con (LR8) are much higher than those observed on the surface of sphalerite in Con 1 (LR3) sample. The lead intensities in the Gen Tail (LR14) and Zn Con (LR15) are not as high as the Gen Con (LR8) but are still elevated.

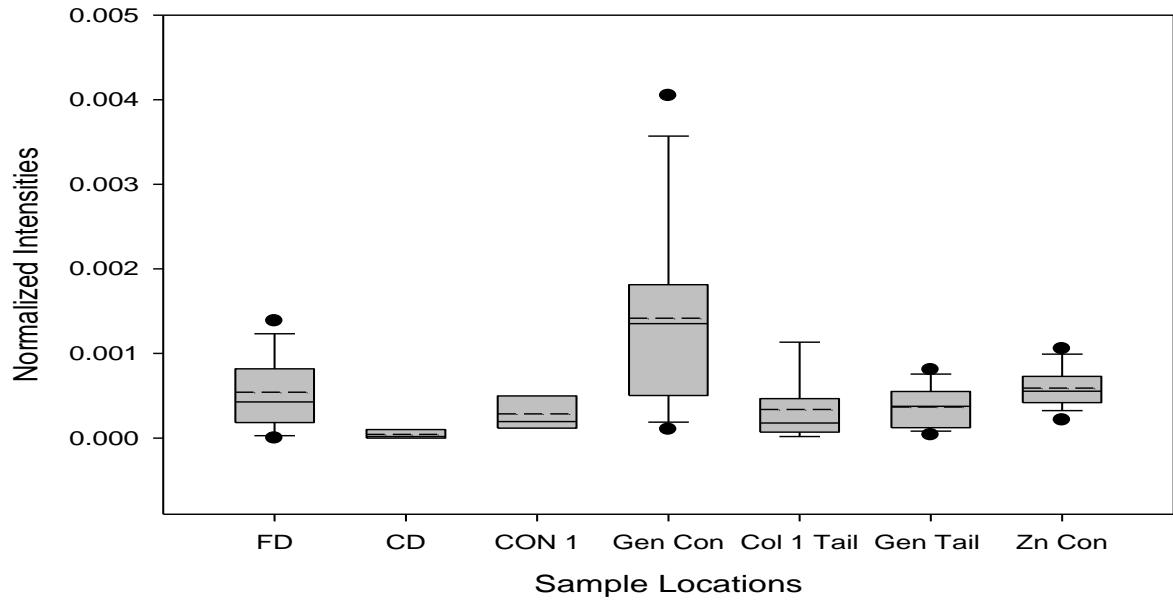


Figure 3-5 Vertical box plot of lead intensities on the surface of sphalerite grains. For sample location abbreviations refer to Table 3-2.

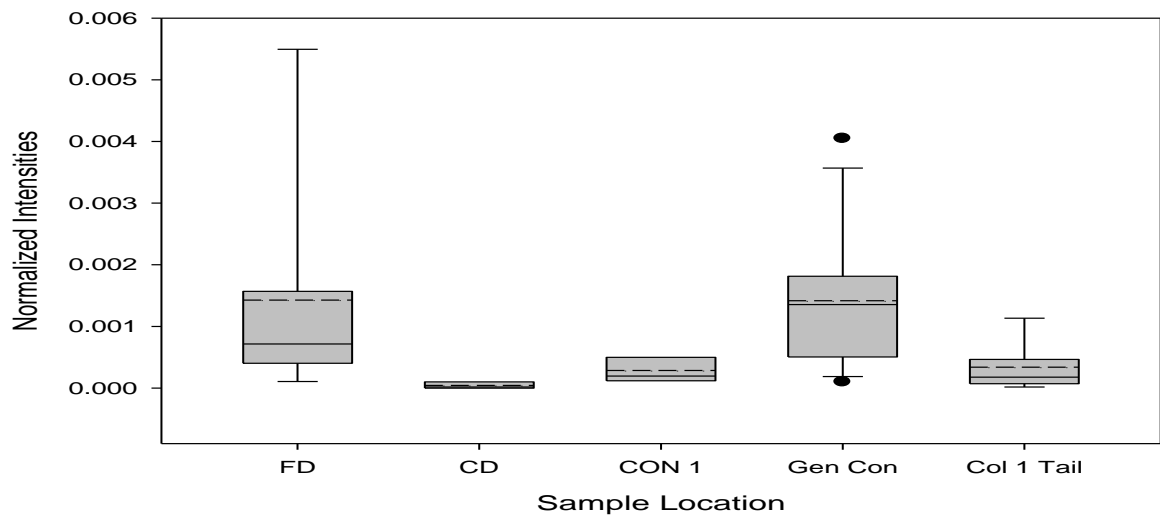


Figure 3-6 Vertical box plots of lead on sphalerite grains in the Cu/Pb circuit. For sample location abbreviations refer to Table 3-2.

3.2.1 TOF-SIMS results: LaRonde Mill Samples: Discussion

The sphalerite grains from the feed (LR1) have copper and lead intensities on their surface at similar levels to those from LR3 (rougher concentrate 1). This indicates that a significant proportion of the copper and lead is transferred to the sphalerite surface during grinding in the ball mill. The source of the copper and possibly the lead ions is from partial dissolution of chalcopyrite (or other copper minerals) and galena in the ore.

The data indicate that sphalerite grains reporting to the concentrate samples (LR3 and LR8) from the copper/lead circuit have significantly higher intensities of both copper and lead on their surfaces suggesting inadvertent activation and flotation likely in response to associated collector attachment (Figures 3–4 and 3–6).

The elevated intensities of copper and lead associated with sphalerite grains could also represent the analyses of a mixed mineral particle; where the copper and lead intensities represent that of associated mineral phases. Liberation analyses (not included) have shown that, at an 80% passing of 75 microns, more than 90% of the sulphide grains are liberated largely ruling out the possibility that the surface data represents that from mixed mineral grains (personal communication – Caroline Olsen).

It is noteworthy that in the copper/lead flotation, both copper and lead intensities are highest on the surface of sphalerite grains reporting to the Gen Con (LR8). This agrees with the suggestion that sphalerite is being activated by copper and lead.

Copper intensities on sphalerite surfaces are also very high in the general tail (LR14). As this sample represents the feed to the zinc flotation circuit, the high intensities reflect the use of re-cycled plant water from the zinc concentrate, upstream from the collection point LR14 in order to promote sphalerite recovery.

3.3 TOF-SIMS results: Instrumented Mill Tests

TOF-SIMS analyses were performed on sphalerite grains from the mill discharge sample, the first concentrate and reject samples from 3 tests: baseline (STD), copper sulphate (5ppm) and zinc sulphate (25ppm). The data revealed that copper transfer occurred under

all test conditions (Figure 3–7); higher copper intensities were recorded on the surface of sphalerite grains for all concentrate samples relative to the paired rejects. The greatest paired differences were noted for the baseline and the copper sulphate addition tests, where the intensity of copper on the sphalerite grains from both concentrates is very similar. The smallest paired difference, as well as the lowest copper intensity, was observed on grains from the zinc sulphate test.

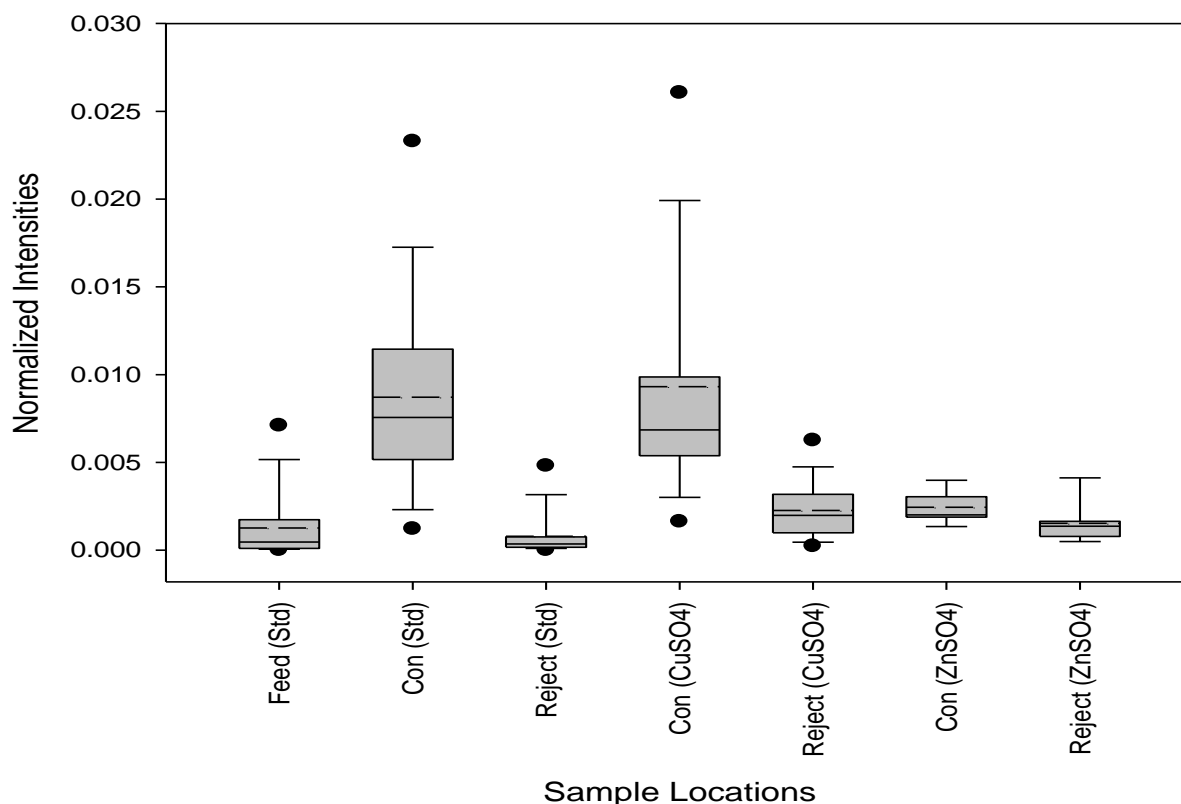


Figure 3-7 Vertical box plot of Cu on sphalerite grains from the instrumented mill test samples.

The zinc hydroxide intensities as measured on sphalerite surfaces from the three tests reveal the following: no discrimination for the concentrate/reject pair in the base line samples, elevated zinc hydroxide intensity on sphalerite surfaces but no discrimination between the concentrate/reject pair from the test with copper sulphate addition and

significant zinc hydroxide discrimination favouring the reject sample in the test with added zinc sulphate (Figure 3–8).

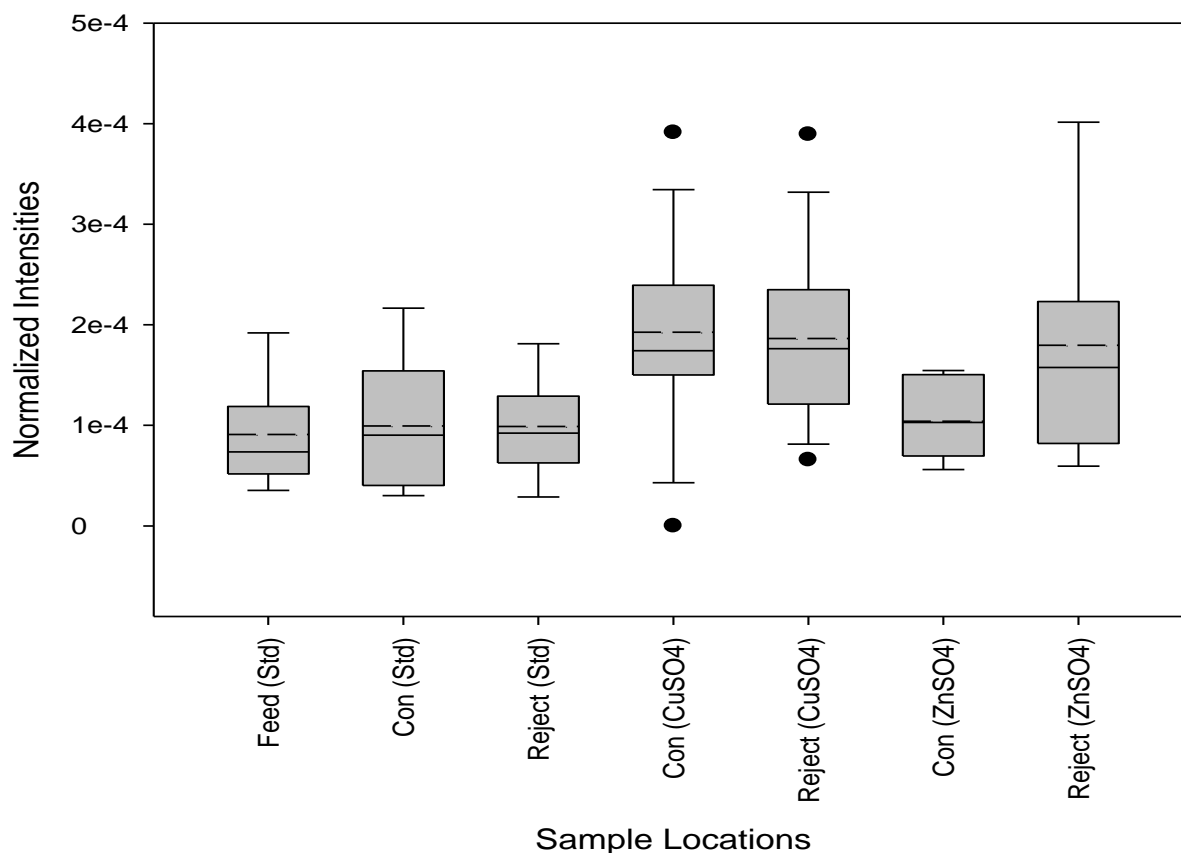


Figure 3-8 Vertical box plot of ZnOH on sphalerite grains from the instrumented mill test samples.

Similar to the distribution of zinc hydroxide on the surface of sphalerite grains, the measured sulphite intensities showed no discrimination between the concentrate/reject pair from the baseline test. In the test with copper sulphate addition there is intensity discrimination favouring the sphalerite grains from the concentrate relative to the reject where as in the test with zinc sulphate addition, the intensity discrimination is significant and favours grains from the reject sample (Figure 3–9).

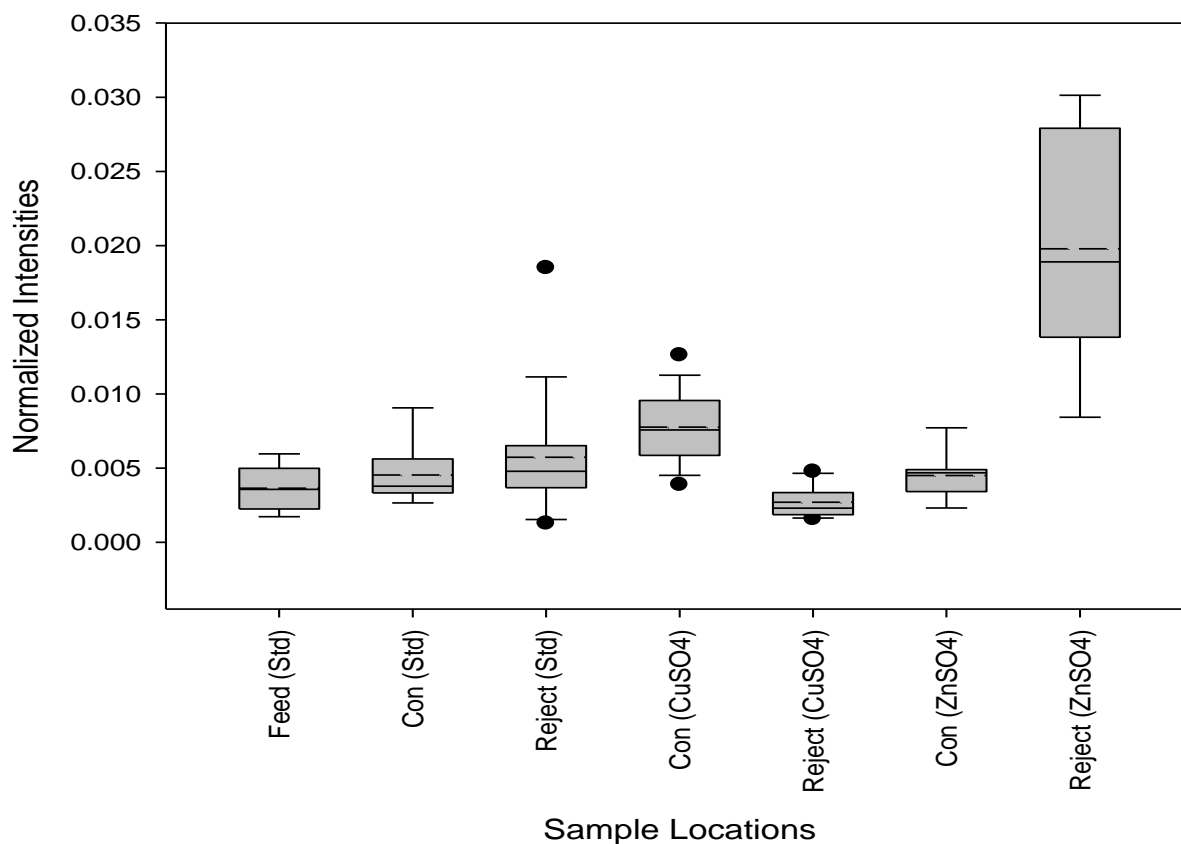


Figure 3-9 Vertical box plot of SO₃ on sphalerite grains from the instrumented mill test samples.

The distribution of the collector 3418A (Figure 3–10) on the surface of sphalerite grains is very similar to that of copper; elevated levels on the surface of grains from the concentrate samples. The greatest intensity was noted for grains from the test with copper sulphate addition followed by those from the baseline test. In both of these tests there is significant concentrate/tail discrimination. The collector intensity on concentrate sphalerite grains from the test with zinc sulphate addition, while elevated relative to the tail, is significantly less than that observed for the sphalerite grains from the baseline or copper sulphate addition tests. Furthermore, the collector intensity on sphalerite grains does not show pronounced concentrate/tail discrimination.

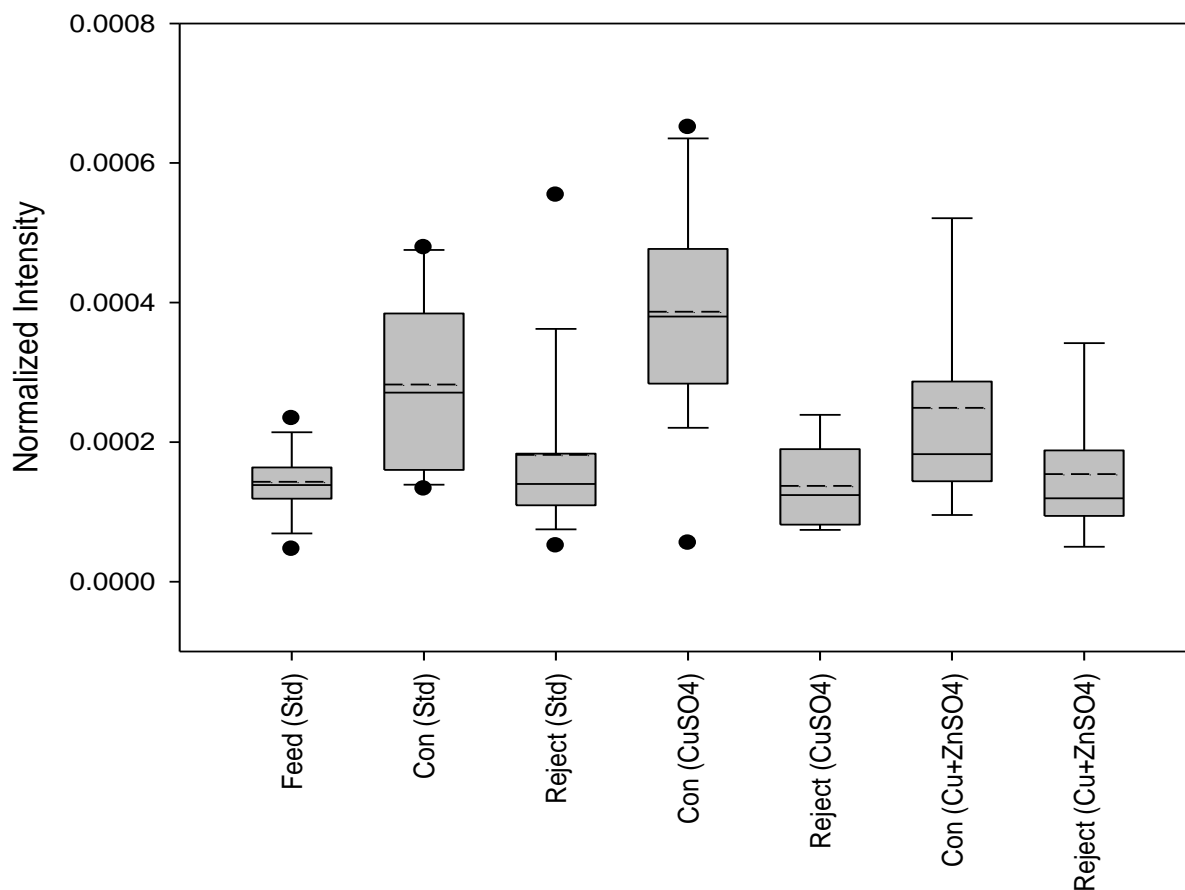


Figure 3-10 Vertical box plot of the collector 3418A on sphalerite grains from the instrumented mill test samples.

3.3.1 TOF-SIMS results: Instrumented Mill Tests: Discussion

The data from Figure 3–7 shows that all sphalerite grains in the concentrate samples had some degree of copper on their surface. The collector data indicates that sphalerite flotation was facilitated by collector attachment and, given that the copper intensity distribution in the samples correlate, it can be argued that copper is involved in inadvertent activation promoting collector attachment and flotation.

Zinc hydroxide on sphalerite surfaces has been implicated in inhibiting the adsorption of copper thereby depressing sphalerite flotation (Chandra and Gerson, 2009).

Concentrate/tail discrimination for zinc hydroxide was only identified on sphalerite surfaces in the samples from the zinc sulphate addition test. These same samples show the lowest intensity of surface copper on grains reporting to the concentrates and only a small intensity discrimination between the concentrate/tail pair. The data from the zinc sulphate test samples suggests that copper may be inhibited from attaching to the surface of the sphalerite grains thereby reducing recovery to the concentrate. The mechanism by which this is thought to occur will be presented in Chapter 4.

3.4 ZnSO₄ bench tests: XPS results

XPS survey spectrum of a fractured sphalerite surface is given in Figure 3–11. The sulphur survey spectrum shows sharp, clearly defined peaks for zinc and sulphur with small rounded indistinct peaks for iron (a naturally occurring substitute for zinc in the sphalerite lattice) and carbon (adventitious hydrocarbon contamination). The oxygen peak is almost non-existent, confirming the vacuum-fractured surface was not previously exposed to oxygen.

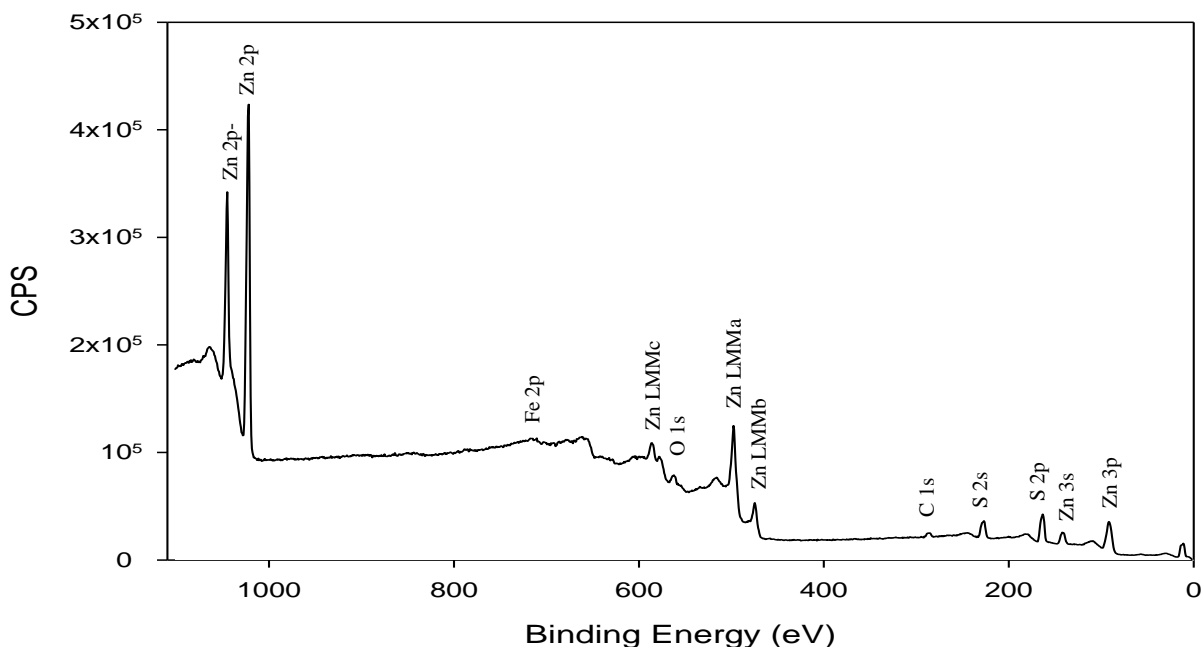


Figure 3-11 XPS survey spectrum of vacuum-fractured sphalerite surfaces.

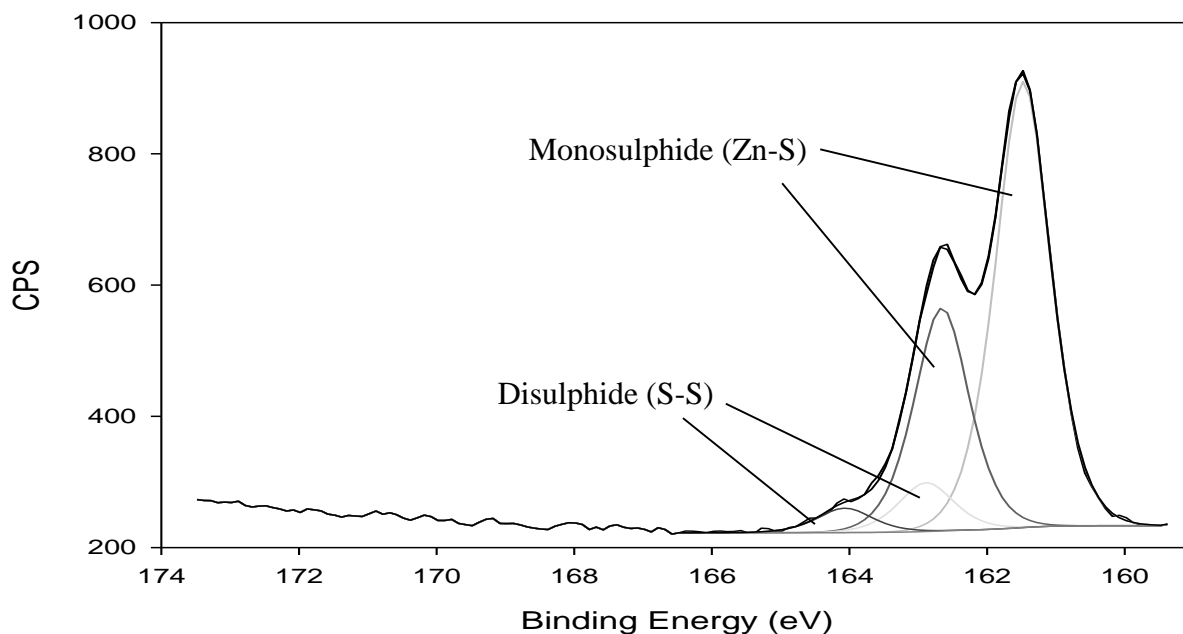


Figure 3-12 XPS high resolution S 2p peak of vacuum-fractured sphalerite surfaces.

The high resolution spectrum for S 2p (Figure 3–12) identified a doublet at 161.6 eV (the S^{2-} species or monosulphide) and a second doublet at 162.8 eV (a disulphide or metal deficient sulphide).

The survey spectra of the sphalerite grains from the de-ionized water test show that there is copper on the surface of the sphalerite grains (Figure 3–13). The atomic percentages (At%) of copper from these spectra range from 1.9-4.9%, (Table 3–3). The oxygen and carbon peaks have also become more pronounced than the vacuum-fractured sphalerite spectra.

Table 3-3 Range, median and average concentration of Cu as measured on the surface of sphalerite grains by XPS.

Test	Range (%)	Median (%)	Average (%)
De-ionized Water	1.9-4.9	2.5	3.1
CuSO ₄	1.8-2.5	2.2	2.2
ZnSO ₄	1.7-3.4	2.6	3
CuSO ₄ + ZnSO ₄	1.8-3.1	2.7	2.5

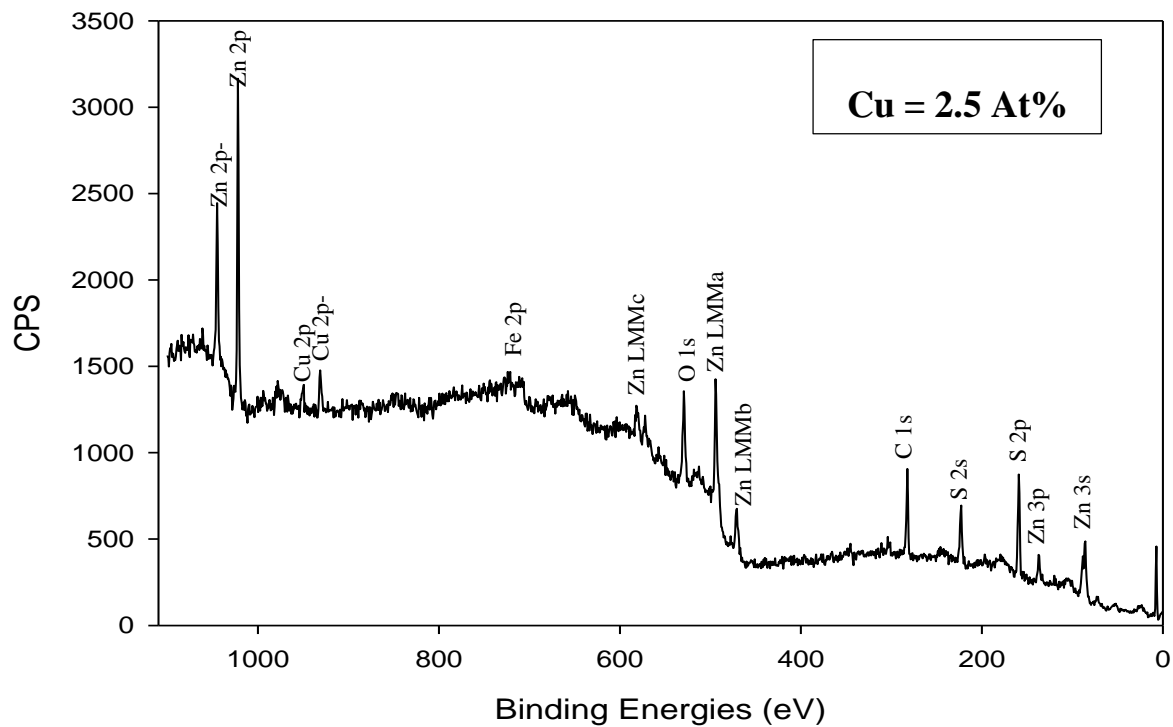


Figure 3-13 XPS survey spectra of sphalerite surfaces in de-ionized water.

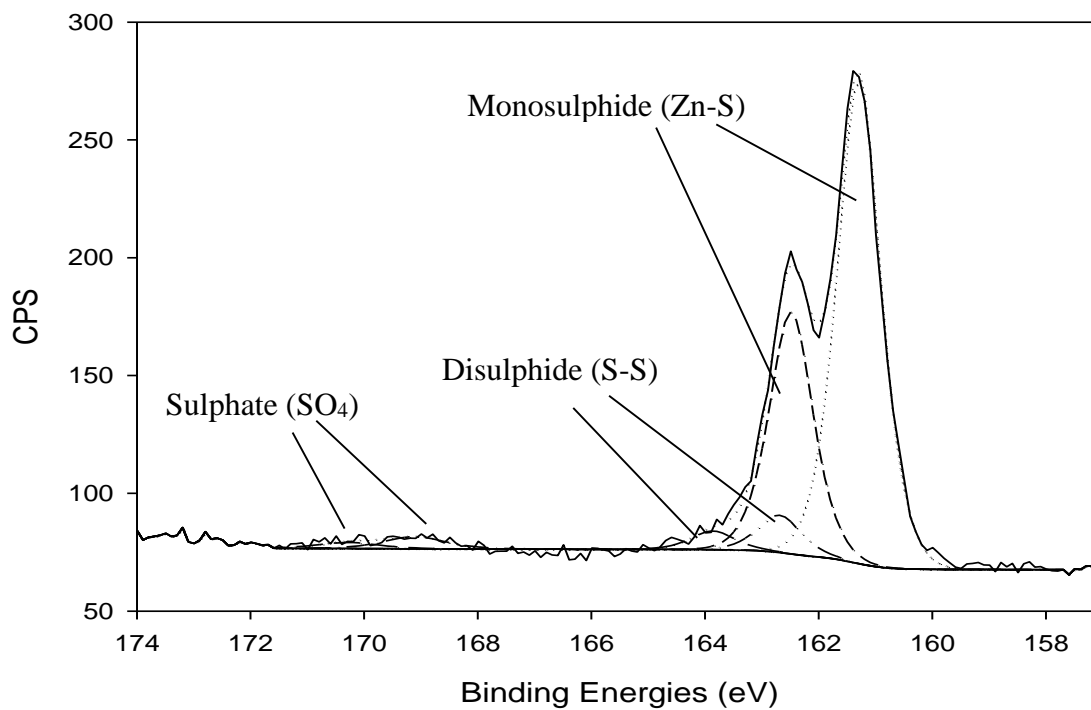


Figure 3-14 XPS high resolution S 2p peak of sphalerite surfaces in de-ionized water.

The high resolution S 2p spectra of the sphalerite surfaces from the de-ionized water test show, similar to the fractured sample, a doublet at 161.6 eV (the S^{2-} species or monosulphide) a second doublet at 162.8 eV (a disulphide or metal deficient sulphide) along with a broad band at 168eV indicating the presence of sulphates (Figure 3–14).

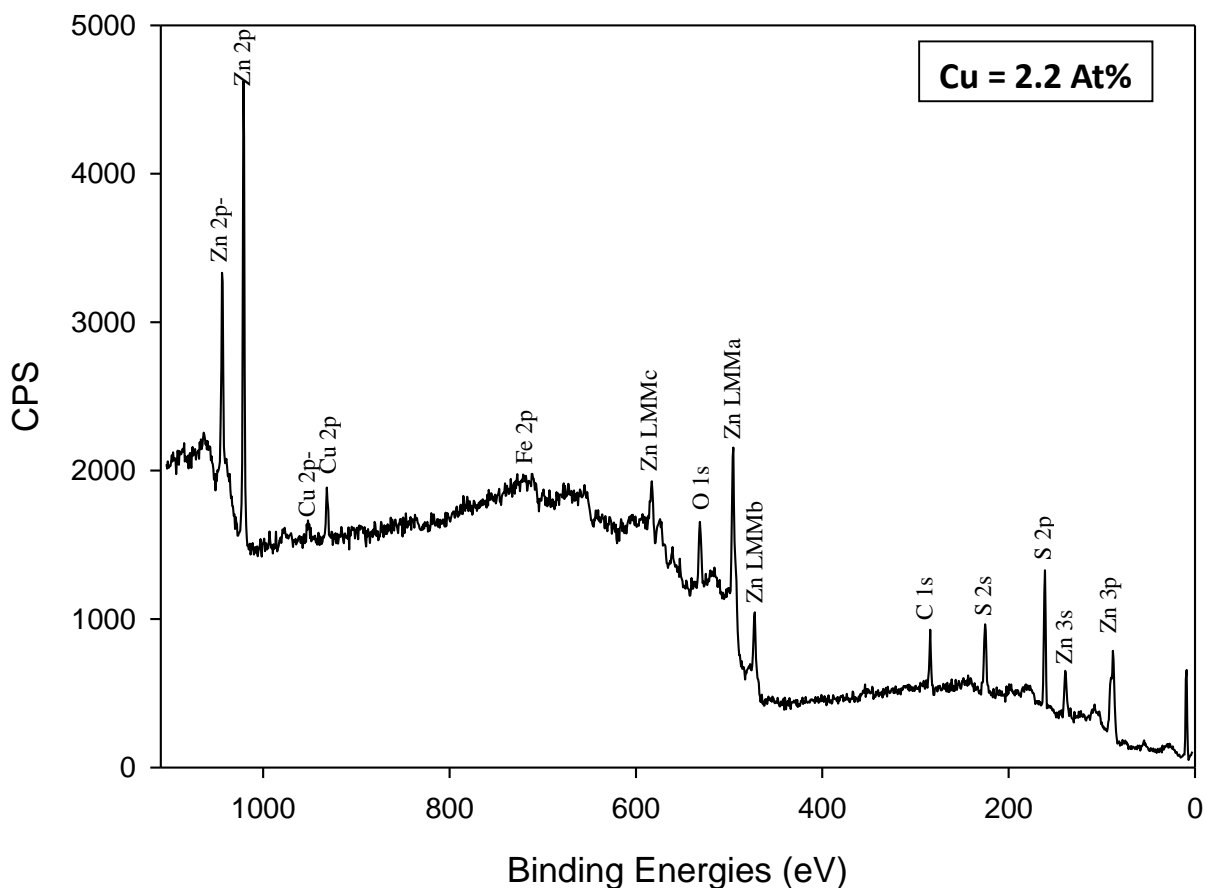


Figure 3-15 XPS survey spectra of sphalerite surfaces in de-ionized water with 5 ppm $CuSO_4$.

The survey spectra of the sphalerite grains from the de-ionized H_2O + 5 ppm $CuSO_4$ test (Figure 3-15) show that there is copper on the surface of the sphalerite grains. The At% of copper from these spectra range from 2.1-2.6% with a median of 2.2%, (Table 3–3).

The proportion of copper on the sphalerite surface in this test is similar to but slightly less than that from the de-ionized water test (Figure 3–13).

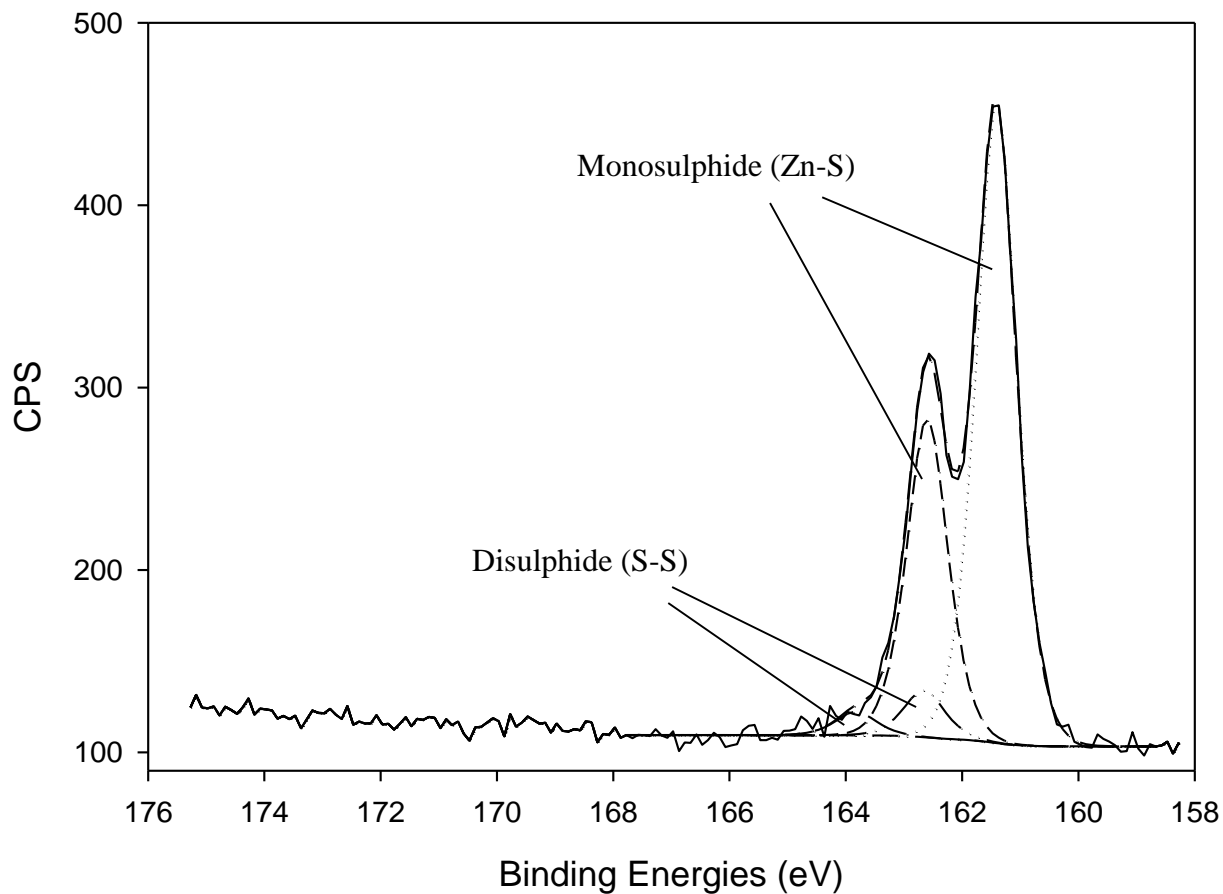


Figure 3-16 XPS high resolution S 2p spectra of sphalerite surfaces in de-ionized water with 5 ppm of CuSO₄.

The high resolution S 2p spectra of the sphalerite surfaces from the de-ionized H₂O + 5 ppm CuSO₄ identified a doublet at 161.6 eV (the S²⁻ species or monosulphide) and a second doublet at 162.8 eV (a disulphide or metal deficient sulphide). Curiously, a weak broad band at 168 eV (sulphate) was only observed on one of the grains examined and not on the grain shown in Figure 3-16.

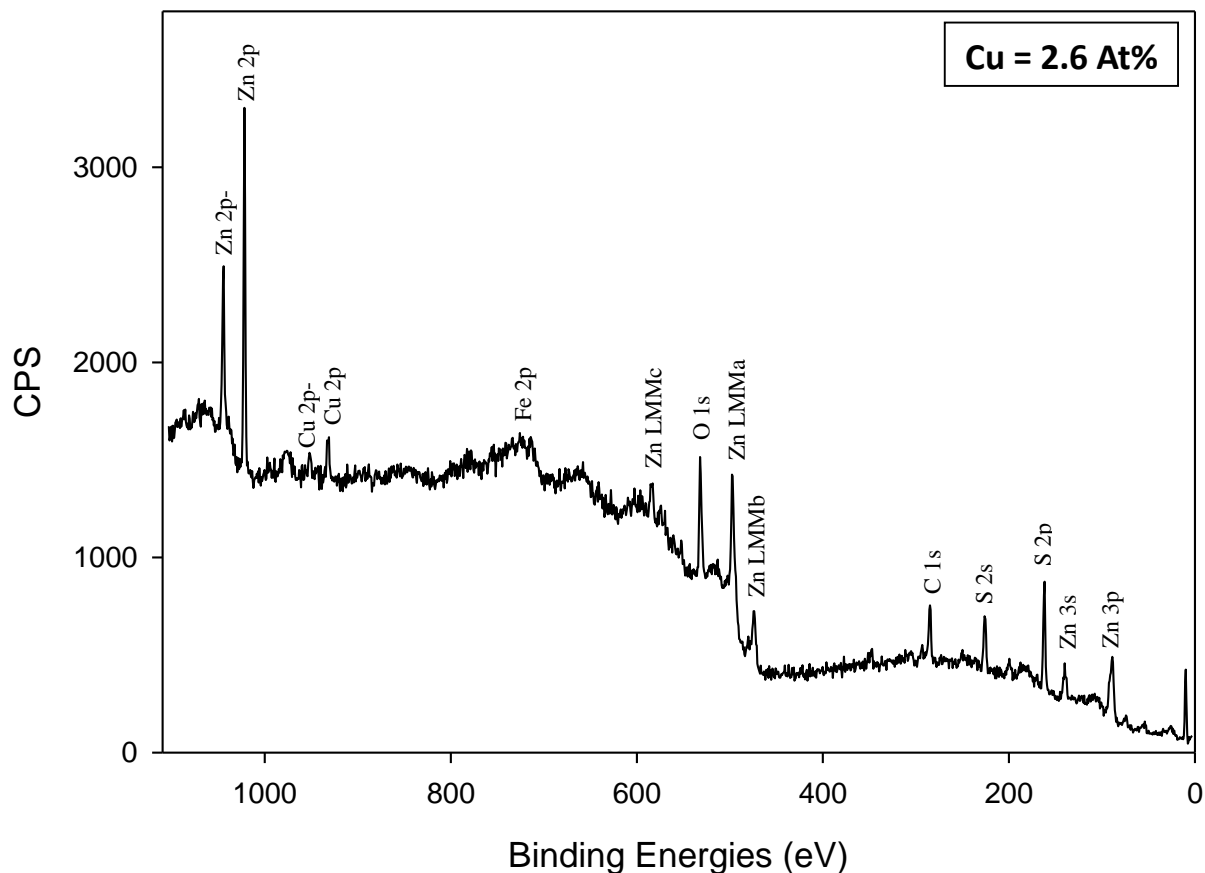


Figure 3-17 XPS survey spectra of sphalerite surfaces in de-ionized water with 25 ppm of ZnSO₄.

The survey spectra of the sphalerite grains from the de-ionized H₂O + 25 ppm ZnSO₄ test (Figure 3–17) show that there is an addition of copper to the surface of the sphalerite grains. The At% of copper in these spectra range from 1.7-3.4%, (Table 3–3). The proportion of copper on the sphalerite surface in this test is very similar to the de-ionized water test (Figure 3–13).

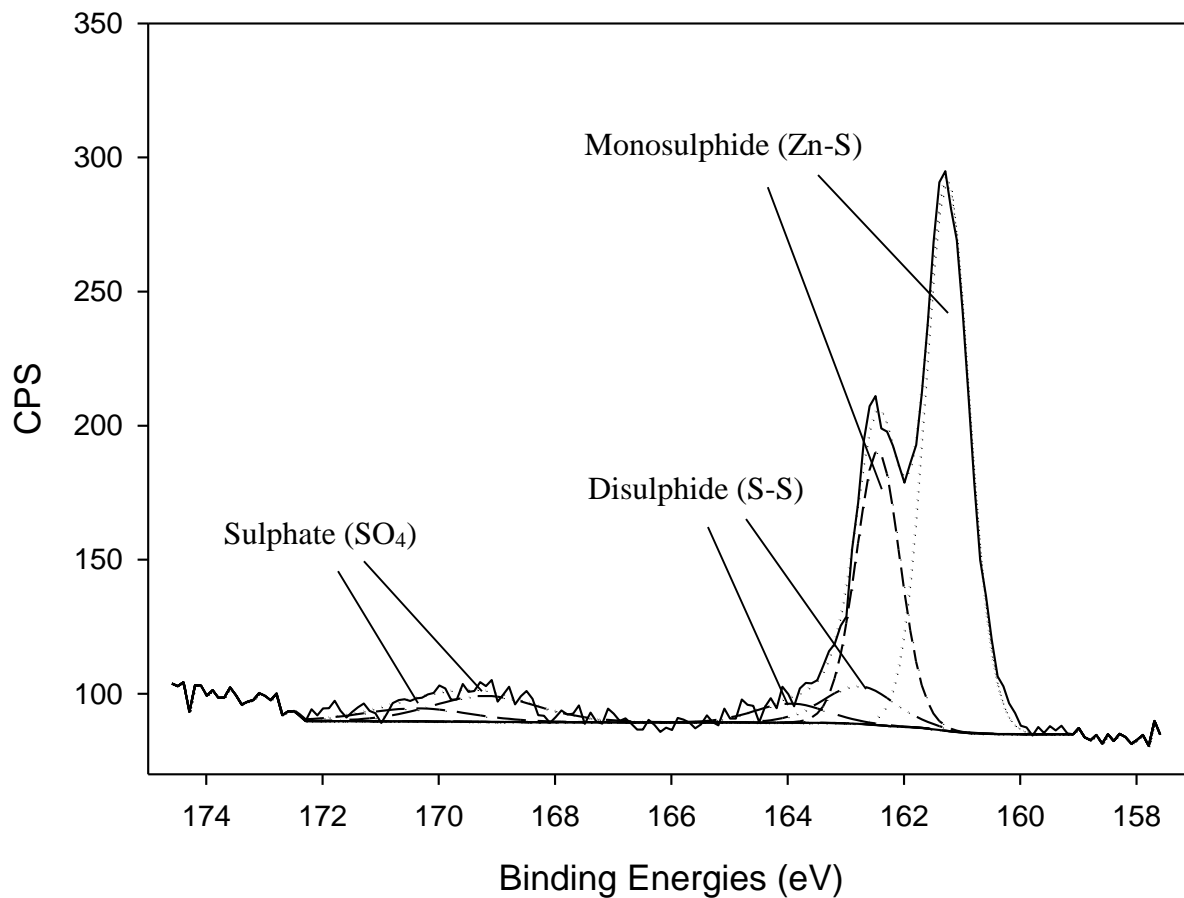


Figure 3-18 XPS high resolution S 2p peak of sphalerite surfaces in de-ionized water with 25 ppm of ZnSO₄.

The high resolution S 2p spectra of the sphalerite surfaces from the de-ionized H₂O + 25 ppm ZnSO₄ test identified the doublet at 161.6 eV (the S²⁻ species or monosulphide) a second doublet at 162.8 eV (a disulphide or metal deficient sulphide) along with a broad band at 168 eV indicating the presence of sulphate on their surfaces (Figure 3–18).

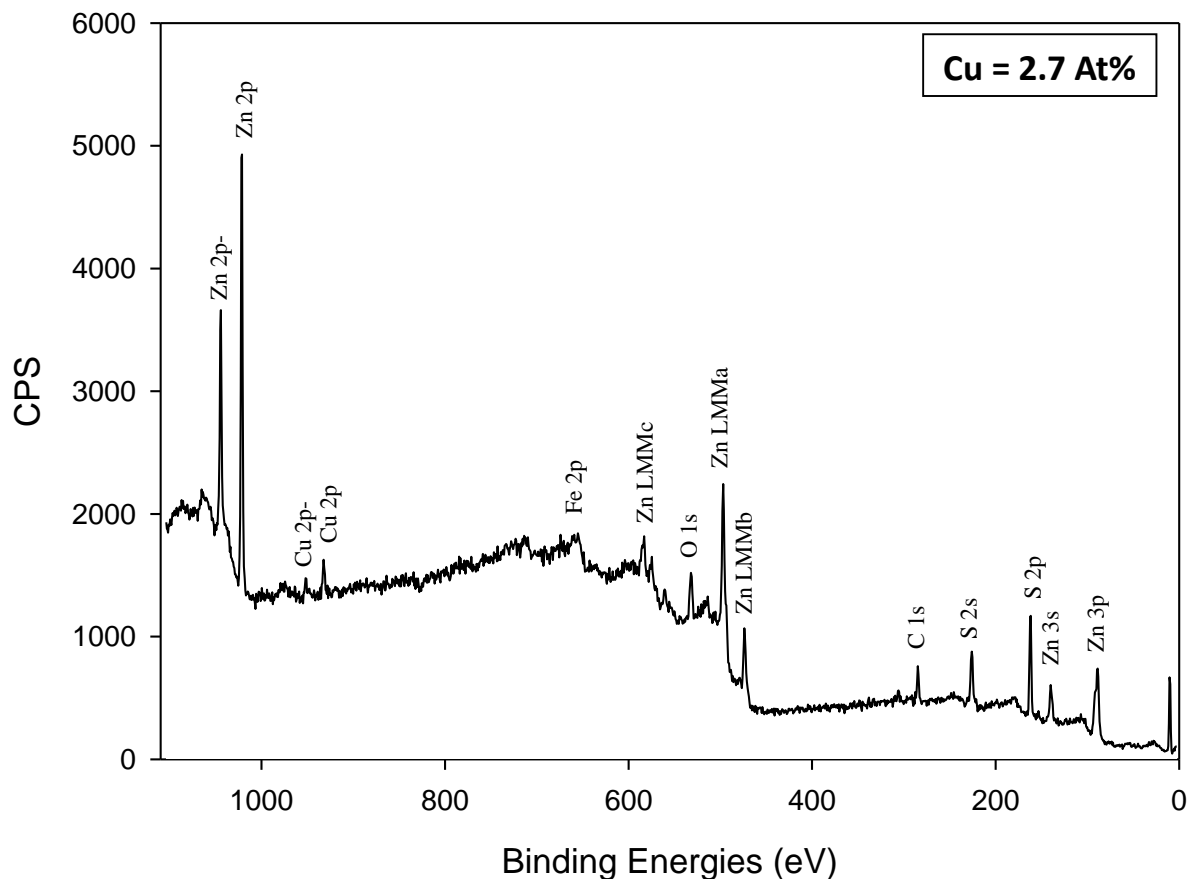


Figure 3-19 XPS survey spectra of sphalerite in de-ionized water with 5 ppm CuSO_4 and 25 ppm ZnSO_4 .

The survey spectra of the sphalerite grains from the de-ionized H_2O + 5 ppm CuSO_4 and 25 ppm ZnSO_4 test (Figure 3–19) show that there is an addition of copper to the surface of the sphalerite grains. The At% of copper in these spectra range from 1.8-3.1% (Table 3–3). The proportion of copper on the sphalerite surface in this test is slightly higher but still very similar to the previous tests (Figure 3–13, 3–15 and 3–17).

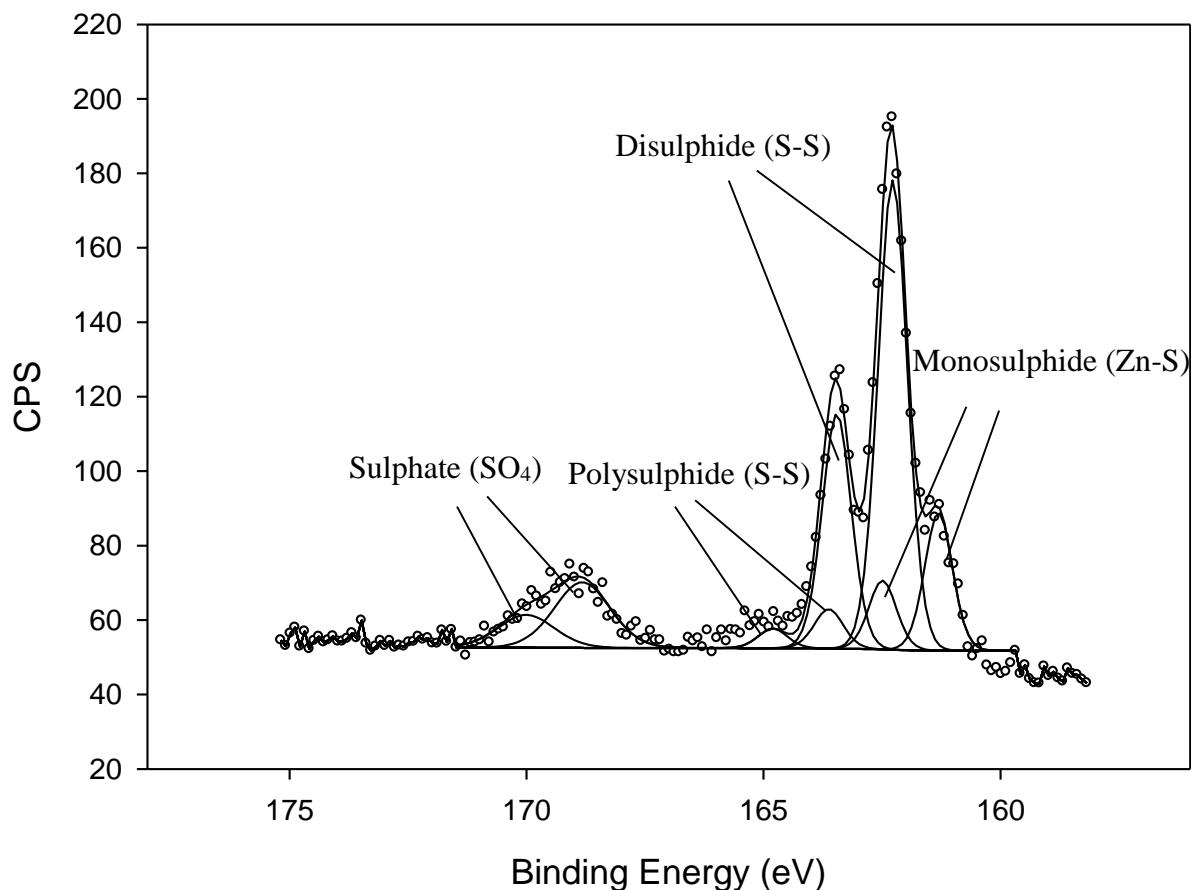


Figure 3-20 XPS high resolution S 2p of sphalerite in de-ionized water with 5 ppm CuSO_4 and 25 ppm ZnSO_4 .

The high resolution S 2p spectra of the sphalerite surfaces from the de-ionized H_2O + 5 ppm CuSO_4 and 25 ppm ZnSO_4 test (Figure 3–20) identified the doublet at 161.6 eV (the S^{2-} species or monosulphide) a second doublet at 162.8 eV (a disulphide or metal deficient sulphide), a polysulphide specie at 163 eV along with a broad band at 168 eV indicating the presence of sulphate. The proportion of sulphate on the surfaces is slightly higher than that from the de-ionized water test (Figure 3–13) but similar to the H_2O + ZnSO_4 test (Figure 3–17).

3.4.1 ZnSO_4 bench tests: Discussion

The XPS data from the bench tests corroborate a number of results from the LaRonde mill samples and the samples from the flotation tests using the instrumented mill. The

surface data from all bench tests show that for all cases copper is transferred between chalcopyrite and the sphalerite grains (Table 3–3). The data show significant variability in surface copper content but the median values for copper are fairly similar between test samples.

Along with the increase in surface copper, changes to the sulphur speciation can be readily identified in the XPS S 2p spectra. The most striking features include a decrease in the proportion of monosulphide (S^{2-} , S bonded to Zn) an increase in the proportion of disulphide (metal deficient S) along with an increase in SO_4 and the identification of a polysulphide (S_n^{2-}) (Figure 3–21).

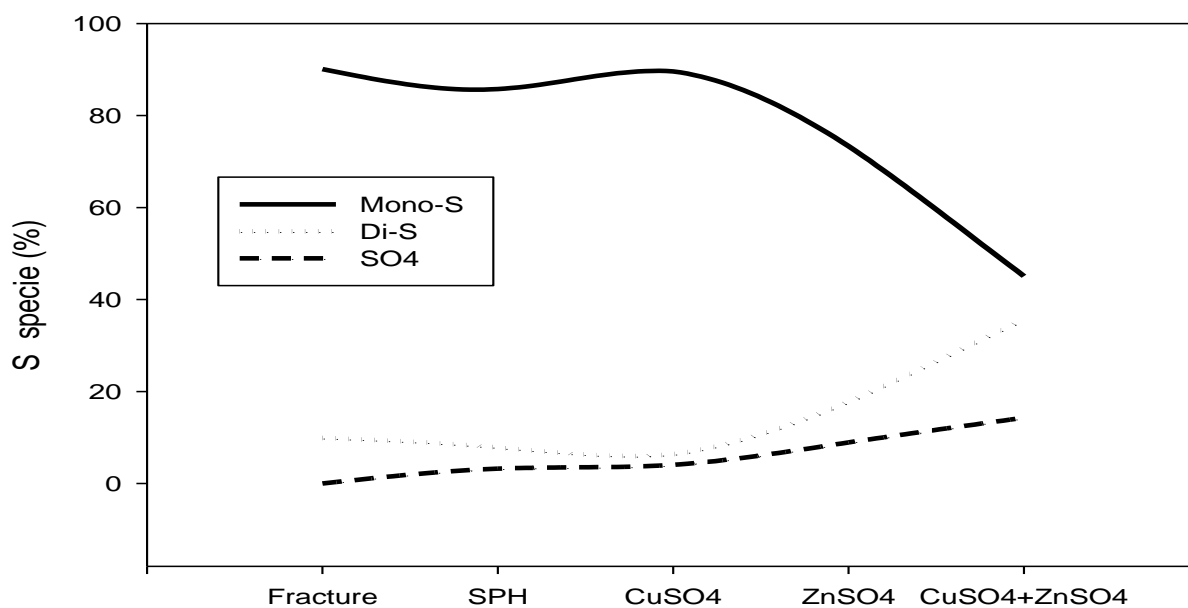


Figure 3-21 The variability in dominant S species as identified on sphalerite grains by XPS in the bench test samples. Fracture: freshly fractured; SPH: in DIW; CuSO₄: DIW + CuSO₄; ZnSO₄: DIW + ZnSO₄; CuSO₄ + ZnSO₄: DIW + CuSO₄ + ZnSO₄.

Table 3-4 Relative proportion in % of S species identified from the S2p spectra on the surface of sphalerite grains from the various bench tests.

Test Conditions	BE(eV) for S 2p 3/2 doublets				
	Monosulphide	Disulphide	S-SO ₃	SO ₃	SO ₄
	161.6	162.8	163	167.4	168.9
Fracture	90.1	9.9	BD	BD	BD
DIW+SPH	85.8	7.8	3.2	BD	3.2
DIW+SPH+CuSO ₄	89.6	6.4	BD	BD	4.0
DIW+SPH+ZnSO ₄	73.3	17.8	BD	BD	8.9
DIW+SPH+CuSO ₄ +ZnSO ₄	45.0	35.7	5.0	?	14.3

Other species identified on sphalerite grains from the CuSO₄ + ZnSO₄ bench test sample include a polysulphide (S_n²⁻) and/or thiosulphite (S-SO₃) and potentially sulphite (SO₃) (Table 3–4). The uncertainty about SO₃ is marked by the (?) and BD stands for Below Detection in Table 3–4.

Given the general consensus that copper substitutes for zinc in the upper layers of sphalerite (see Chandra & Gerson, 2009, and the discussion Chapter 4), the data should reveal some linked variability in the proportion of zinc in relation to sulphur. A plot of the Zn:S ratio for the 5 bench test samples is given in Figure 3–22. The data shows very similar Zn:S ratios for the fractured and CuSO₄ + ZnSO₄ samples, around 1.4. This might indicate limited copper introduction in the upper layers of the sphalerite in the CuSO₄ + ZnSO₄ test but is not supported by the surface copper content (see Table 3–3). More likely it represents a greater proportion of zinc on the surface possibly in the form of zinc hydroxide, which is indeed supported by the TOF-SIMS data from the instrumented mill test with the addition of zinc sulphate. The substitution of copper and corresponding reduction of zinc in the surface layers resulting in the lower Zn:S ratio (approximately 0.8) seen in the DIW, and CuSO₄ tests again cannot be supported by the current XPS data which shows a rather consistent surface copper content.

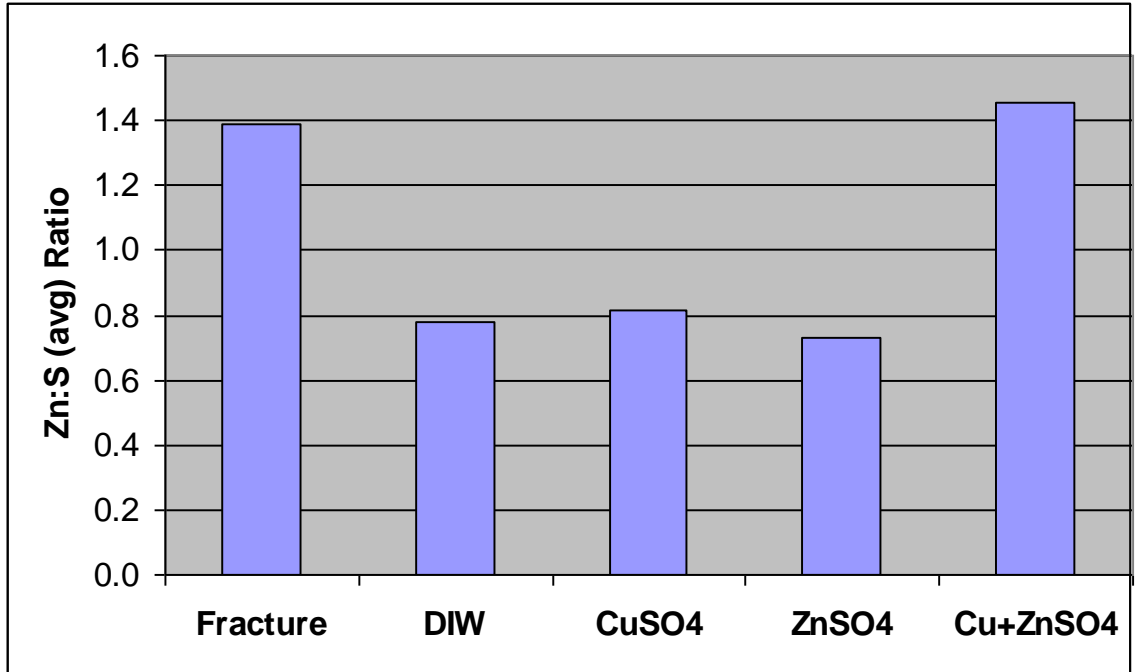


Figure 3-22 Average Zn:S ratio as determined by XPS analyses for sphalerite grains from the 5 bench tests.

Chapter 4

4 Final discussion

Complex polysulphide ores are usually difficult to process without incurring inadvertent activation of unwanted minerals (Aslan & Boz, 2010); in this case ZnS (sphalerite) in the LaRonde copper and precious metal flotation circuit. It is well established that the activation of sphalerite is linked to the dissolution and transfer of copper and lead sulphides (yielding Cu^{2+} and Pb^{2+}) in solution (Ralston & Healy, 1980; Finkelstein, 1999; Chandra & Gerson, 2009; Chen et al., 2010; Mehrabini et al., 2010; Pulido & Salus, 2011). Dissolution and transfer can occur during grinding (Chen et al., 2010; Peng & Grano, 2010; Ye et al., 2010; Simpson et al., 2011) with surface modification continuing during conditioning and flotation (Ruonala et al., 1997; Smart et al., 1998; Biesinger et al., 2007; Chelgani & Hart, 2014). Understanding the surface chemical impacts on minerals reporting to various streams in flotation circuits has been greatly enhanced by the use of modern surface characterization techniques (Smart et al., 2013). Detailed surface chemical evaluations linked to flotation testing can establish a correlation between mineral surface chemistry and flotation response (Abreu & Skinner, 2011; Peng et al., 2011) and potentially provide some valuable insight towards surface mechanisms promoting a flotation phenomenon in response to the addition of a particular reagent. The objective of this study was to examine the surface chemical effects on sphalerite in response to zinc sulphate addition in flotation testing scenarios designed to evaluate changes in zinc recovery.

4.1 Flotation Laboratory Test

In the lab, a six minute copper rougher flotation test was used to duplicate the grinding, conditioning and first kinetics of copper flotation in the mill. This test was performed at mill operating conditions with a mill representative feed ore sample. The conditions and results of this test are considered as the flotation baseline. In the test nearly 21% of the zinc in the feed ore was recovered as sphalerite in the final copper concentrate. In the mill, subsequent cleaning and grinding steps in the copper flotation circuit reduce this

percentage to around 6-7%, however, a large proportion of zinc is still lost to the copper concentrate.

As part of a zinc reduction testing program, a series of flotation tests (Table 4–1) were performed in order to investigate the effect of various reagent additions on zinc recovery.

Table 4-1 Flotation testing conditions

Test	Material	Conditions
1	Feed Ore	Base Line (Mill parameters)
2	Feed Ore	addition of 3mg/l Cu
3	Feed Ore	addition of 25g/t ZnSO ₄
4	Feed Ore	addition of 200g/t ZnSO ₄
5	Feed Ore	addition of 3mg/l Cu + 50g/t ZnSO ₄
6	Feed Ore	addition of 3mg/l Cu + 200g/t ZnSO ₄

Figure 4–1 illustrates the results of the tests. The use of zinc sulphate reduces the zinc recovery in the copper concentrate from 21% (baseline without Cu²⁺ addition) to 17.5% (25g/t ZnSO₄) and 18.6% (200g/t ZnSO₄). Inadvertent zinc recovery with Cu²⁺ addition is reduced from 32.2% to around 17.5% for both 50g/t and 100g/t ZnSO₄. From other flotation tests performed by COREM for Agnico-Eagle (not presented here) it was determined that inadvertent Cu²⁺ activation occurs mainly during the flotation stages.

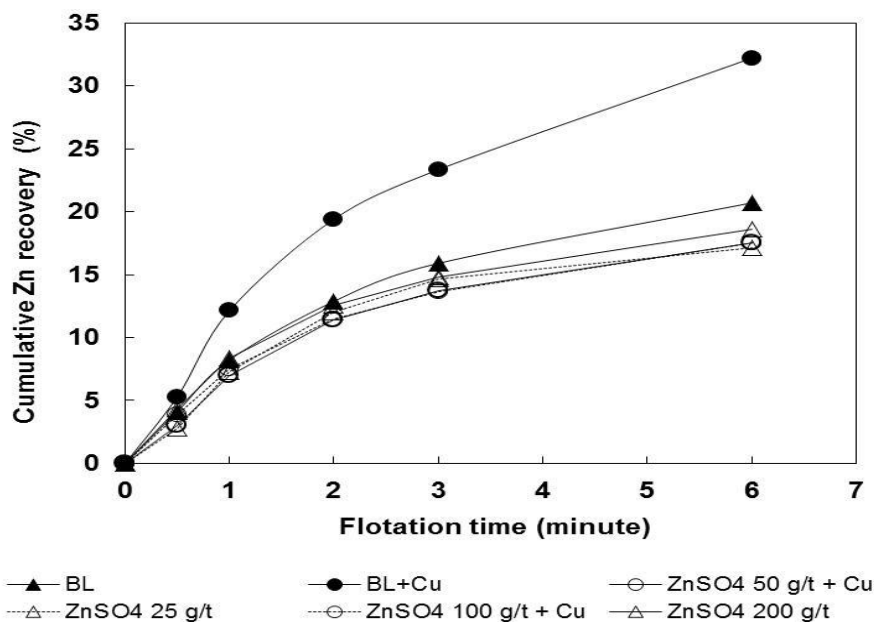


Figure 4-1 Effect of zinc sulphate on ZnS in Cu rougher flotation tests, with and without Cu²⁺

4.2 Instrumented Mill

In order to better understand the effect of the zinc sulphate addition to the flotation of sphalerite, TOF-SIMS analyses were performed on sphalerite grains from a series of milling and flotation tests: samples analysed include the mill discharge sample, the first concentrate and reject samples of 3 tests: baseline, baseline + 5ppm Cu²⁺, and baseline + 5ppm Cu²⁺ + 25ppm ZnSO₄. The sphalerite surface analysis data revealed that copper transfer occurred under all test conditions. The intensity distribution of the collector, 3418A, mirrored that of copper indicating that sphalerite flotation was in response to copper induced collector attachment (Figures 3–7 and 3–10).

The results from the zinc sulphate tests show that copper was partially inhibited from attaching to the surface of the sphalerite grains. This could be attributed to the development of oxidative species on sphalerite grains such as Zn(OH)₂ (Fuerstenau, 1985; Cao & Liu, 2006; Bulatovic, 2007) and SO₃ (Khmeleva et al., 2006). As identified by TOF-SIMS in figures 3–8 and 3–9, the sphalerite grain surfaces in the zinc sulphate test displayed the highest proportion of these oxidative species. The identification of

hydroxide and sulphoxyl species, in concert with the reduction of zinc on the surface of the sphalerites from the copper concentrate, supports the theory that hydroxide and sulphite may inhibit collector attachment, produce hydrophilic surfaces, and, in combination, result in poor flotation (Khmeleva et al., 2006; Chandra & Gerson, 2009).

4.3 Bench Tests

The XPS analyses of sphalerite grains from the bench test agree with a number of results observed by the TOF-SIMS study. This is not definitive however, because the XPS analyses did not confirm the presence of Zn(OH)_2 , as the Zn 2p peak at 1021.5 eV is characteristic of both ZnS and Zn(OH)_2 (Prestige, 1997; Shen, 2001). However, the calculated modified Zn Auger parameter at 2011.05 eV falls into the oxide category (Wagner et al., 2003; Biesinger et al., 2010) while the broad oxide peak at 531.8 eV possibly represents Zn(OH)_2 and/or a sulphoxy species (Grano, 1997; Prestige et al., 1997). The characteristic Cu^{2+} shake up peak at 942 eV is not present in any of the Cu 2p spectra (Figure 4–2) indicating that the copper is present as Cu^{1+} and thus, not as $\text{Cu(OH)}_{2(\text{solid})}$. Furthermore, $(\text{CuOH})^+$ which could be weakly held to the sphalerite surface, is not likely present as it was not identified in the TOF-SIMS analysis and is generally not stable in this pH range (Laskowski et al., 1997).

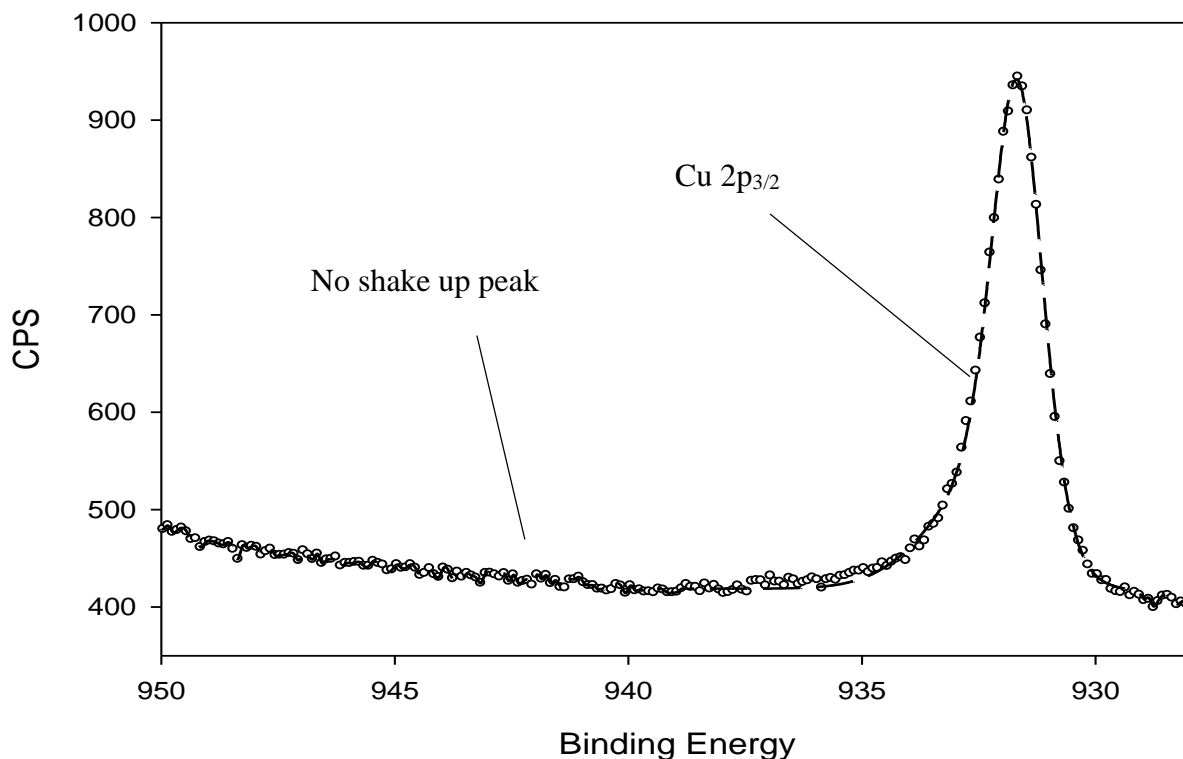


Figure 4-2 High resolution XPS spectrum of the Cu $2p_{3/2}$ peak with no “shake-up” peak.

Thus, copper present as Cu^{1+} can be interpreted as the copper that substituted for zinc in the upper layers of the mineral lattice and supports conclusions by Ralston, (1980), Gerson et al., (1999) and Smart, (2003).

The S $2p_{3/2}$ XPS spectra (Figures 4–3 and 4–4) show the presence of a number of sulphur species including the sulphony species, which likely play an integral part in the depression of sphalerite. Figure 4–4 shows both sulphates and sulphites were identified in the $\text{CuSO}_4 + \text{ZnSO}_4$ test. The identification of thiosulphite in the 163.5 eV region (Figure 3–25) coupled with the strong presence of sulphite in the TOF-SIMS spectra (Figure 3–9) make it likely that sulphite rather than sulphate is linked to the depression of sphalerite. It should be pointed out that other interpretations of the XPS spectra are possible; however, it seems relevant when supported by the TOF-SIMS data. These data indicate a process similar to that outlined by Khmeleva et al., (2006) who studied sphalerite depression in response to NaHSO_3 addition. They concluded that sulphite ions specifically interact with

the reduced coordination sulphur associated with copper activation (which results in a trigonally coordinated Cu-S species, as opposed to the quadruple coordinated Zn-S species) and report into solution as a thiosulphate, which is then oxidized to sulphate. At the same time, zinc hydroxide is formed at the sphalerite surface and in solution thus reducing surface hydrophobicity and depressing sphalerite flotation.

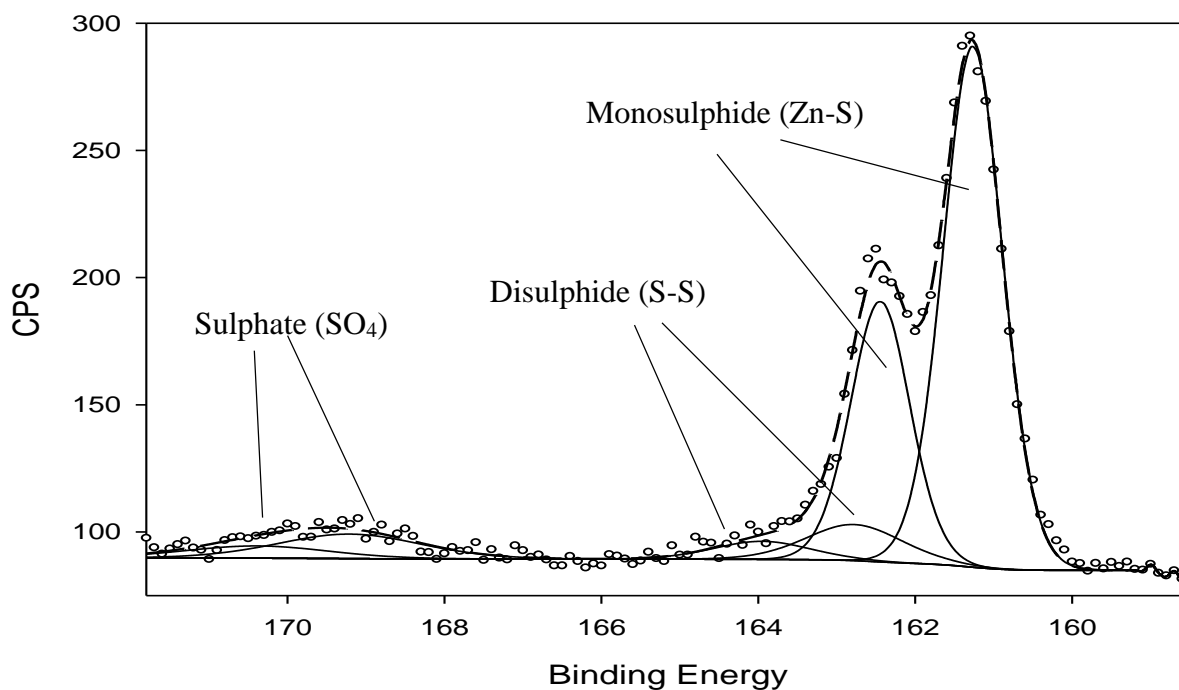


Figure 4-3 High resolution XPS spectrum of S 2p_{3/2} peaks on sphalerite in de-ionized water.

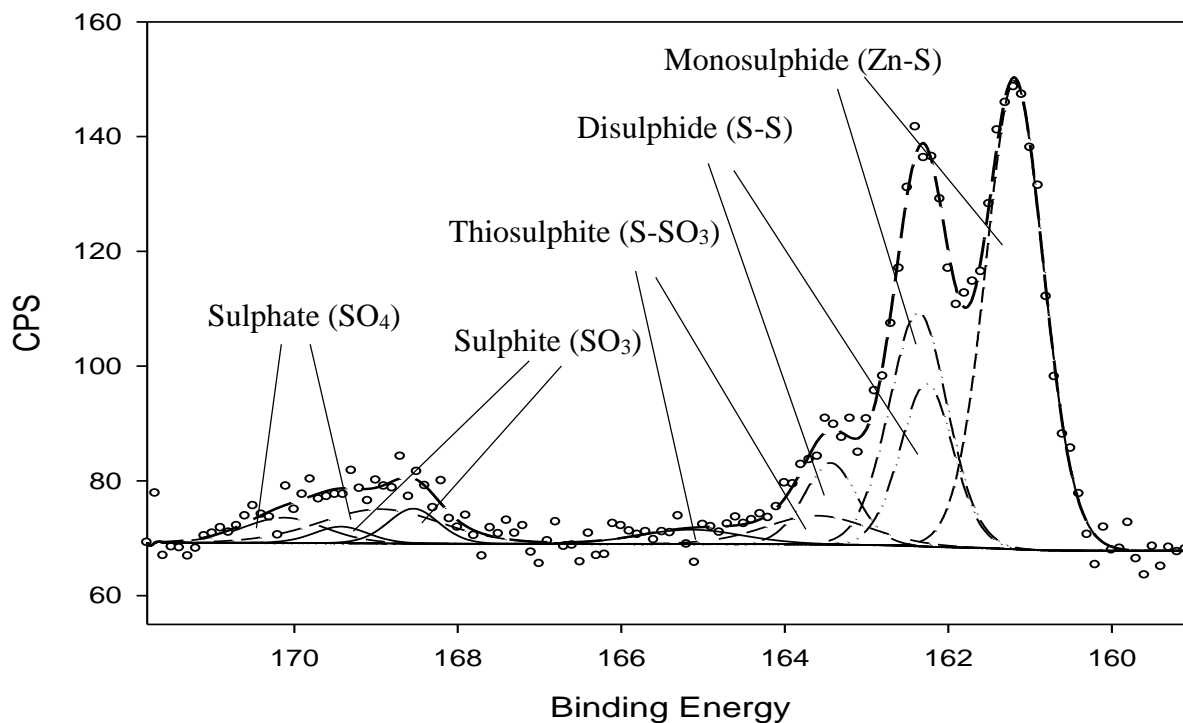


Figure 4-4 High resolution spectrum of S $2p_{3/2}$ peaks on sphalerite in 25ppm $ZnSO_4$ and 5ppm $CuSO_4$ solution.

The following proposed mechanism for sphalerite depression is based on the results primarily identified in the XPS analyses of the bench tests:

1. Cu substitution for Zn results in hydrophobic Cu coordinated S (polysulphide).
2. Sulphite ions present in solution as a result of $ZnSO_4$ dissociation, adsorb to the polysulphides.
3. The sulphite ion decomposition of the polysulphides, generates thiosulphate, which is subsequently oxidized to sulphate.
4. $Zn(OH)_2$, identified in the TOF-SIMS analysis, likely forms concurrently at the surface of sphalerite as a result of liberated Zn ions combining with hydroxyls.

The XPS spectrum of a sphalerite surface in Figure 4–4 potentially represents a snapshot into this process.

4.4 Plant Implementation

The LaRonde Division of Agnico-Eagle Mines Limited tested zinc sulphate as a reagent to control sphalerite activation in the copper flotation circuit over the course of more than one year. Before the addition of zinc sulphate, zinc recovery in the final copper concentrate was around 6%; after, this value dropped to almost 3.5% (Figure 4–5). Continued zinc sulphate additions during 2010 resulted in an average zinc recovery reduction of 2%.

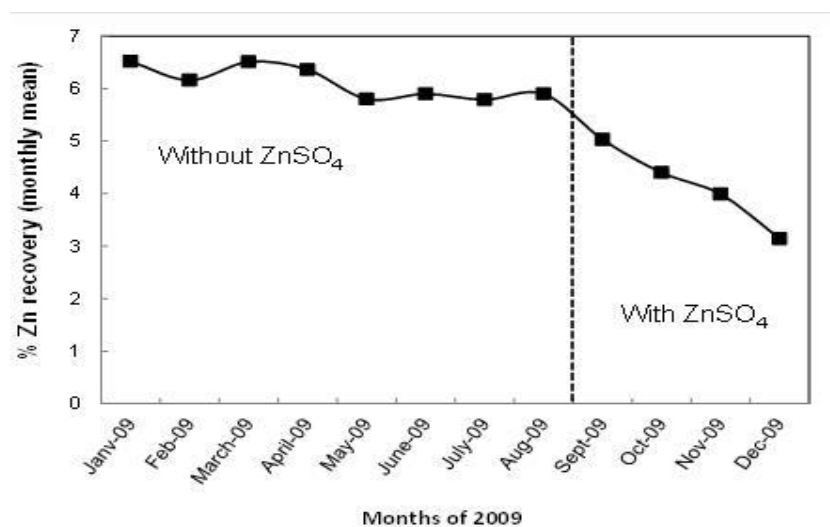


Figure 4-5 Monthly mean Zn recovery in the Cu flotation circuit at LaRonde (2009).

Two sources of Cu^{2+} were identified by tracking dissolved copper in the copper and zinc flotation circuits at LaRonde. The main source, reused process water was due to over addition of copper sulphate in the downstream zinc flotation circuit. The secondary source of Cu^{2+} was reclaimed water from the tailings pond. Excess Cu^{2+} in reused process water was reduced by the installation of an automatic valve that optimized copper sulphate addition based on zinc feed values. Cu^{2+} enrichment in the tailings pond was linked to operational problems and evaporation during summer. Means to provide online monitoring of this water are under study. A third source is from the ore itself. Dissolution of inherent copper minerals and the introduction of copper to solution and subsequent transfer to sphalerite is a common problem in many polymetallic ores. From the better

understanding of the chemistry of flotation circuits and water quality gained in this study, the addition of zinc sulphate is still applied in 2014 but only as required.

5 Conclusions

Inadvertent sphalerite activation by Cu^{2+} in the copper flotation circuit at LaRonde was confirmed by a detailed mineralogical and surface chemical evaluation. The addition of zinc sulphate was tested to control sphalerite activation and samples from a series of tests designed to reproduce the electrochemical conditions during grinding and flotation in the mill. Surface chemistry data indicate that when zinc sulphate is added, copper is partially inhibited from attaching to the surface of sphalerite grains. This is likely due to adsorption of oxidation species on sphalerite grains. Data also suggest that zinc sulphate could inhibit collector attachment by promoting the development of sulphoxyl and hydroxide species on sphalerite surfaces. Based on these tests, the LaRonde mill implemented the addition of 40g/t zinc sulphate at the conditioning or cleaning stages which has led to the reduction of the zinc in the copper concentrate by one third.

References

- Abreu, S.Be. and Skinner, W. (2011). ToF-SIMS-derived hydrophobicity in DTP flotation of chalcopyrite: contact angle distributions in flotation streams. *International Journal of Mineral Processing*, 98, 35- 41.
- Allison, S. A., Goold, L. A., Nicol, M. J. and Granville, A. (1972). A determination of the products of reaction between various sulphide minerals and aqueous xanthate solution, and a correlation of the products with electrode rest potential. *Metallurgical Transactions*, 3, 2613- 2618.
- Aslan, A. and Boz, H. (2010). Effect of air distribution profile on selectivity at zinc cleaner circuit. *Minerals Engineering*, 23, 885-887.
- Ayer, J., Amelin, Y., Corfu, F., Kamo, S., Ketchum, J., Kwok, K. and Trowell, N.F. (2002). Evolution of the southern Abitibi greenstone belt based on U-Pb geochronology: autochthonous volcanic construction followed by plutonism, regional deformation and sedimentation. *Precambrian Research*, 115, 63-95.
- Basilio, C.I., Kartio, I.J. and Yoon, R.H. (1996). Lead activation during galena flotation. *Mineral Engineering*, 9, 8, 869-879.
- Biesinger, M.C., Hart, B.R., Polack, R., Kobe, B.A. and Smart, R.S.C. (2007). Analysis of mineral surface chemistry in flotation separation using imaging XPS. *Minerals Engineering*, 20, 152-162.
- Biesinger M.C., Lau, L.W.M., Gerson, A.R. and Smart, R.St.C. (2010). Resolving surface chemical states in XPS analysis of first row transition metals, oxides and hydroxides: Sc, Ti, V, Cu and Zn. *Applied Surface Science*, 257, 887-898.
- Boulton, A., Fornasiero, D. and Ralston, J. (2005). Effect of iron content in sphalerite on flotation. *Journal of Mineral Engineering*, 18, 1120-1122.

Buckley, A.N. & Woods, R. (1987). The surface oxidation of pyrite. *Applied Surface Science*, 27, 4, 437-452.

Buckley, A.N., Woods, R. and Wouterlood, H.J. (1989). An XPS investigation of the surface of natural sphalerites under flotation-related conditions. *International Journal of Mineral Processing*, 26, 29-49.

Buckley, A.N., Skinner, W.M., Harmer, S.L., Pring, A., Lamb, R.N., Fan, L. and Yang, Y.W. (2007). Examination of the proposition that Cu(II) can be required for charge neutrality in a sulfide lattice - Cu in tetrahedrites and sphalerite. *Canadian Journal of Chemistry*, 85, 767-781.

Bulatovic, S.M. (2007). *Handbook of flotation reagents: chemistry, theory and practice. Flotation of Sulphide Ores*. Elsevier, S&T Books.

Cao, M. and Liu, Q. (2006). Re-examining the functions of zinc sulphate as a selective depressant in differential sulphide flotation—the role of coagulation. *Journal of Colloid and Interface Science*, 301, 2, 523-531.

Card, K.D. (1990). A review of the Superior Province of the Canadian Shield, a product of Archean accretion. *Precambrian Research*, 48, 1, 99-156.

Cengage, G., Ed. Lerner K.L. and Lerner B.W. (2003). Greenstone Belt. *World of Earth Science*. <http://www.enotes.com/earth-science/greenstone-belt>

Chandra, A.P. & Gerson, A.R. (2009). A review of the fundamental studies of the copper activation mechanisms for selective flotation of the sulfide minerals, sphalerite and pyrite. *Advances in Colloid and Interface Science*, 145, 97-110.

Chen, Z. & Yoon, R.H. (2000). Electrochemistry of copper activation of sphalerite at pH 9.2. *International Journal of Mineral Processing*, 58, 57-66.

Chen, Y., Chen, J.H., Guo, J. (2010). A DFT study on the effect of lattice impurities on the electronic structures and floatability of sphalerite. *Minerals Engineering*, 23, 1120-1130.

Clarke, P., Fornasiero, D., Ralston, J. and Smart, R.St.C. (1995). A study of the removal of oxidation products from sulphide mineral surfaces. *Minerals Engineering*, 8, 11, 1347–1357.

Corfu, F. (1993). The evolution of the Southern Abitibi greenstone belt in light of precise U-Pb geochronology. *Economic Geology*, 88, 1323-1340.

Dana, J.D., Hurlbut, C.S. and Klein, C. (editors) (1977). *Manual of mineralogy (after James D. Dana) 19th edition*. New York: Wiley

Dávila-Pulido, G.I., Uribe-Salas, A. and Espinosa-Gómez, R. (2011). Comparison of the depressant action of sulfite and metabisulfite for Cu-activated sphalerite, *International Journal of Mineral Processing*, 101, 71–74.

Davis, D.W. (2002). U-Pb geochronology of Archean metasedimentary rocks in the Pontiac and Abitibi subprovinces, Quebec, constraints on timing, provenance and regional tectonics. *Precambrian Research*, 115, 97-117.

De Wit M. J. & Ashwal L. D. (1995). Greenstone belts: what are they? *South African Journal of Geology*, 98, 4, 505-520.

De Wit M. J. and Hynes A. (1995). The onset of interaction between the hydrosphere and oceanic crust, and the origin of the first continental lithosphere. *Geological Society Special Publication*, 95, 1-9.

Dimroth, E., Imreh, L., Rocheleau, M. and Goulet, N. (1982). Evolution of the south-central part of the Archean Abitibi belt, Quebec. Part I: stratigraphy and paleogeographic model. *Canadian Journal of Earth Sciences*, 19, 1729-1758.

Dimroth, E., Imreh, L., Goulet, N. and Rocheleau, M. (1983). Evolution of the south-central part of the Archean Abitibi Belt, Quebec: Part II: Tectonic evolution and geomechanical model. *Canadian Journal of Earth Sciences*, 20, 1355-1373.

Dimroth, E., Imreh, L., Cousineau, P., Leduc, M., and Sanschagrin, Y. (1985). Paleogeographic analysis of mafic submarine flows and its use in the exploration for

- massive sulphide deposits. In L.D. Ayres, P.C. Thurston, K.D. Card and W. Weber (Editors), Evolution of Archean Supracrustal Sequences. *Geological Association of Canada, Special Paper, 28*, 203-222.
- Duarte, A.C.P. and Grano, S.R. (2007). Mechanism for the recovery of silicate gangue minerals in the flotation of ultrafine sphalerite. *Mineral Engineering, 20*, 766-775.
- Dube, B., Gosselin, P. Mercier-Langevin, P., Hannington, M. and Galley, A. (2007). Gold-rich volcanogenic massive sulphide deposits. In Goodfellow, W.D., ed., Mineral Deposits of Canada: A Synthesis of Major Deposit-Types, District Metallogeny, the Evolution of Geological Provinces, and Exploration Methods. *Geological Association of Canada, Mineral Deposits Division, Special Publication 5*, 75-94.
- Duke, C.B., Wang, Y.R. (1988). Surface structure and bonding of the cleavage faces of tetrahedrally coordinated II–VI compounds. *Journal of Vacuum Science & Technology B: Microelectronics and Nanometer Structures, 6, 4*, 1440.
- El-Shall, H.E., Elgillani, D.A. and Abdel-Khalek, N.A. (2000). Role of zinc sulfate in depression of lead-activated sphalerite. *International Journal of Mineral Processing, 58*, 67-75.
- Finch, J.A., Rao, S.R. and Nessel, J.E. (2007). Iron control in mineral processing, 39th annual meeting of the Canadian mineral processors 23-25 January. *Ottawa: Canadian Institute of Mining, Metallurgy and Petroleum*
- Finkelstein, N.P. (1997). The activation of sulfide minerals for flotation: a review. *International Journal of Mineral Processing, 52*, 81-120.
- Fornasiero, D. and Ralston, J. (2006). Effect of surface oxide/hydroxide products on the collectorless flotation of copper-activated sphalerite. *International Journal of Mineral Processing, 78*, 231-237.
- Franklin, J.M., Lydon, J.W. and Sangster, D.F. (1981). Volcanic-Associated Massive Sulfide Deposits. *Economic Geology 75th Anniversary Volume*, 485-627.

- Franklin, J.M. (1995). Volcanic-associated sulphide base metal: Geological Survey of Canada. *Geology of Canada*, 8, 158-183.
- Fuerstenau, M.C., Kuhn, M.C. and Elgillani, D.A. (1968). The role of dixanthogen in xanthate flotation of pyrite. *AIME, Society of Mining Engineers, Transactions*, 241, 148-156.
- Fuerstenau, M.C. and Palmer, B.R. (1976). In Fuerstenau, M.C. (editor). *Flotation. A.M. Gaudin memorial volume, 1*, AIME, New York, N.Y.
- Fuerstenau, M.C. (1985). *Chemistry of Flotation*, AIME, New York, N.Y.
- Gerson, A.R., Lange, A.G., Prince, K.E. and Smart, R.S.C. (1999). The mechanism of copper activation of sphalerite. *Applied Surface Science*, 137, 207-223.
- Gerson, A.R., Cookson, D.J. and Prince, K.C. (2008). In Riviere, J.C., Myhra, S. (editors). *Handbook of surface and interface analysis: methods for problem solving, 2nd Edition*. Chapter 10.
- Gigowski, B., Vogg, A., Wierer, K., Dobias, B. (1991). Effect of Fe-lattice ions on adsorption, electrokinetic, calorimetric and flotation properties of sphalerite. *International Journal of Mineral Processing*, 33, 103-120.
- Goodwin, A.M. (1982). Archean volcanoes in southwestern Abitibi belt, Ontario and Quebec: form, composition, and development. *Canadian Journal of Earth Sciences*, 1, 1140-1155.
- Goodwin, A.M. and Ridler, R.H. (1970). The Abitibi orogenic belt; In Baer, A. J., (editor). Symposium on Basins and Geosynclines of the Canadian Shield. *Geological Survey of Canada Paper 70, 40*, 1-24.
- Goold, L. A. and Finkelstein, N. P., (1972). Product of reaction between galena and aqueous xanthate solutions. *South Africa, IMM, Report No.1439*

Grano, S.R. (1997). Mechanisms for the action of sulphite and carbonate ions in the flotation of the Hilton ore of Mount Isa Mines limited. PhD Thesis. University of Australia.

Groves, D.I. and Bierlein, F.P. (2007). Geodynamic settings of mineral deposit systems. *Journal of the Geological Society, London*. 164, 19-30.

Hannington, M.D., Poulsen, K.H., Thompson, J.F.H., and Sillitoe, R.H., (1999). Volcanogenic gold in the massive sulfide environment. In Barrie, C.T., and Hannington, M.D., eds., Volcanic-Associated Massive Sulfide Deposits: Processes and Examples in Modern and Ancient Settings. *Reviews in Economic Geology*, 8, 325-356.

Harmer, S.L., Goncharova, L.V., Kolarova, R., Lennard, W.N., Munoz-Marquez, M.A., Mitchell, I.V. and Nesbitt, H.W. (2007). Surface structure of sphalerite studied by medium energy ion scattering and XPS. *Surface Science*, 601, 352-361.

Harmer, S.L., Mierczynska-Vasilev, A., Beattie, D.A., and Shapter, J.G. (2008). The effect of bulk iron concentration and heterogeneities on the copper activation of sphalerite. *Minerals Engineering*, 21, 1005-1012.

Hart, B., Biesinger, M. and Smart, R.S.C. (2006). Improved statistical methods applied to surface chemistry in minerals flotation. *Minerals Engineering*, 19, 790-798.

Hu, Y., Qiu, G., Sun, S., Wang, D. (2000). Recent developments in the research of the electrochemistry of sulphide flotation at Central South University of Technology. *Transactions Nonferrous Metalurgical Society of China*, 10, 1- 7

Hu, Y. Sun, W. Wang, D. (2009). *Electrochemistry of flotation of sulphide minerals*. Tsinghua University Press: Springer 316 pgs.

Huston, D.L., (2000). Gold in volcanic-hosted massive sulfide deposits; distribution, genesis, and exploration, In Hagemann, S.G. ed., Gold in 2000. *Reviews in Economic Geology*, 13, 401-426.

- Hyde, R.S. (1980). Sedimentary facies in the Archean Timiskaming Group and their tectonic implications; Abitibi greenstone belt, northeastern Ontario, Canada. *Precambrian Research*, 12, 161-195.
- Jolly, W. T. (1978). Metamorphic history of the Archean Abitibi belt. In Metamorphism in the Canadian Shield. Fraser, I. A. and Heywood, W. W., (editors). *Geological Survey of Canada, Paper 78, 10*, 63-78.
- Kalliokoski, J. (1968). Structural features and some metallogenic patterns in the southern part of the Superior Province, Canada. *Canadian Journal of Earth Sciences*, 5, 1199-1208.
- Kartio, I.J., Basilio, C.I. and Yoon, R.H. (1998). An XPS study of sphalerite activation by copper. *Langmuir*, 14, 5274-5278.
- Klein C. (2002). *The 22nd edition of the manual of mineral science*. New York: John Wiley and Sons, 646 pgs.
- Khmeleva, T.N., Chapelet, J.K., Skinner, W.M. and Beattie, D.A. (2006). Depression mechanisms of sodium bisulfate in the xanthate-induced flotation of copper activated sphalerite. *International Journal of Mineral Processing*, 79, 61-75.
- Lafrance, B., Davis, D.W., Goutier, J., Moorhead, J., Pilote, P., Mercier-Langevin, P., Dubé, B., Galley, A.G., and Mueller, W.U. (2005). New isotopic ages in the Quebec portion of the Blake River Group and adjacent units. Ministère des Ressources naturelles et de la Faune, Québec, Report RP 2005-01, 15.
- Lascelles, D., Sui, C.C., Finch, J.A. and Butler, I.S. (2001). Copper ion mobility in sphalerite activation. *Colloids and Surfaces A: Physicochemical and Engineering Aspects*, 186, 163-172.
- Laskowski, J.S., Liu, Q. and Zhan, Y. (1997). Sphalerite activation: flotation and electrokinetic studies. *Minerals Engineering*, 10, 787-802.

Leppinen, J.O. (1990, December 30). FTIR and flotation investigation of the adsorption of ethyl xanthate on activated and non-activated sulfide minerals. *International Journal of Mineral Processing*, 30, 3-4, 245-263.

Ludden, J. Hubert, C. Gariépy, C. (1986). The tectonic evolution of the Abitibi greenstone belt of Canada. *Geology Magazine* 123, 153-166.

Marquis, P., Hubert, C., Brown, A.C., and Rigg, D.M. (1990a). Overprinting of early, redistributed Fe and Pb-Zn mineralization by late-stage Au- Ag-Cu deposition at the Dumagami mine, Bousquet district, Abitibi, Quebec. *Canadian Journal of Earth Sciences*, 27, 1651-1671.

McNicoll, V., Goutier, J., Dubé, B., Mercier-Langevin, P., Ross, P.S., Dion, C., Monecke, T., Legault, M., Percival, J. and Gibson, H. (2014). U-Pb geochronology of the Blake River Group, Abitibi Greenstone Belt, Quebec, and implications for base metal exploration. *Economic Geology*, 109, 27-59.

Mehrabani, J.V., Noaparast, M., Mousavi, S.M., Dehghan, R. and Ghorbani, A. (2010). Process optimization and modeling of sphalerite flotation from a low-grade Zn-Pb ore using response surface methodology. *Separation and Purification Technology*, 72, 234-249.

Morey, M.S., Grano, S.R., Ralston, J., Prestidge, C.A. and Verity, B. (2001). The electrochemistry of PbII activated sphalerite in relation to flotation. *Mineral Engineering*, 14, 9, 1009-1017.

Mortensen, J. K. & Card, K. D. (1993). U-Pb age constraints for the magmatic and tectonic evolution of the Pontiac subprovince, Quebec. *Canadian Journal of Earth Sciences*, 30, 1970-1980.

Mueller, W. and Donaldson, J.A. (1992). Development of sedimentary basins in the Archean Abitibi belt, Canada: an overview. *Canadian Journal of Earth Sciences*, 29, 2249-2265.

Mueller, W. U. Stix, J. Corcoran, P. L. Daigneault, R. (2009). Subaqueous calderas in the Archean Abitibi greenstone belt: An overview and new ideas. *Ore Geology Reviews*, 35, 4-46.

Norman, G. W. H. (1946). Major faults, Abitibi Region, Quebec. *Canadian Mining and Metallurgical Bulletin*, 406, 129–144.

Ojakangas, R.W. (1985). Review of Archean clastic sedimentation, Canadian Shield: major felsic volcanic contributions to turbidite and alluvial fan-fluvial facies associations. In Ayres, L.D., Thurston, P.C., Card, K.D. and Weber, W., (Editors), Evolution of Archean supracrustal sequences. *Geological Association of Canada, Special Paper*, 8, 23-48.

Olsen, C., Makni, S., Hart, B., Laliberty, M., Pratt, A., Blatter, P. and Lanouette, M. (2012). The successful application of a laboratory-developed test protocol utilizing electrochemical and surface chemical analysis to the industrial flotation process of a complex sulphide (Cu-Pb-Zn-Au-Ag) ore. *XXVI International Mineral Processing Congress (IMPC 12)*. September 24-28, 2012, New Delhi, Paper 771.

Patrick, R.A.D., England, K.E.R., Charnock, J.M. and Mosselmans, J.F.W. (1999). Copper activation of sphalerite and its reaction with xanthate in relation to flotation: an X-ray absorption spectroscopy (reflection extended X-ray absorption spectroscopy fine structure) investigation. *International Journal of Mineral Processing*, 55, 247-265.

Pearse, M.J. (2005). An overview of the use of chemical reagents in mineral processing. *Minerals Engineering*, 18, 139-149.

Peng, Y. and Grano, S. (2010). Effect of iron contamination from grinding media on the flotation of sulphide minerals of different particle size. *International Journal of Mineral Processing*, 97, 1-6.

Peng, Y., Wang, B. and Bradshaw, D. (2011). Pentlandite oxidation in the flotation of a complex nickel ore in saline water. *Minerals Engineering*, 24, 85-87.

Piantadosi, C., Jasieniak, M., Skinner, W. M. and Smart R.St.C. (2000). Statistical comparison of surface species in flotation concentrates and tails from ToF-SIMS evidence. *Minerals Engineering*, 13, 1377-1394.

Popov, S.R. & Vucinic, D.R. (1990, December 30). The ethyl xanthate adsorption on copper-activated sphalerite under flotation-related conditions in alkaline media. *International Journal of Mineral Processing*, 30, 3-4, 229-244.

Poulsen, K.H. & Hannington, M.D. (1996). Volcanic-associated massive sulphide gold. In Eckstrand, O.R., Sinclair, W.D. and Thorpe, R.I., eds., *Geology of Canadian Mineral Deposit Types*. *Geology of Canada*, 8, 183-196.

Poulsen, K.H., Robert, F. and Dube, B. (2000). Geological classification of Canadian gold deposits. *Geological Survey of Canada, Bulletin 540*, 106 p.

Powell W.G. & Hodgson, C.J. (1992). Deformation of the Gowganda Formation, Matachewan area, Ontario, by post- Early Proterozoic reactivation of the Archean Larder Lake - Cadillac break, with implications for gold exploration. *Canadian Journal of Earth Sciences*, 29, 1580-1589.

Powell, W.G., Hodgson, C.J., Hanes, J.A., Carmichael, D.M., McBride, S. and Farrar, E. (1995a). $^{40}\text{Ar}/^{39}\text{Ar}$ geochronological evidence for multiple postmetamorphic hydrothermal events focused along faults in the southern Abitibi greenstone belt. *Canadian Journal of Earth Sciences*, 32, 768-786.

Prestige, C.A., Skinner, W.M., Ralston, J. and Smart, R.S.C. (1997). Copper (II) activation and cyanide deactivation of zinc sulphide under mildly alkaline conditions. *Applied Surface Science*, 108, 333-344.

Pulido, G.I.D. and Salus, A.U. (2011). Contact angle study on the activation mechanisms of sphalerite with Cu(II) and Pb(II). *Revista de Metalurgia*, 47, 329-340.

Rao, S.R. and Leja, J. (2004). *Surface chemistry of froth flotation volume 1: fundamentals. 2nd edition*. New York: Kluwer Academic/Plenum Publishers

- Rao, S.R. (2004). *Surface chemistry of froth flotation volume 2: reagents and mechanisms. 2nd edition*. New York: Kluwer Academic/Plenum Publishers
- Ralston, J. and Healy, T.W. (1980). Activation of zinc sulphide with CuII, CdII and PbII: II. Activation in neutral and weakly alkaline media. *International Journal of Mineral Processing*, 7, 203-217.
- Rashchi, F., Sui, C. and Finch, J.A. (2002). Sphalerite activation and surface Pb ion concentration. *International Journal of Mineral Processing*, 67, 1, 43-58.
- Richardson, P. E. & Maust, E. E. Jr. (1976). Flotation. In Fuerstenau, M.C., ed., Gaudin Memorial Volume. AIME, 1, 364p.
- Robert, F. (1989). Internal structure of the Cadillac tectonic zone southeast of Val d'Or, Abitibi belt, Quebec. *Canadian Journal of Earth Sciences*, 26, 2661-2690.
- Robb, L.J. (2005). *Introduction to Ore-Forming Processes*. Malden: Blackwell Science Ltd.
- Rollinson, H. (2007). *Early Earth Systems A Geochemical Approach*. Oxford, Malden, Carlton: Blackwell Publishing. 285 pgs
- Ruonala, M. Heimala, S. Jounela, S. (1997). Different aspects of using electrochemical potential measurements in mineral processing. *International Journal of Mineral Processing*, 51, 97-110.
- Savoie, A., Sauve, P., Trudel, P. and Perrault, G. 1990: Geologie de la mine Doyon, Cadillac, Quebec. In The northwestern Quebec polymetallic belt. Rive, M., Verpaelst, P., Gagnon, Y., Lulin, J.M., Riverin, G. and Simard, A., eds., *Canadian Institute of Mining and Metallurgy, Special Volume 43*, 401-412.
- Savoie, A., Trudel, P., Sauvé, P., Hoy L. and Kheang L. (1991). Géologie de la mine Doyon (Région de Cadillac). Ministère de l'Énergie et des Ressources, Québec, ET 90-05.

- Seke, M.D. and Pistorius, P.C. (2005). The effect of mode of occurrence of galena and sphalerite on the selective flotation of ore samples from the Rosh Pinah Mine. *The Journal of the South African Institute of Mining and Metallurgy*, 105, 653-662.
- Shen, W.Z., Fornasiero, D. and Ralston, J. (2001). Flotation of sphalerite and pyrite in the presence of sodium sulfite. *International Journal of Mineral Processing*, 63, 1, 17-18.
- Simpson, D.J., Bredow, T., Chandra, A.P., Cavallaro, G.P. and Gerson, A.R. (2011). The effect of iron and copper impurities on the wettability of sphalerite (110) surface. *Journal of Computational Chemistry*, 32, 2022-2030.
- Smart, R.S.C., Amarantidis, J., Skinner, W., Prestidge, C.A., LaVanier, L. and Grano, S. (1998). Surface analytical studies of oxidation and collector adsorption in sulfide mineral flotation. *Scanning Microscopy*, 12, 4, 553-583.
- Smart, R.St.C., Amarantidis, J., Skinner, W.M., Prestidge, C.A., LaVanier, L. and Grano, S.G. (2003). Surface Analytical Studies of Oxidation and Collector Adsorption in Sulfide Mineral Flotation. In Wandelt, K. and Thurgate, S. (editors). *Solid-Liquid Interfaces. Topics in Applied Physics*, Springer-Verlag, Berlin, 85, 3-60.
- Smart, R.St.C., Gerson, A.R., Hart, B.R., Beattie, D.A. and Young, C. (2013). Innovations in measurement of mineral structure and surface chemistry in flotation: past, present and future. SME Publication In Press.
- Solecki, J., Komosa, A. and Szczypa, J. (1979). Copper ion activation of synthetic sphalerites with various iron contents. *International Journal of Mineral Processing*, 6, 3, 221-228.
- Stanley, S.M. (2009). *Earth system history 3rd Edition*. W.H. Freeman and Company 608 pgs.
- Stockwell, C.H. (1982). Proposals for time classification and correlation of Precambrian rocks and events in Canada and adjacent areas of the Canadian Shield, Part I: a time classification of Precambrian rocks and events. *Geological Survey of Canada, Paper 80, 19*, 135 pp.

Stone, W. E. (1990). Archean volcanism and sedimentation in the Bousquet gold district, Abitibi greenstone belt, Quebec: Implications for stratigraphy and for stratigraphy and gold concentration. *Geological Society of America Bulletin*, 102, 147-158.

Sui, C.C., Lee, D., Casuge, A. and Finch, J.A. (1999). Comparison of the activation of sphalerite by copper and lead. *Minerals and Metallurgical Processing*, 16, 3, 53-61.

Sutcliffe, R.H., Barrie, C.T., Burrows, D.R. and Beakhouse, G.P. (1993). Plutonism in the southern Abitibi Subprovince: a tectonic and petrogenetic framework. *Economic Geology*, 88, 1359-1375.

Sutherland, K.L. & Wark, I.W. eds. (1955). *Principles of flotation*. Melbourne: Australasian Institute of Mining and Metallurgy.

Szczypa, J., Solecki, J. and Komosa, A. (1980). Effect of surface oxidation and iron contents on xanthate ions adsorption of synthetic sphalerites. *International Journal of Mineral Processing*, 7, 151-157.

Thurston, P.C. (2002). Autochthonous development of Superior Province greenstone belts? *Precambrian Research*, 115, 11-36.

Thurston, P.C., Ayer, J.A., Goutier, J. and Hamilton, M.A. (2008). Depositional gaps in Abitibi Greenstone Belt stratigraphy: A key to exploration for syngenetic mineralization. *Economic Geology*, 103, 6, 1097-1134.

Tourigny, G., Doucet, D., and Bourget, A. (1993). Geology of the Bousquet 2 mine: An example of a deformed, gold-bearing, polymetallic sulfide deposit. *Economic Geology*, 88, 1578-1597.

Trahar, W. J. (1984). The influence of pulp potential in sulphide flotation. In Jones, M.H. & Woodcock, J.T., Eds., *Principles of Mineral Flotation*. The Wark symposium. *Australian Institute of Mineral Metallurgy*. Parkville, Victoria, Australia, 117- 135.

Trudel, P., Sauvé, P., Tourigny, G., Hubert, C. & Hoy, L. (1992). Synthèse des Caractéristiques Géologiques des Gisements de la Région de Cadillac (Abitibi). *Ministère des l'Energie et des Ressources, Québec, MM.*

Tukel, C., Kelebek, S., and Yalcin, E. (2010). Eh-pH stability diagrams for analysis of polyamine interaction with chalcopyrite and deactivation of Cu-activated pyrrhotite. *Canadian Metallurgical Quarterly*, 49, 4, 411-418.

Valliant, R.I. & Hutchinson, R.W. (1982). Stratigraphic distribution and genesis of gold deposits, Bousquet Region, North-western Quebec. In Hodder, R.W. and Petruk, W., eds., *Geology of Canadian Gold Deposits. Canadian Institute of Mining and Metallurgy, Special Volume 24*, 27-40.

Von Reeken, F.J.M., Lange, J., Steensma, J.J.S. and Duyvesteyn, W.P.C. (1989). Factors Affecting the Lead-Zinc Separation at the Grund Concentrator. *International Journal of Mineral Processing*, 27, 21-37.

Wagner, C.D., Naumkin, A.V., Kraut-Vass, A., Allison, J.W., Powell, C.J. and Rumble, J.R.Jr. (2003). NIST Standard Reference Database 20, Version 3.4 (web version) (<http://srdata.nist.gov/xps/>).

Wenk, H.R. and Bulakh, A.G. (editors) (2004). *Minerals: their constitution and origin*. Cambridge; New York: Cambridge University Press.

Wilkinson, L., Cruden, A.R. and Krogh, T.E. (1999). Timing and kinematics of post-Timiskaming deformation within the Larder Lake - Cadillac deformation zone, southwest Abitibi greenstone belt, Ontario, Canada. *Canadian Journal of Earth Sciences*, 36, 627-647.

Wills, B.A., ed. (1997). *Mineral processing technology: an introduction to the practical aspects of ore treatment and mineral recovery. 6th ed.* Boston: Butterworth-Heinemann.

Wills, B.A. (2010). *Mineral processing technology, 7th Edition*. Elsevier online Handbook.

Woods, R. (1971). The oxidation of ethyl xanthate on platinum, gold, copper, and galena electrodes, relation to the mechanism of mineral flotation. *Physical Chemistry*, 75, 354–362.

Wyman, D.A., Kerrich, R. and Polat, A. (2002). Assembly of Archean cratonic mantle lithosphere and crust: plume-arc interaction in the Abitibi-Wawa subduction-accretion complex. *Precambrian Research*, 115, 37- 62.

Ye, X., Gredelj, S., Skinner, W. and Grano, S.R. (2010). Regrinding sulphide minerals – breakage mechanisms in milling and their influence on surface properties and flotation behavior. *Powder Technology*, 203, 133-147.

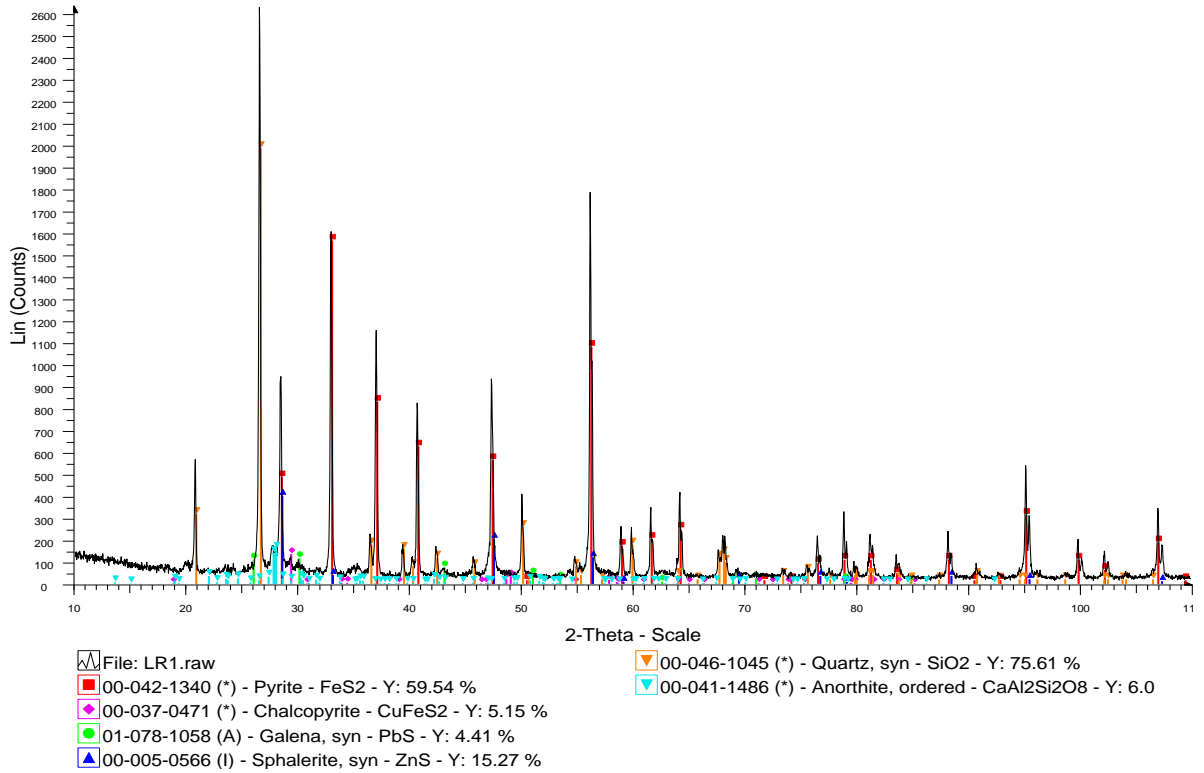
Yu, R., Hu, Y., Qiu, G. and Qin, W. (2004b). A voltammetric study of engineering, 24(1) (in Chinese)

Yu, R., Hu, Y., Qiu, G. and Qin, W. (2004c). Interaction mechanism of jamesonite with flotation collectors by cyclic voltammetry. *Journal of Central South University*, 35(2), 202 - 206 (in Chinese)

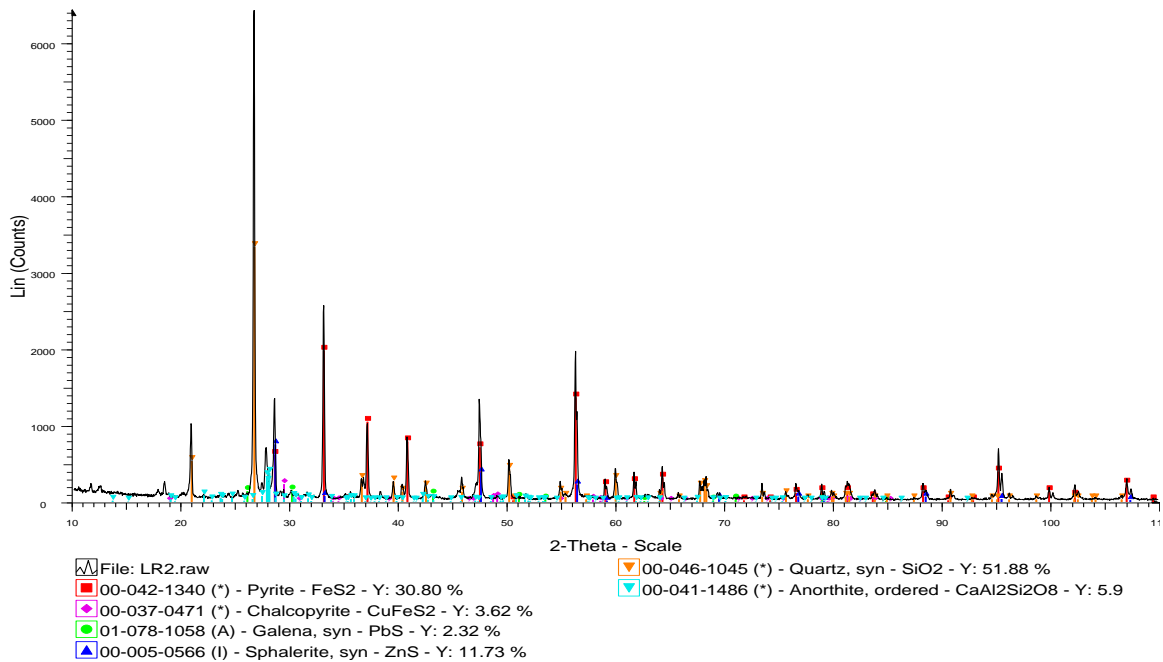
Appendices

1 Appendix A – LaRonde Mill Test

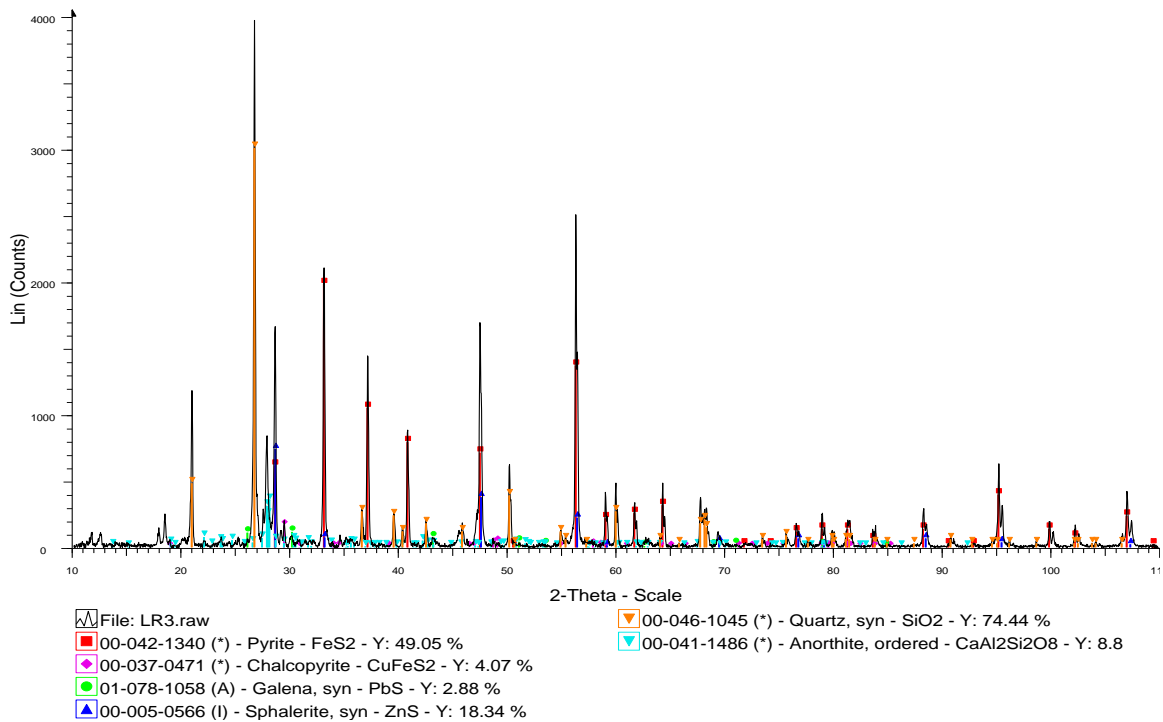
1.1 XRD Plots for LaRonde Mill Samples



A-1 1 XRD Plot for LR1 (LaRonde Mill Feed Sample)

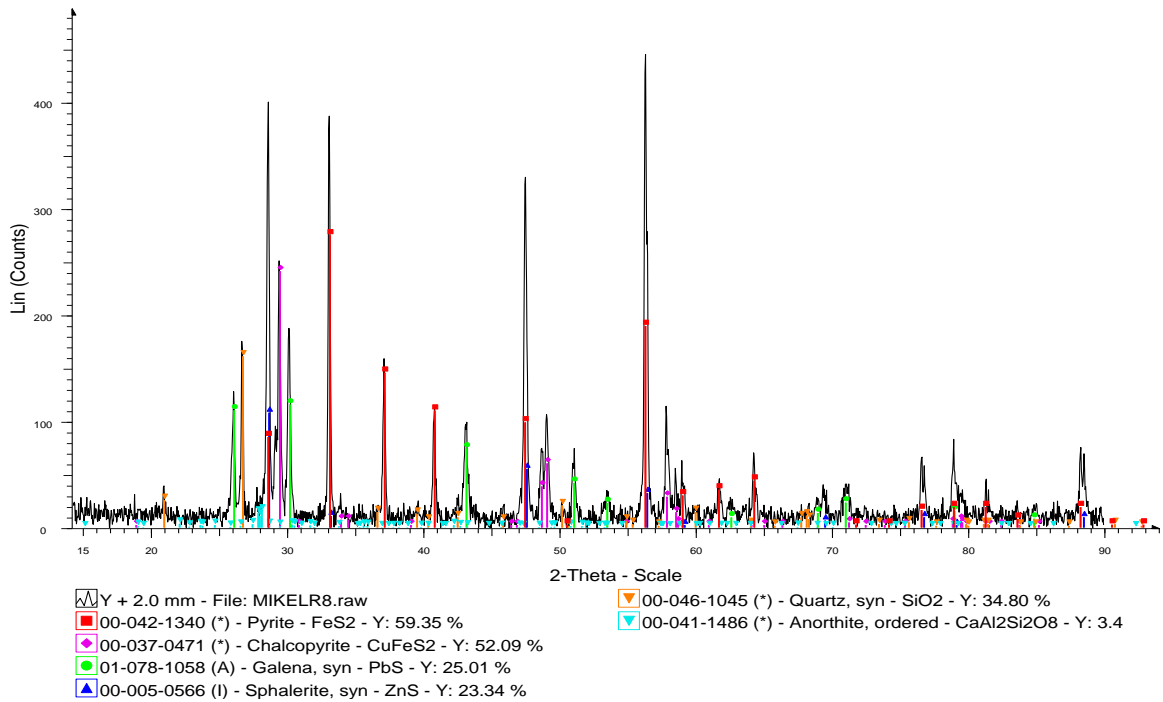


A-1 2 XRD Plot for LR2 (LaRonde Mill Conditioned Feed Sample)

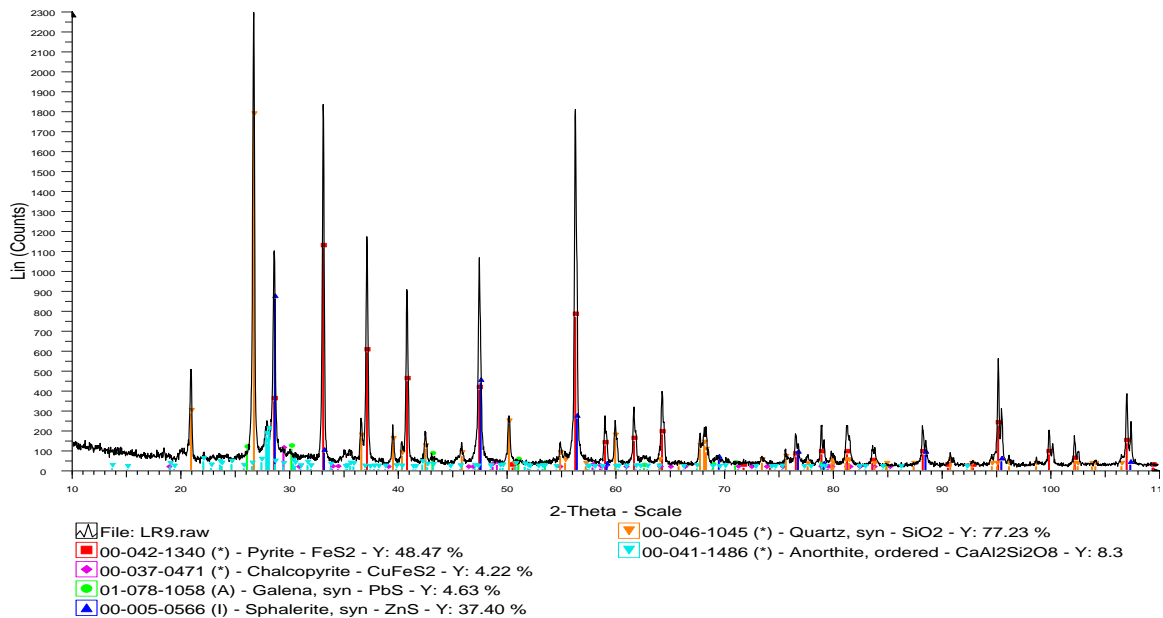


A-1 3 XRD Plot for LR3 (LaRonde Mill Rougher Concentrate Sample from Column

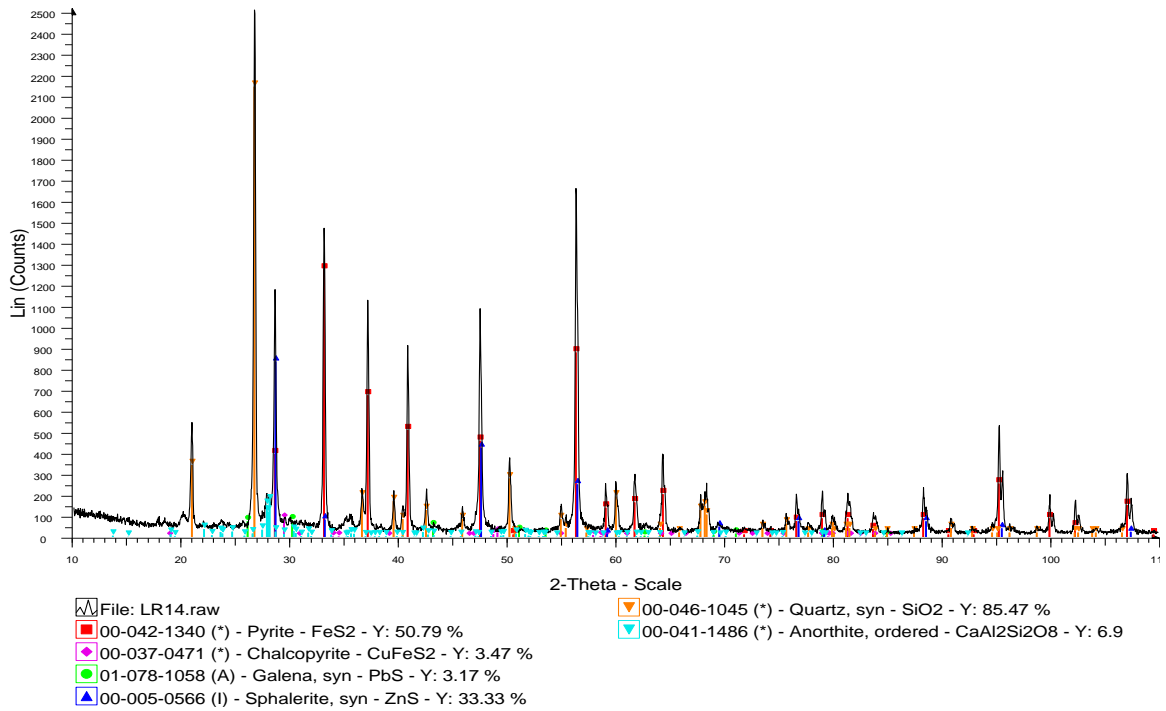
1)



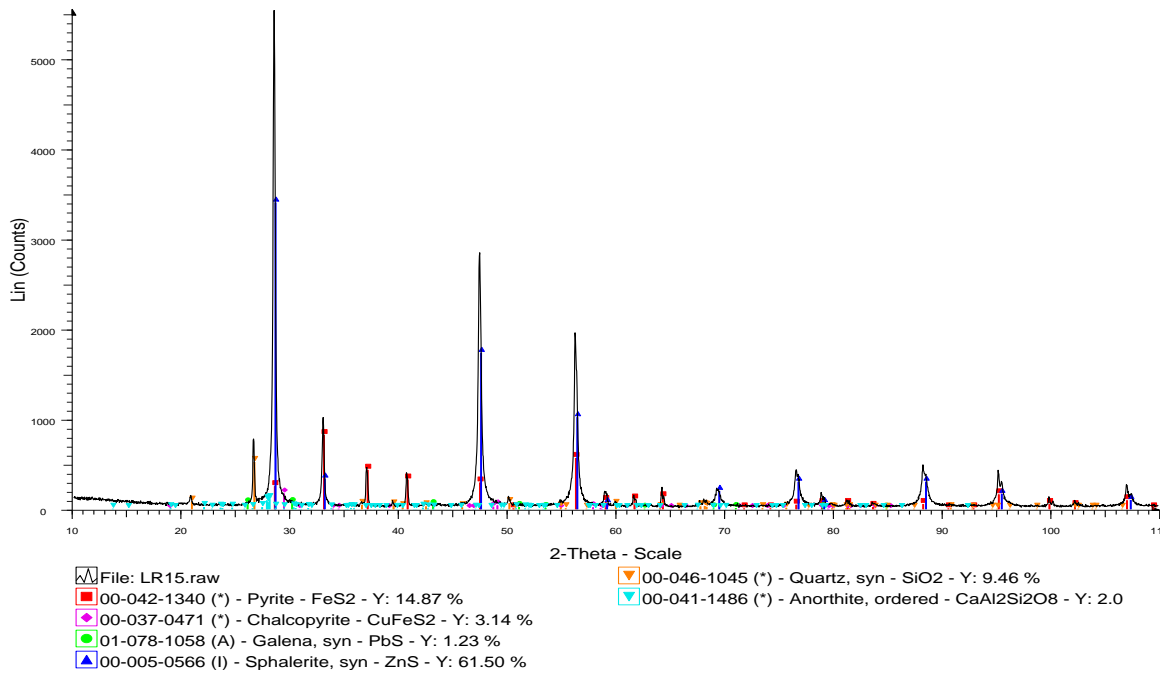
A-1 4 XRD Plot for LR8 (LaRonde Mill Cu Circuit Primary Rougher Concentrate Sample)



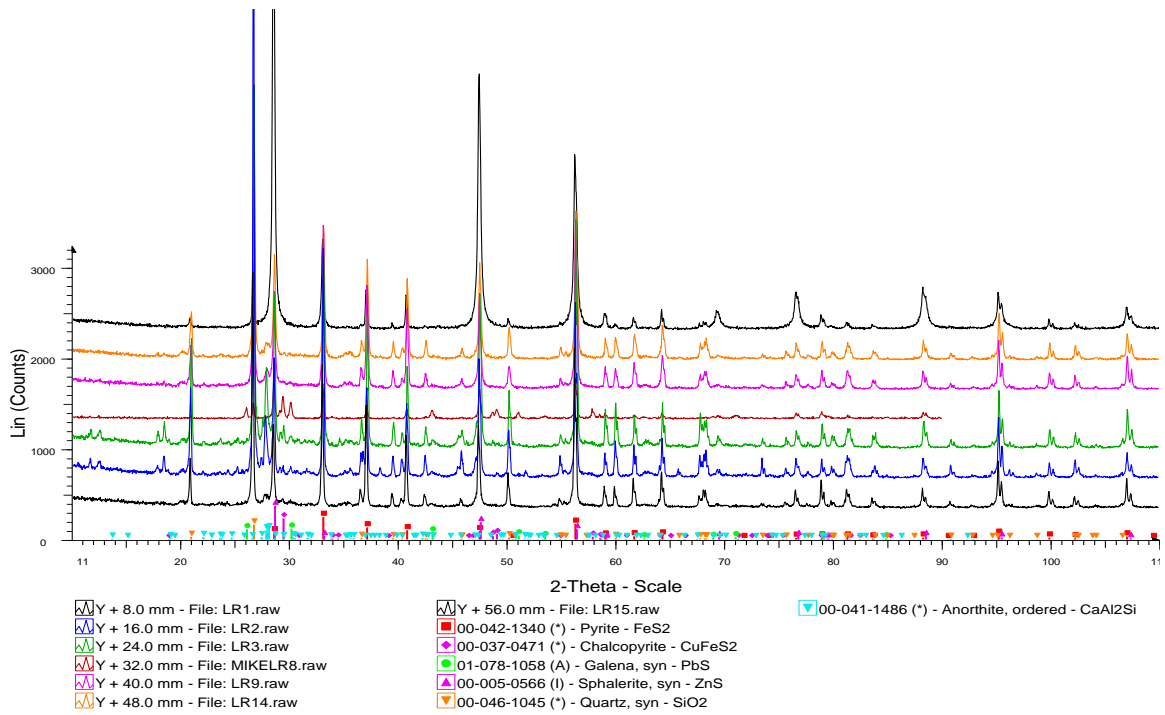
A-1 5 XRD Plot for LR9 (LaRonde Mill Rougher Tail Sample from Column 1)



A-1 6 XRD Plot for LR14 (LaRonde Mill Cu/Pb Circuit Tail – Zn Circuit Feed Sample)

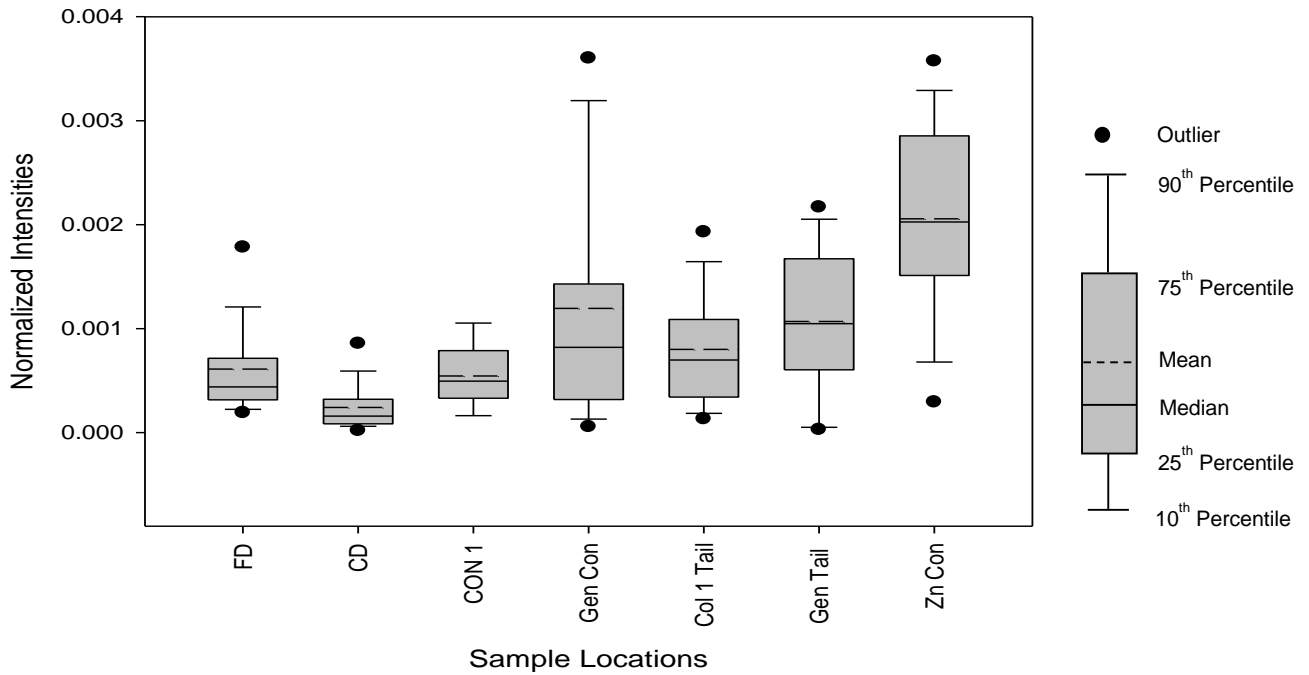


A-1 7 XRD Plot for LR15 (LaRonde Mill Primary Zn Concentrate Sample)

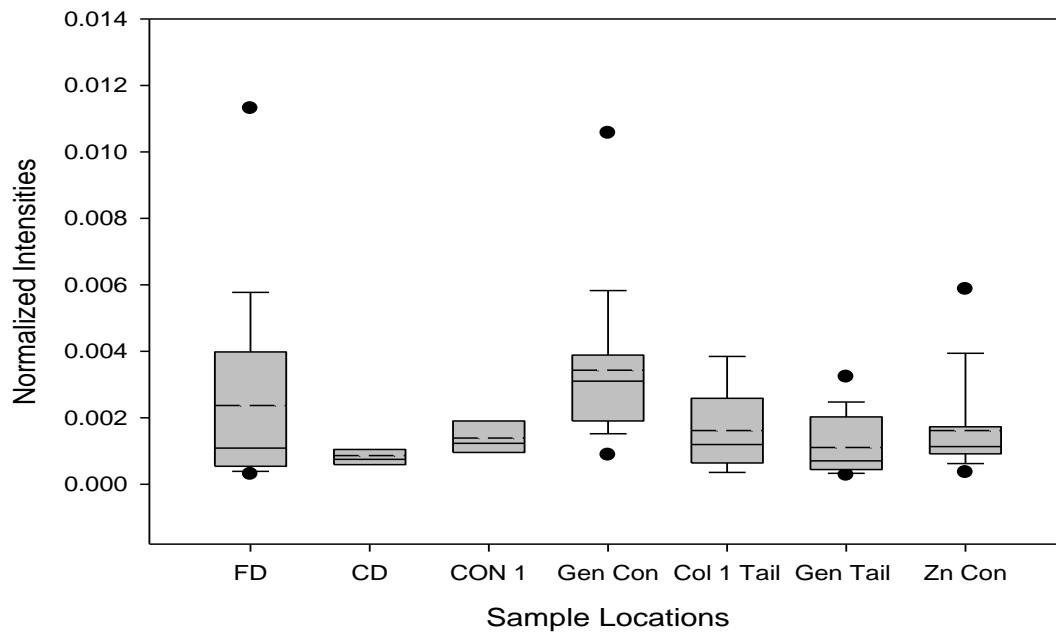


A-1 8 XRD Stacked Plots of the LaRonde Mill Samples

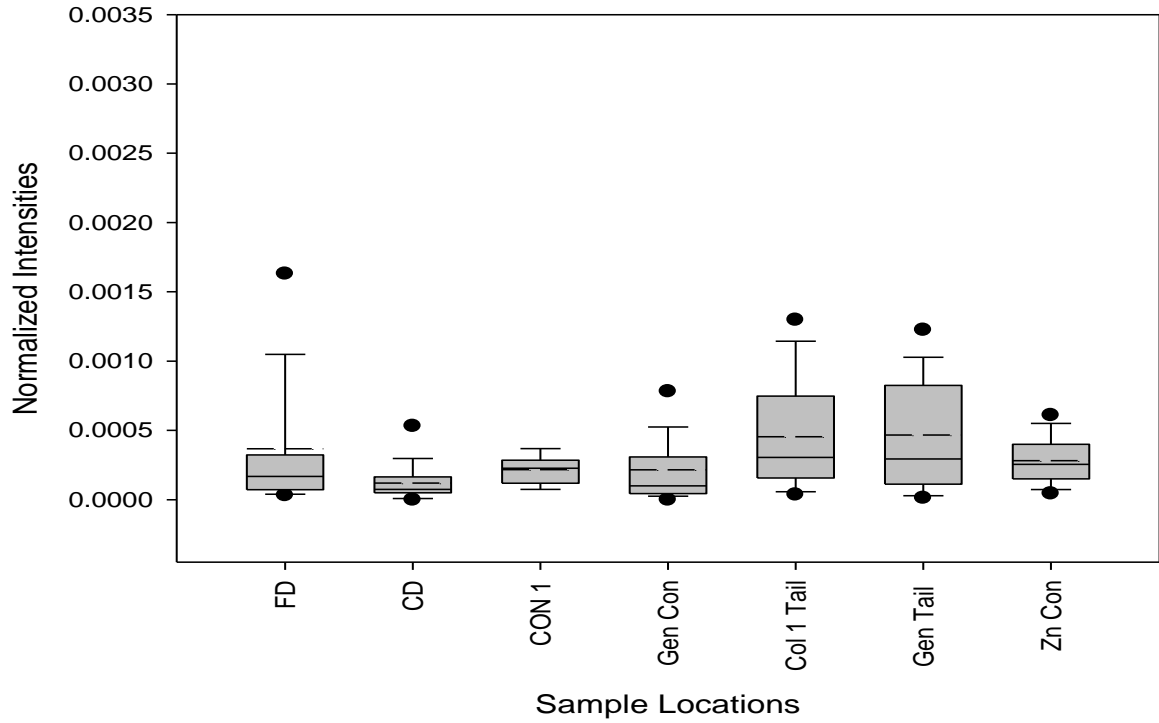
1.2 Vertical Box Plots of TOF-SIMS Data for LaRonde Mill Samples.



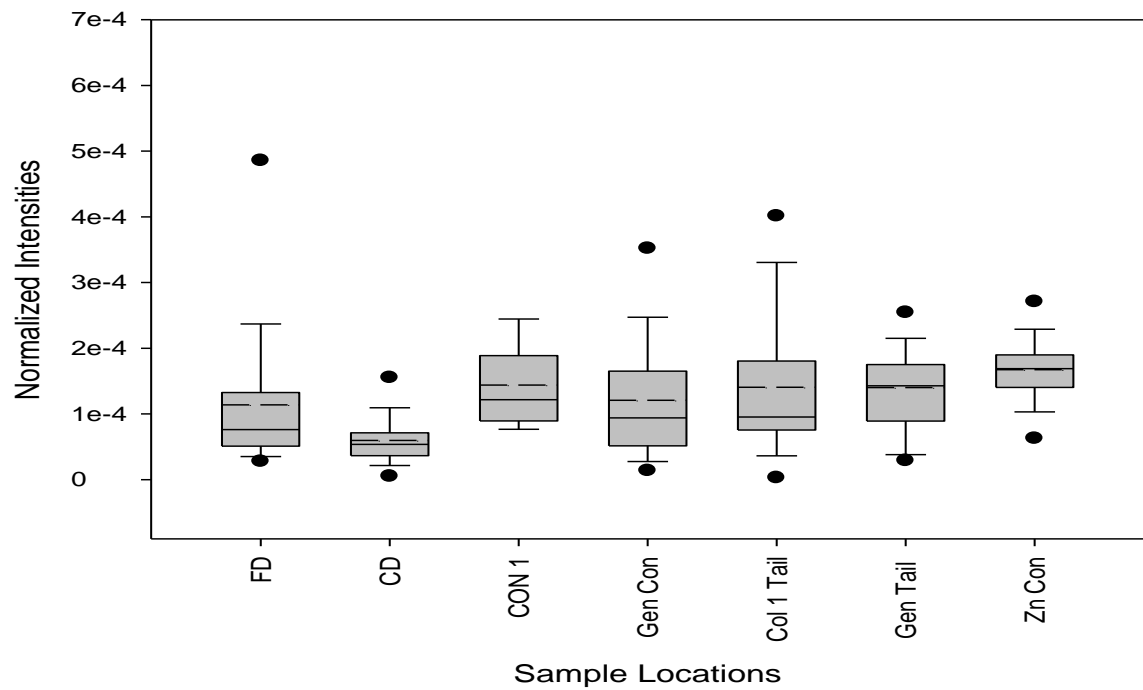
A-2 1 ZnS intensities on sphalerite grains from the LaRonde mill samples



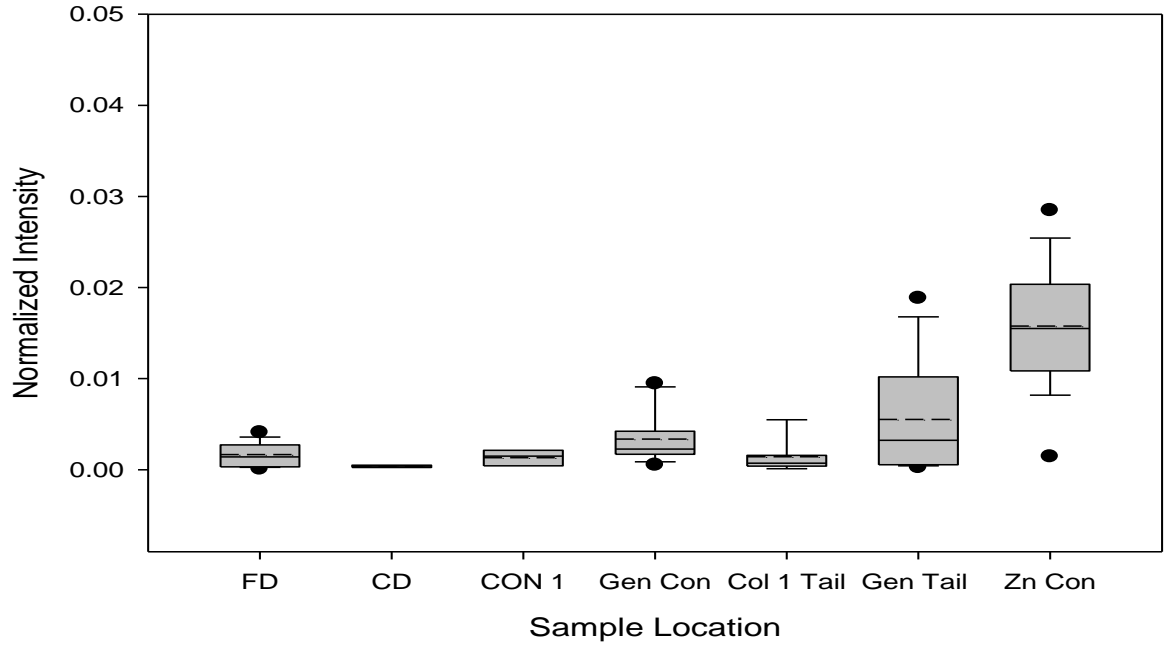
A-2 2 Zn intensities on sphalerite grains from the LaRonde mill samples



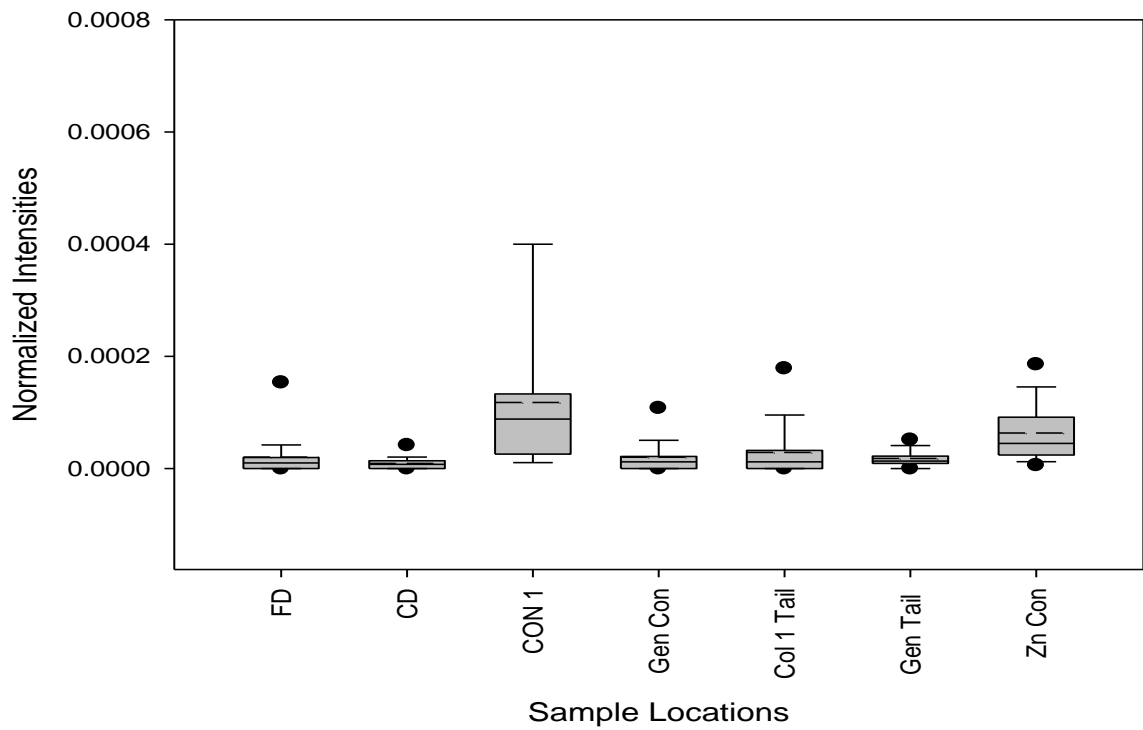
A-2 3 ZnO intensities on sphalerite grains from the LaRonde mill samples



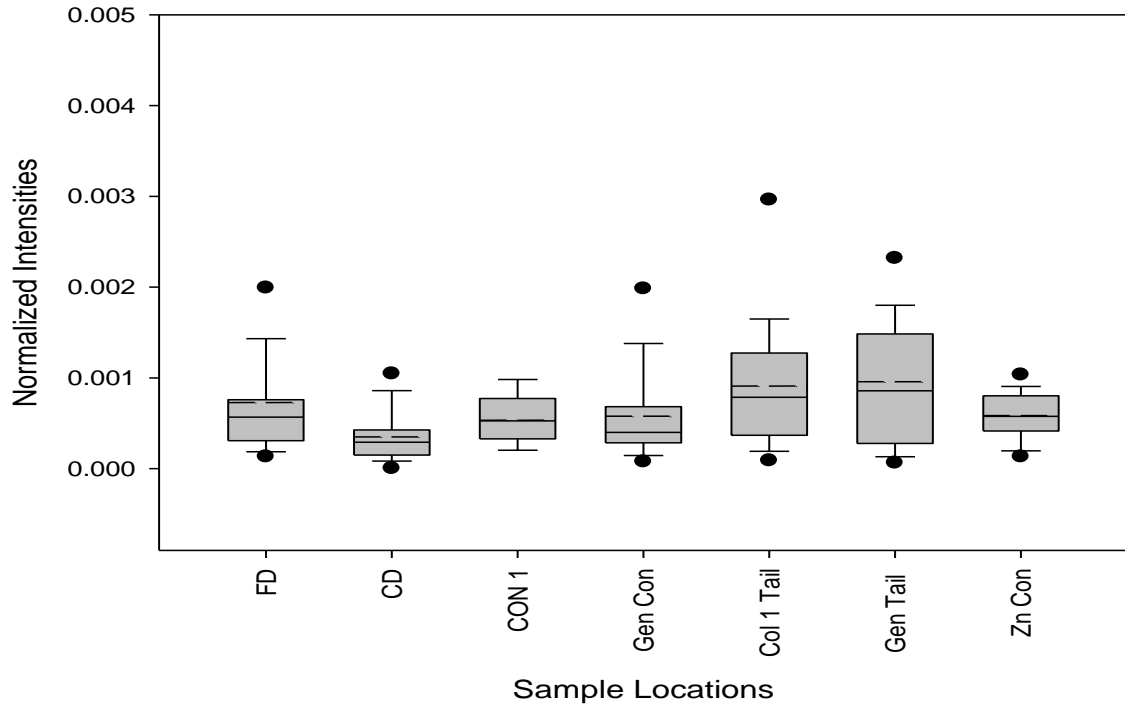
A-2 4 ZnOH intensities on sphalerite grains from the LaRonde mill samples



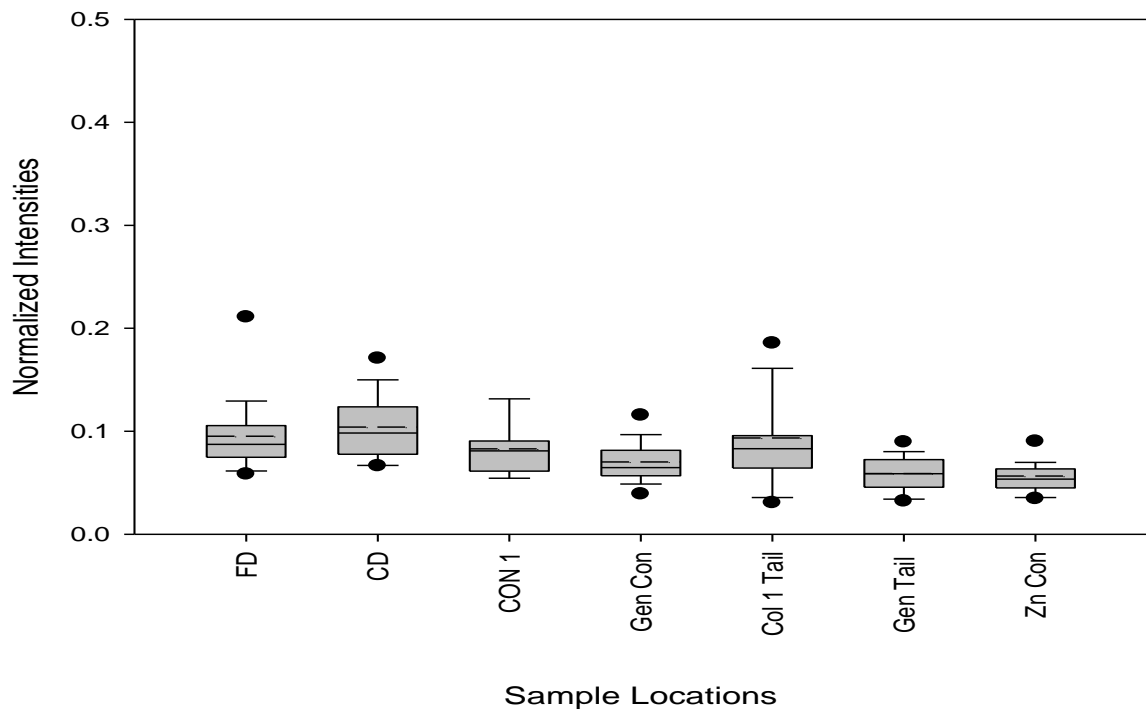
A-2 5 Cu intensities on sphalerite grains from the LaRonde mill samples



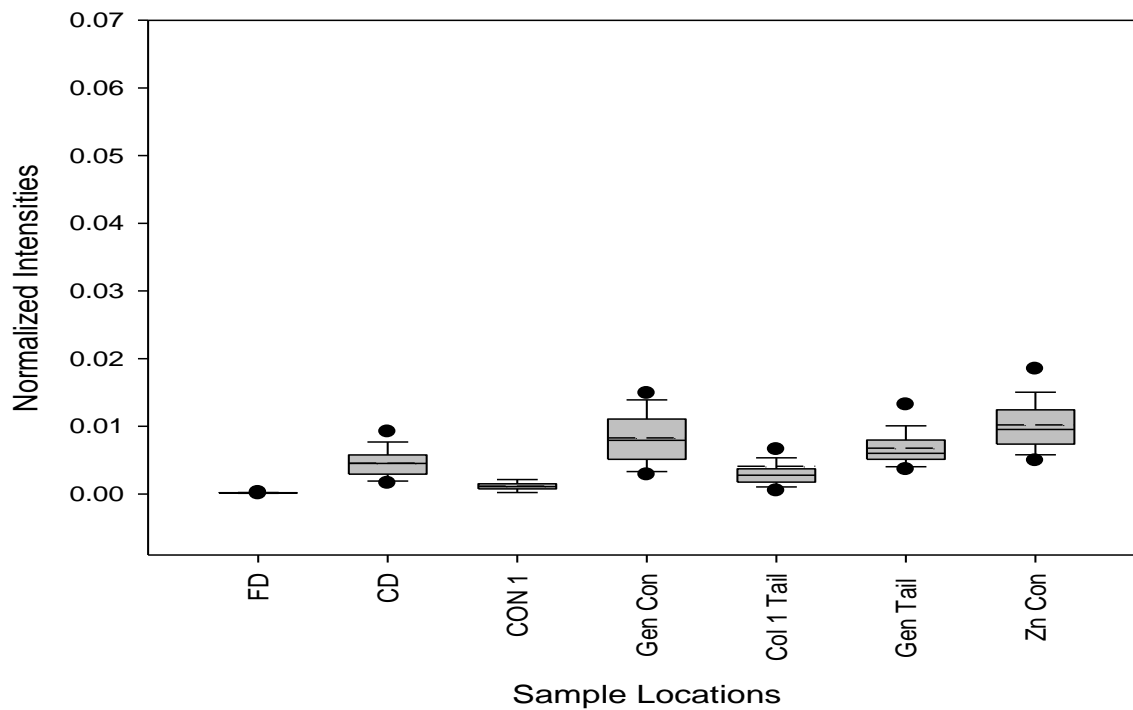
A-2 6 CuO intensities on sphalerite grains from the LaRonde mill samples



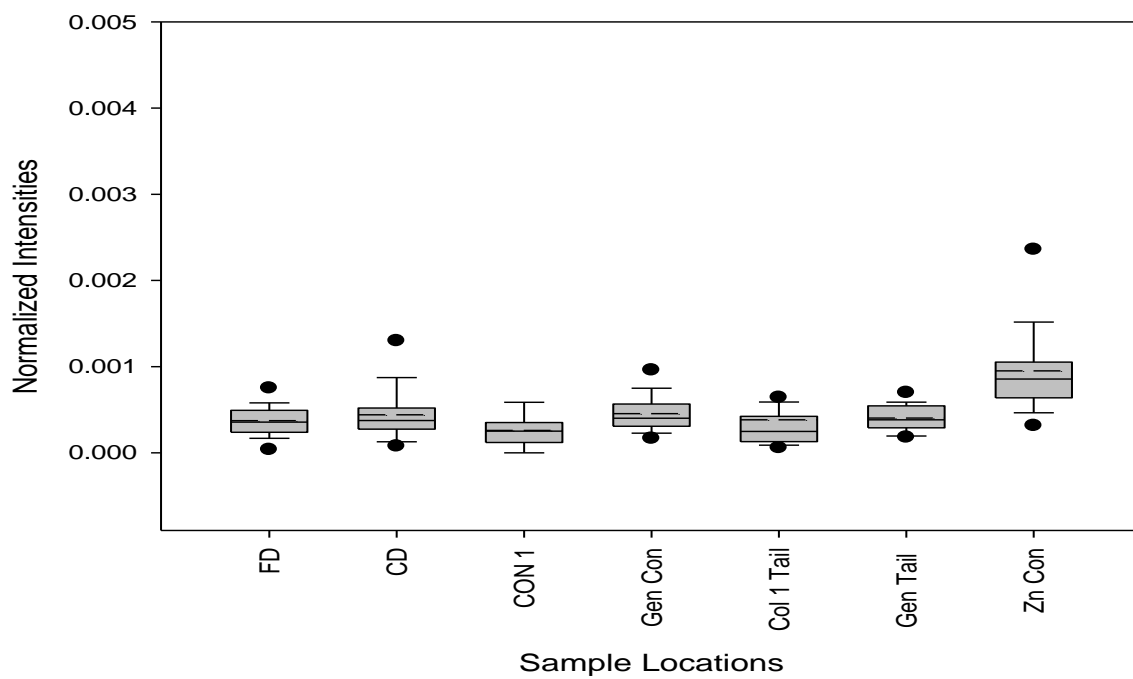
A-2 7 CuOH intensities on sphalerite grains from the LaRonde mill samples



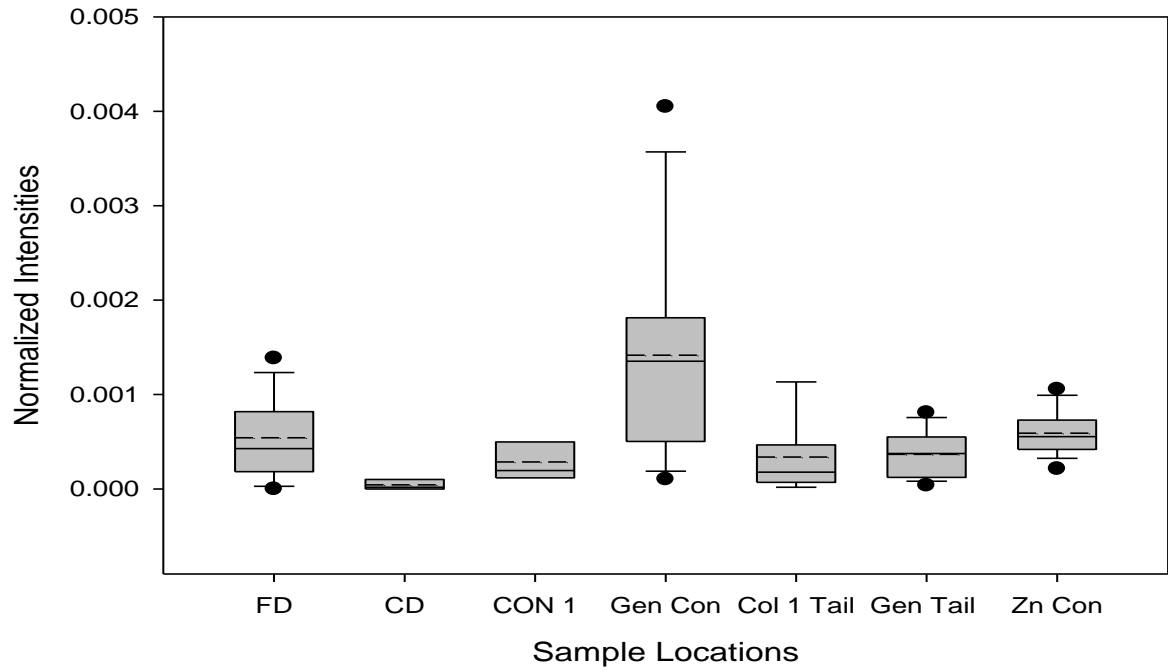
A-2 8 OH intensities on sphalerite grains from the LaRonde mill samples



A-2 9 SO₃ intensities on sphalerite grains from the LaRonde mill samples



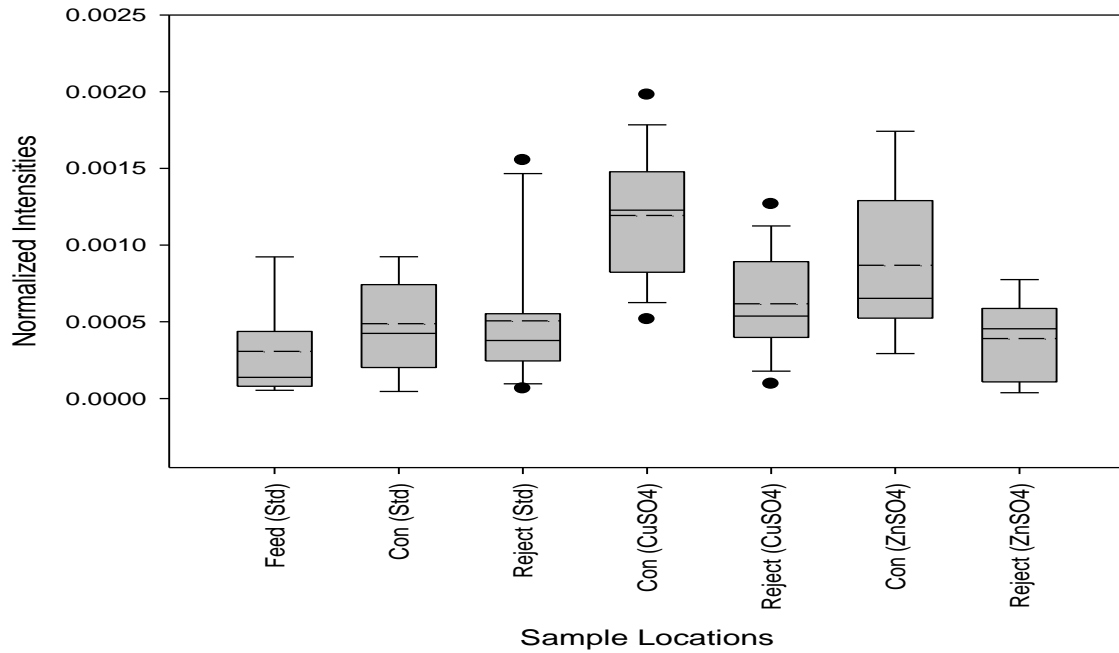
A-2 10 SO₄ intensities on sphalerite grains from the LaRonde mill samples



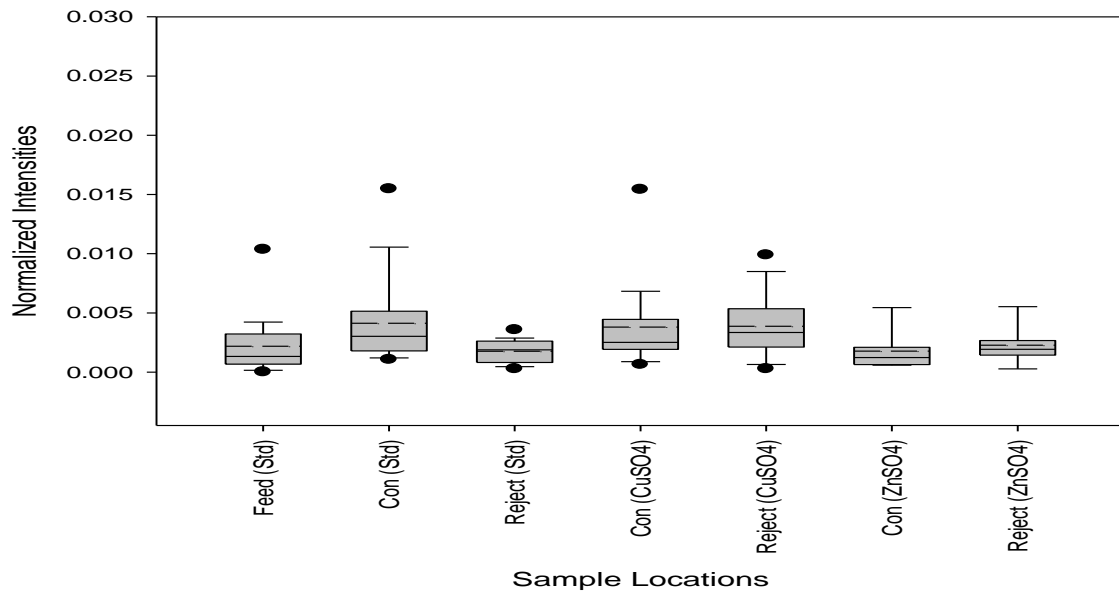
A-2 11 Pb intensities on sphalerite grains from the LaRonde mill samples

2 Appendix B – Instrumented Mill Test

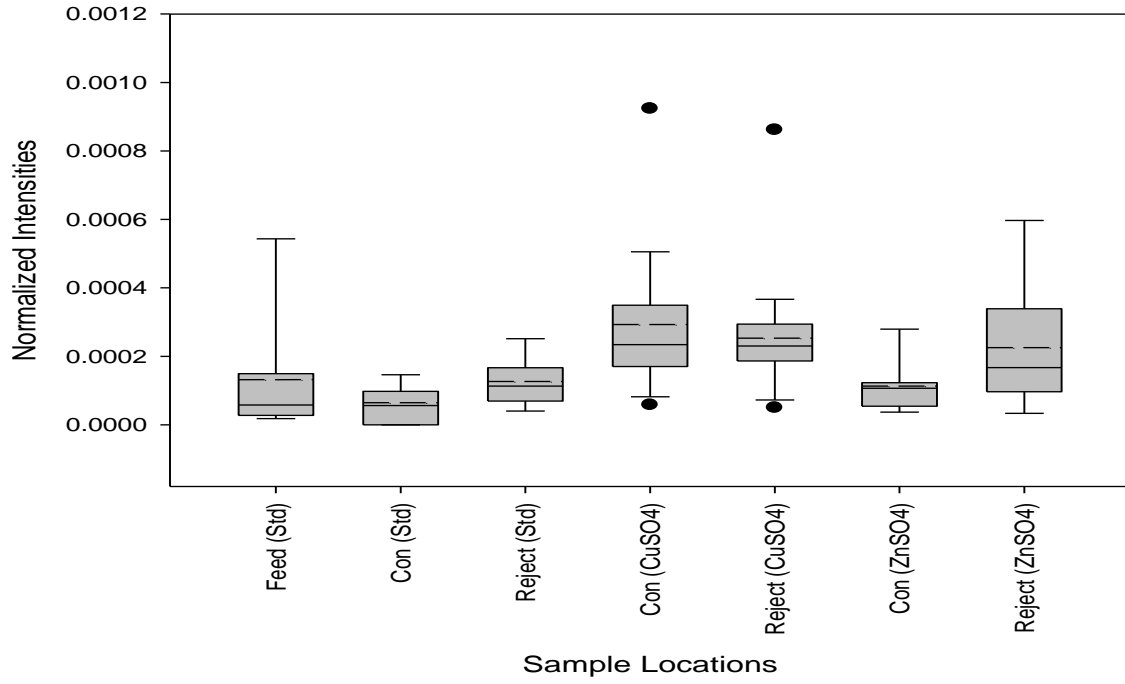
2.1 Vertical Box Plots of TOF-SIMS Data



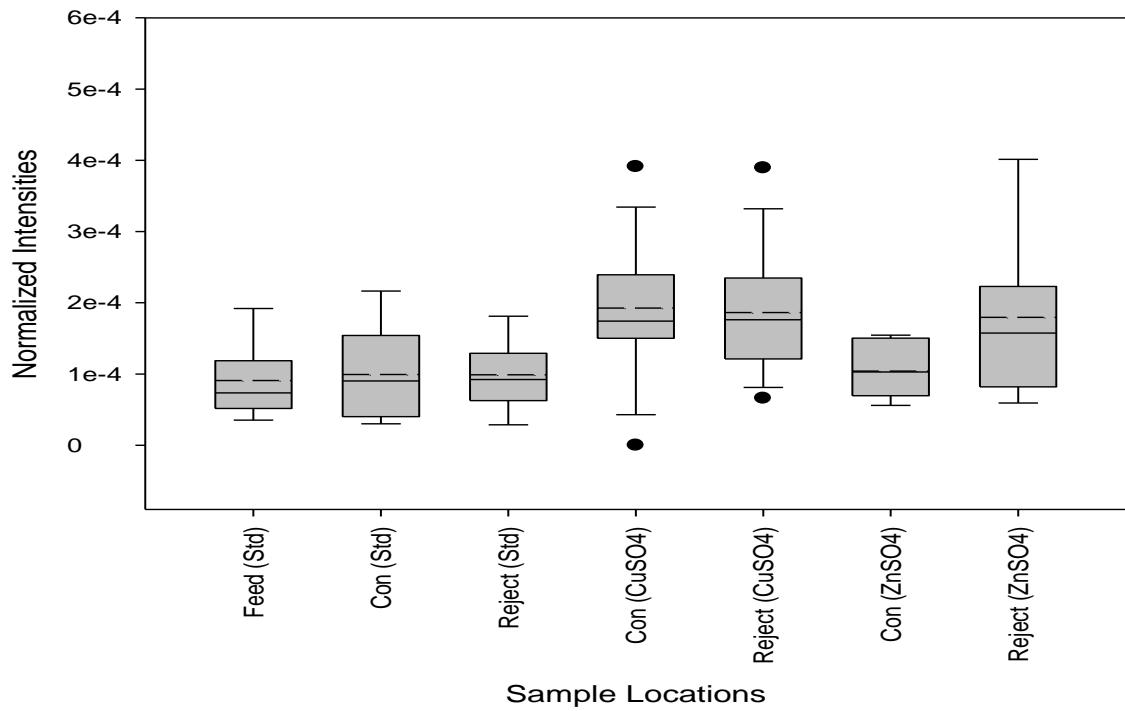
B-1 1 ZnS on sphalerite grains in the instrumented mill samples



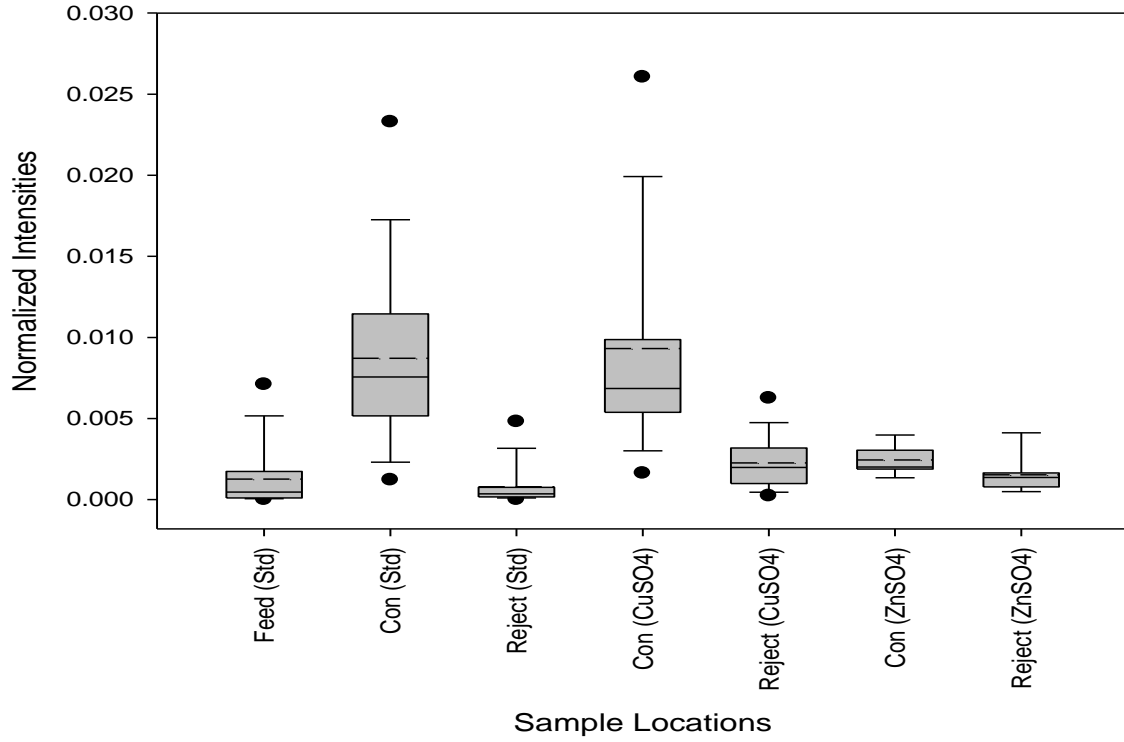
B-1 2 Zn intensities on sphalerite surfaces in instrumented mill tests



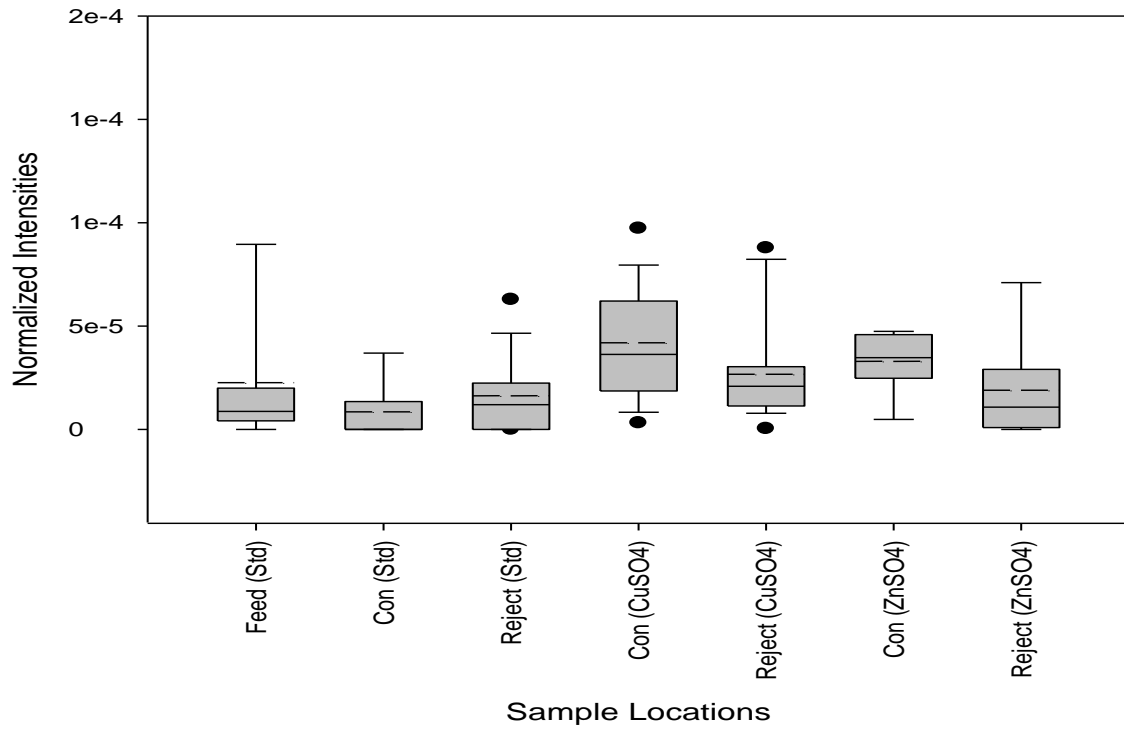
B-1 3 ZnO on sphalerite grains in the instrumented mill tests



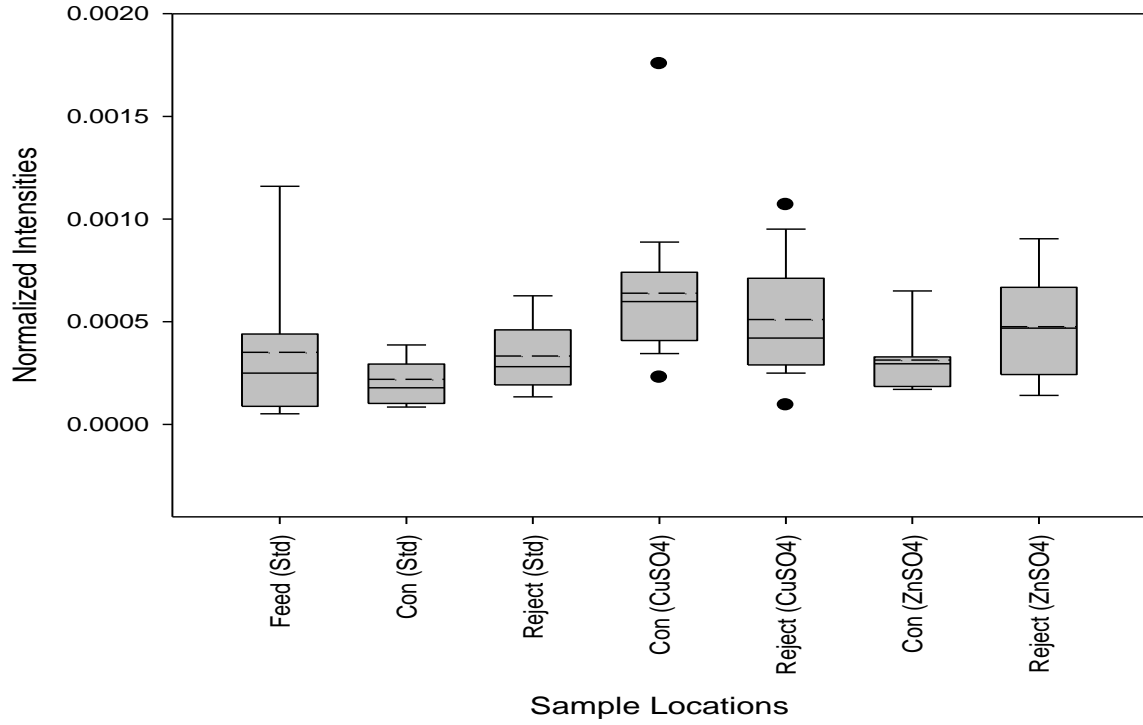
B-1 4 ZnOH on sphalerite grains in the instrumented mill tests



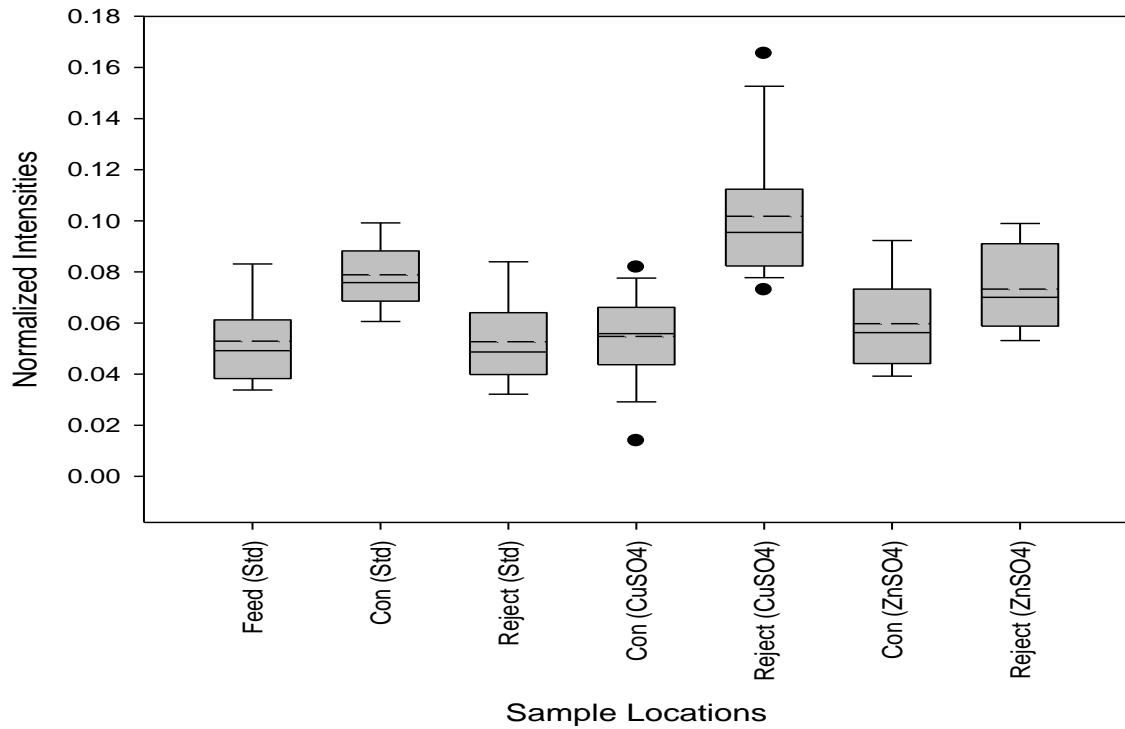
B-1 5 Cu on sphalerite grains in the instrumented mill tests



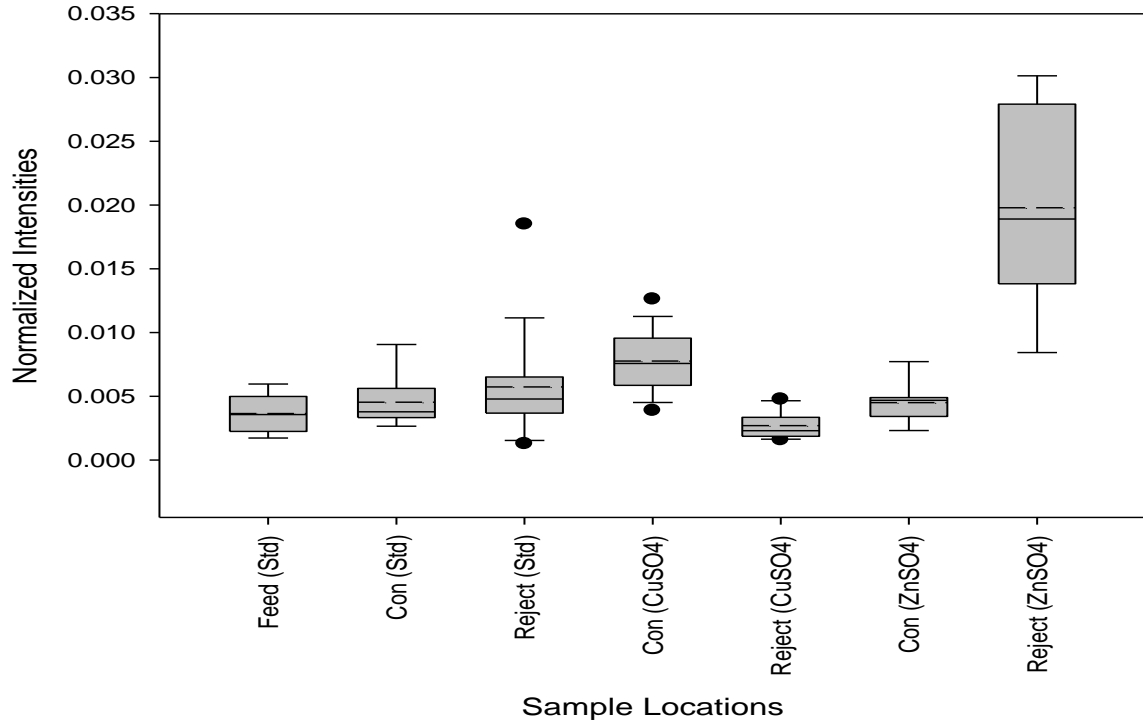
B-1 6 CuO on sphalerite grains in the instrumented mill tests



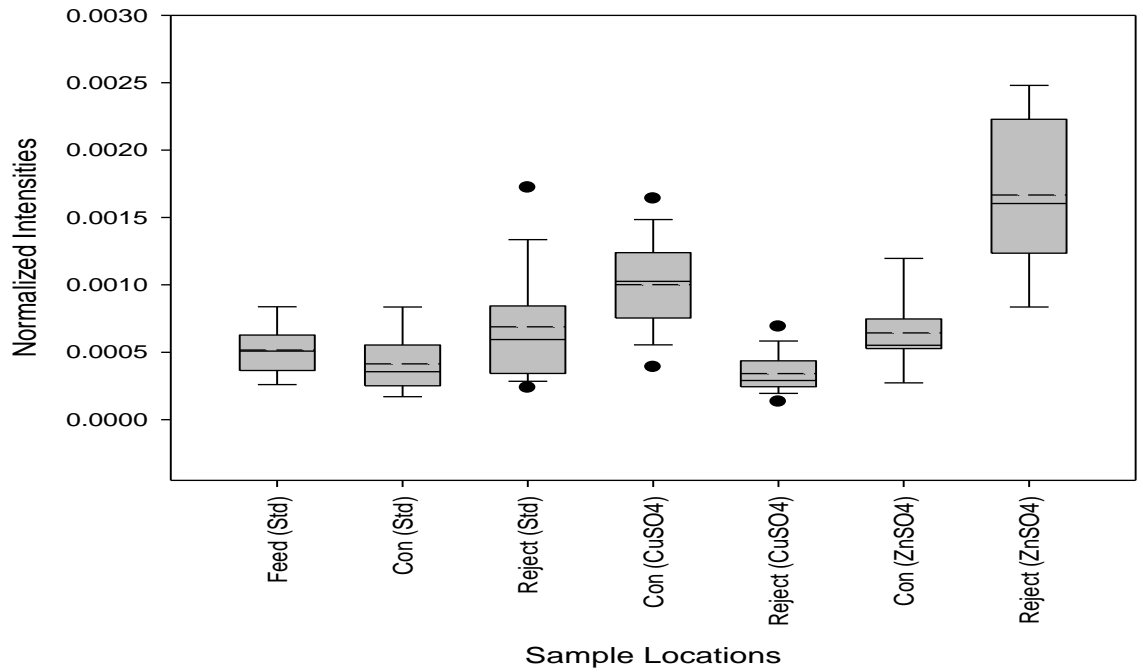
B-1 7 CuOH on sphalerite grains in the instrumented mill tests



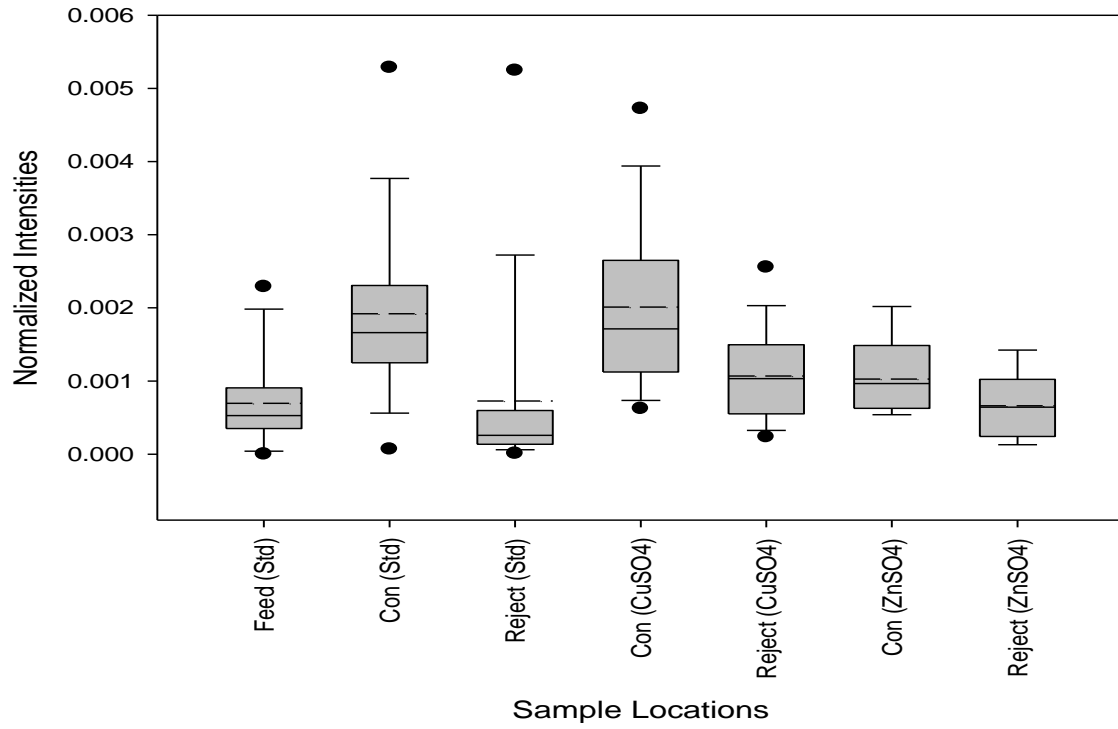
B-1 8 OH on sphalerite grains in the instrumented mill tests



B-1 9 SO₃ on sphalerite grains in the instrumented mill tests



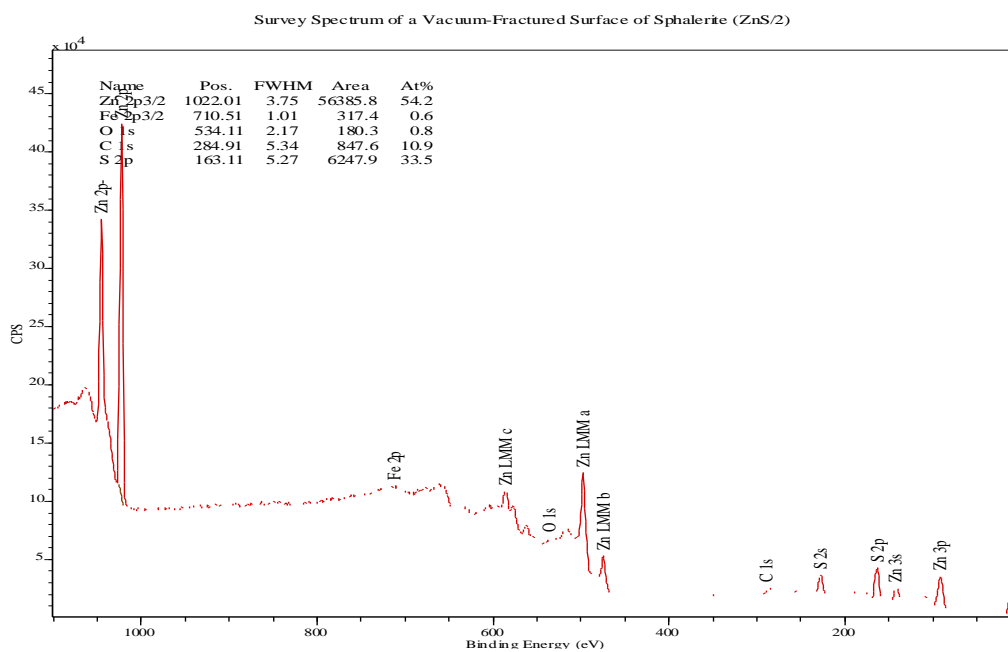
B-1 10 SO₄ on sphalerite grains in the instrumented mill tests



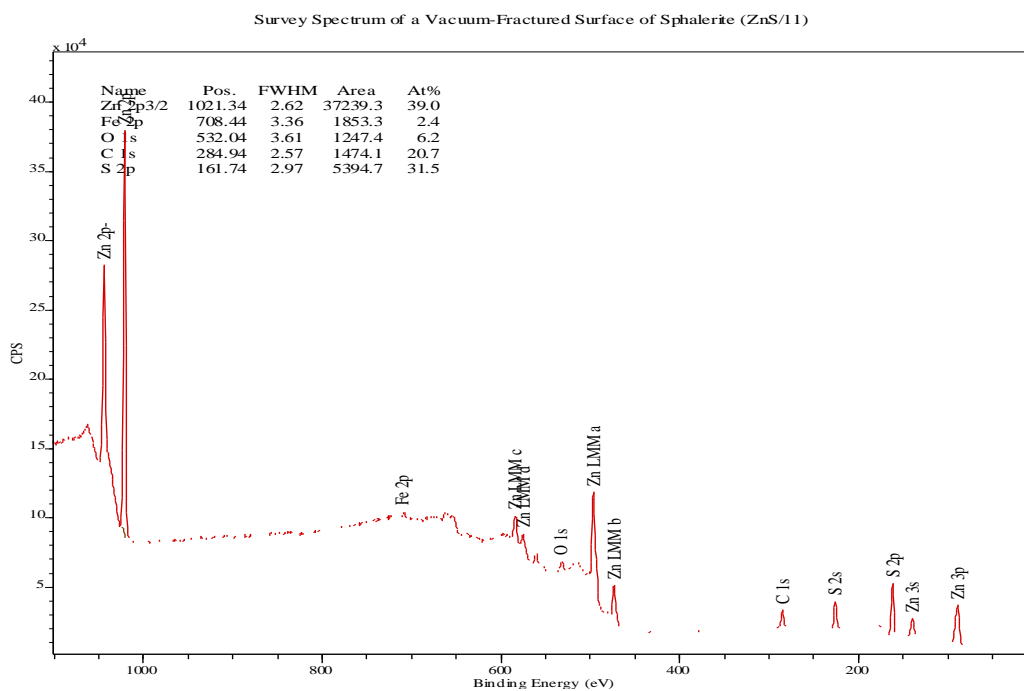
B-1 11 Pb on sphalerite grains in the instrumented mill tests

3 Appendix C – Bench Tests

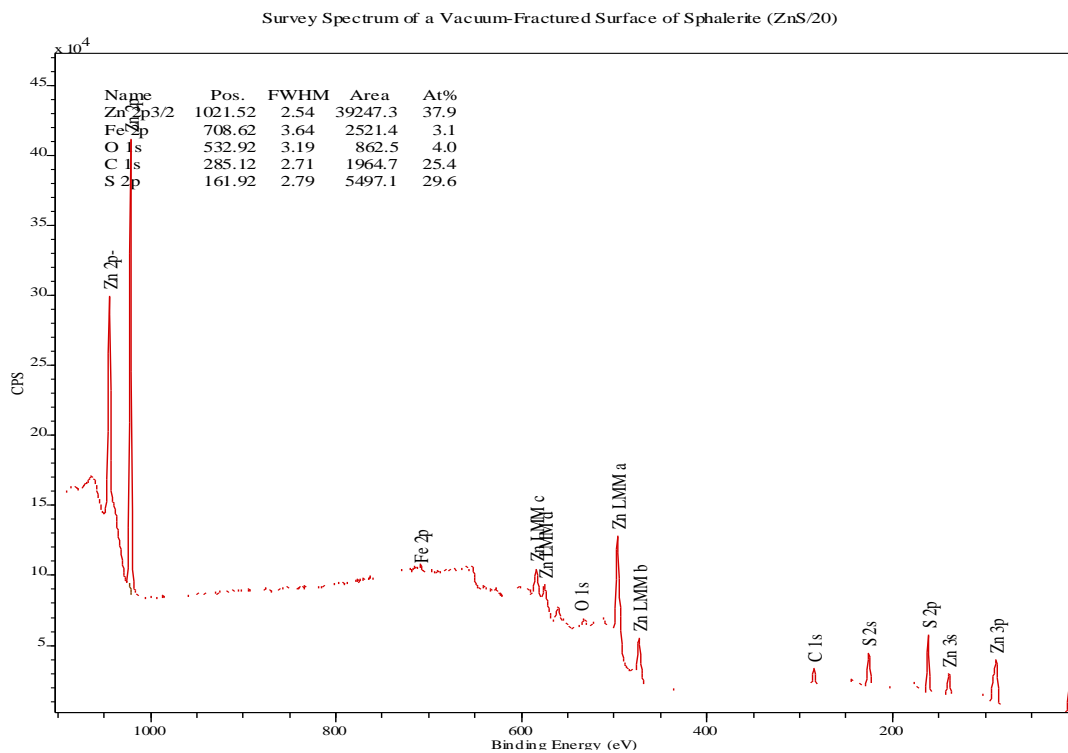
3.1 XPS Survey Spectra



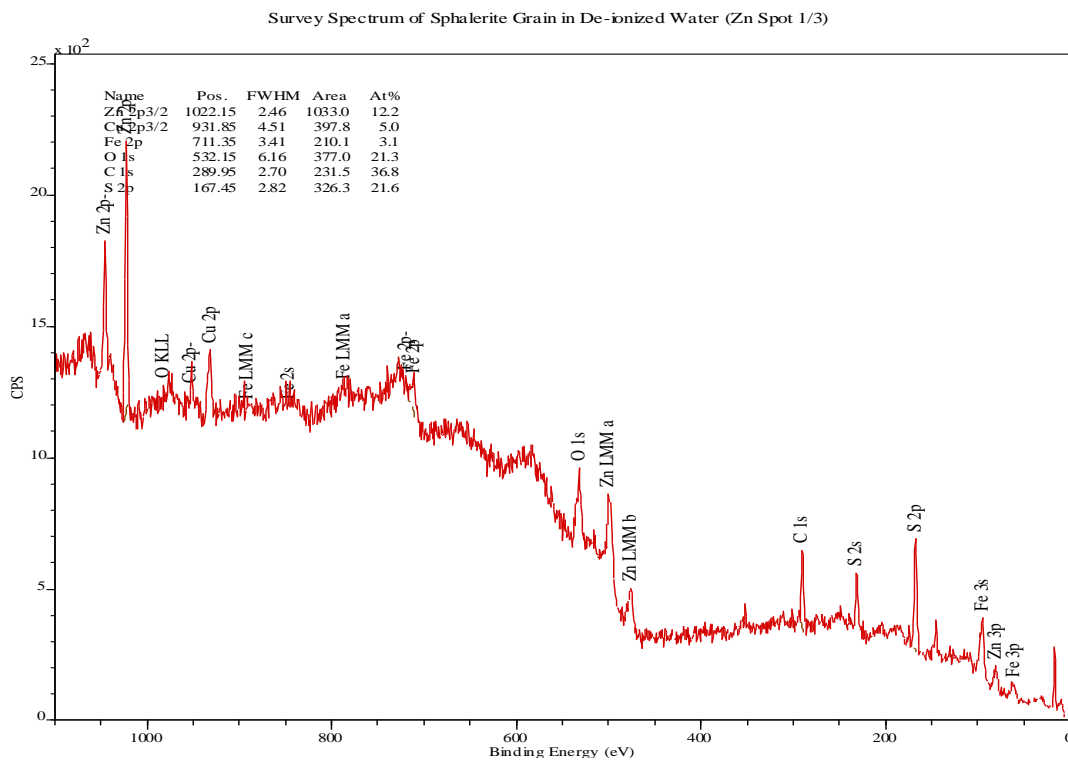
C-1 1 Survey spectrum of a vacuum-fractured sphalerite surface



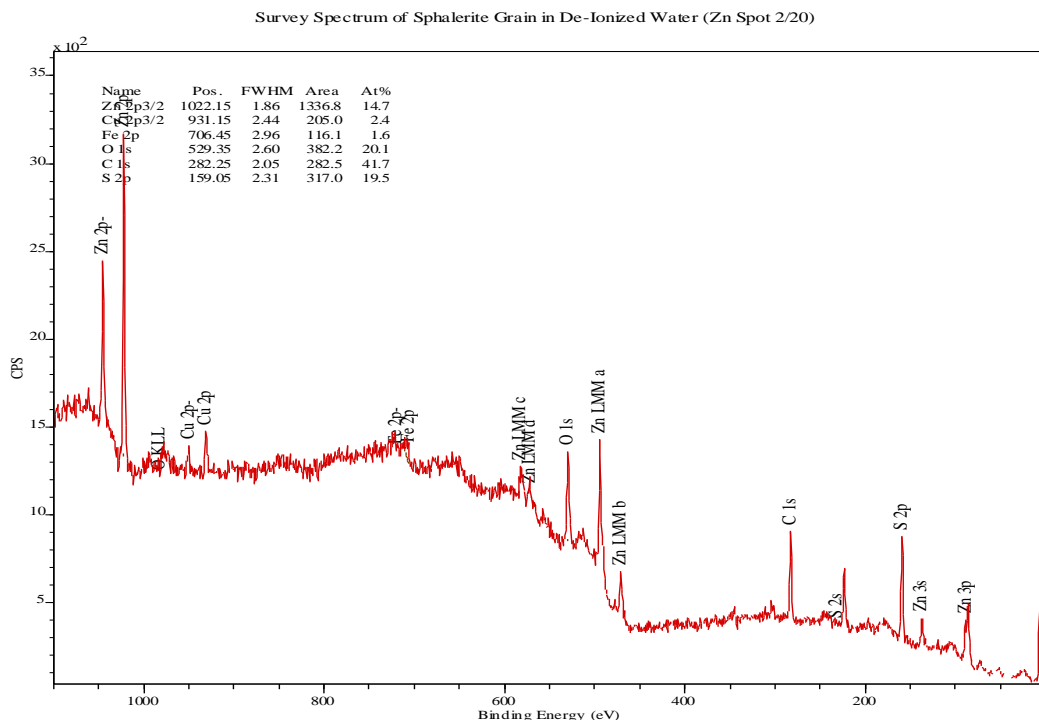
C-1 2 Survey spectrum of a vacuum-fractured sphalerite surface



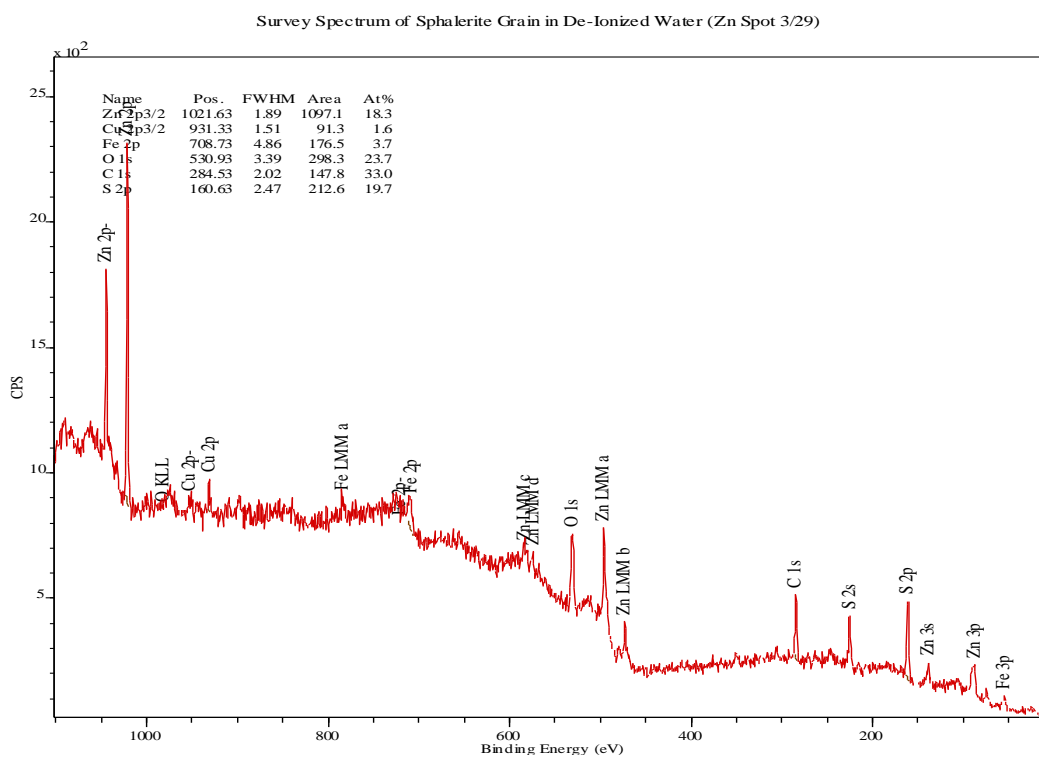
C-1 3 Survey spectrum of a vacuum-fractured sphalerite surface



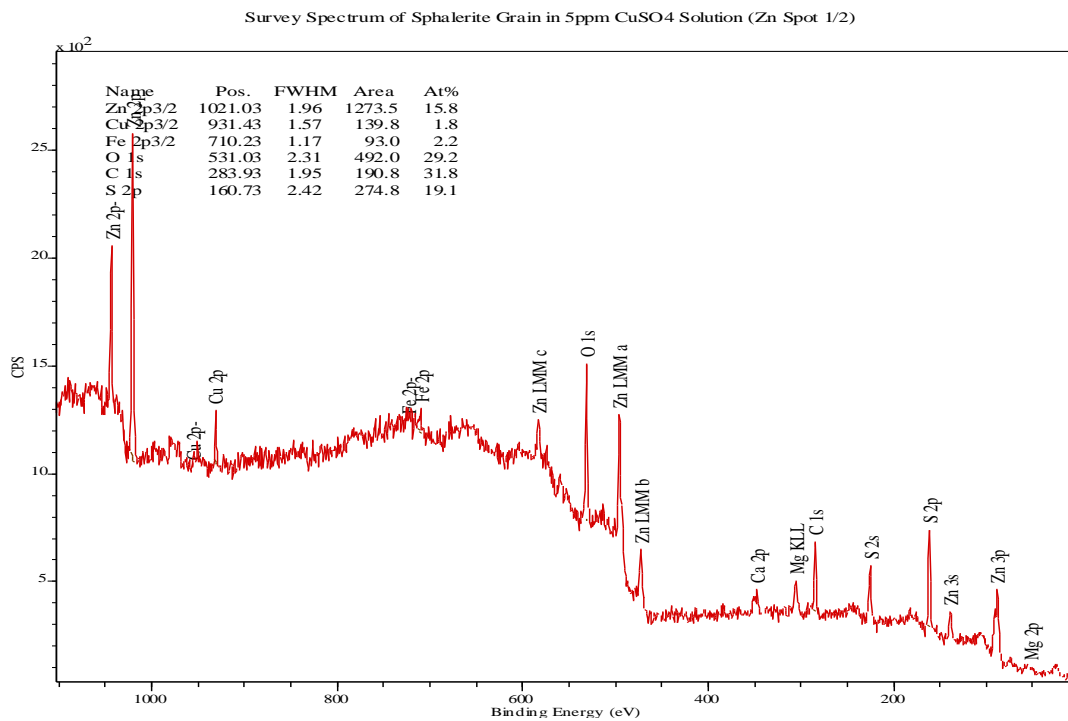
C-1 4 Survey spectrum of a sphalerite grain in de-ionized water



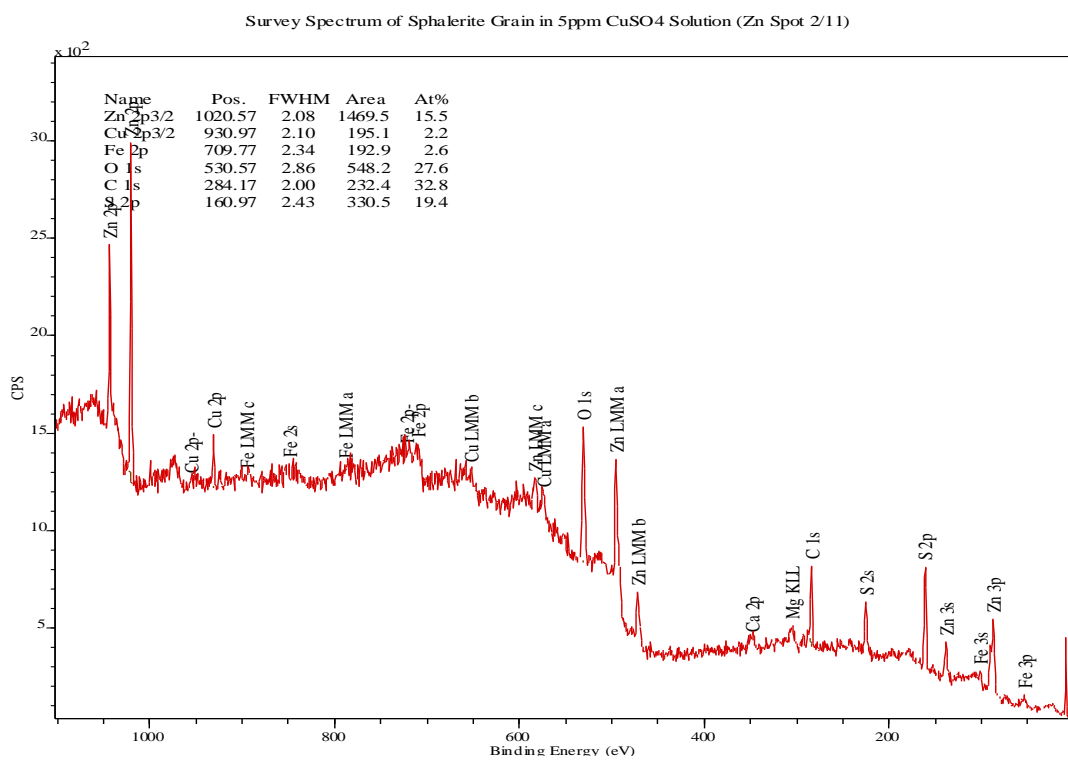
C-1 5 Survey spectrum of a sphalerite grain in de-ionized water



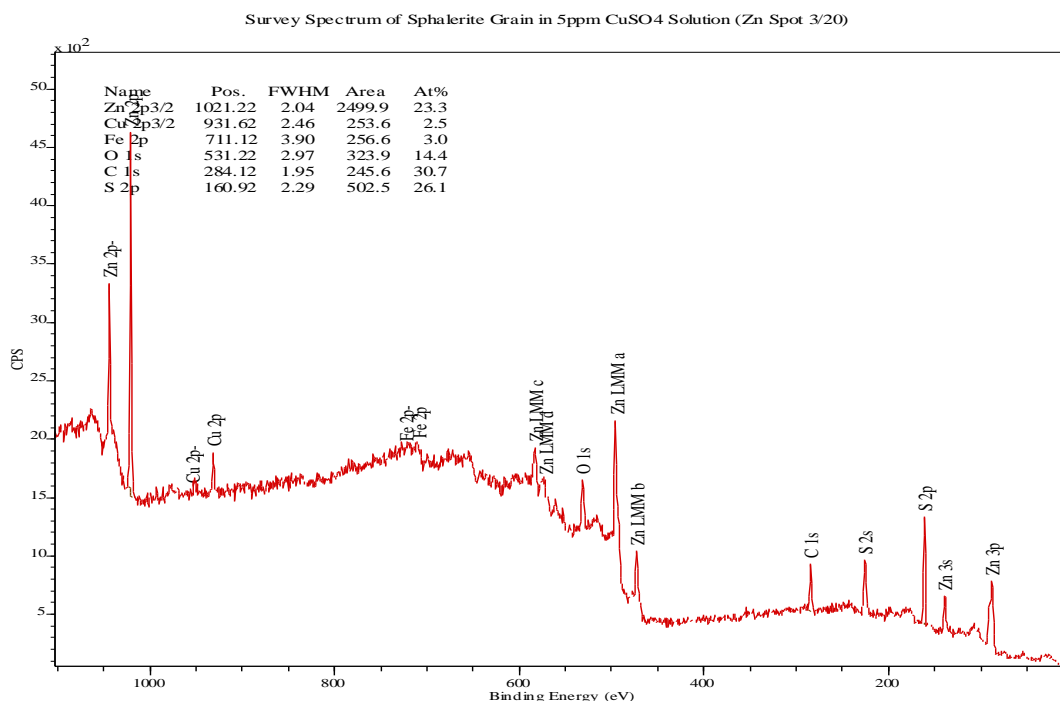
C-1 6 Survey spectrum of a sphalerite grain in de-ionized water



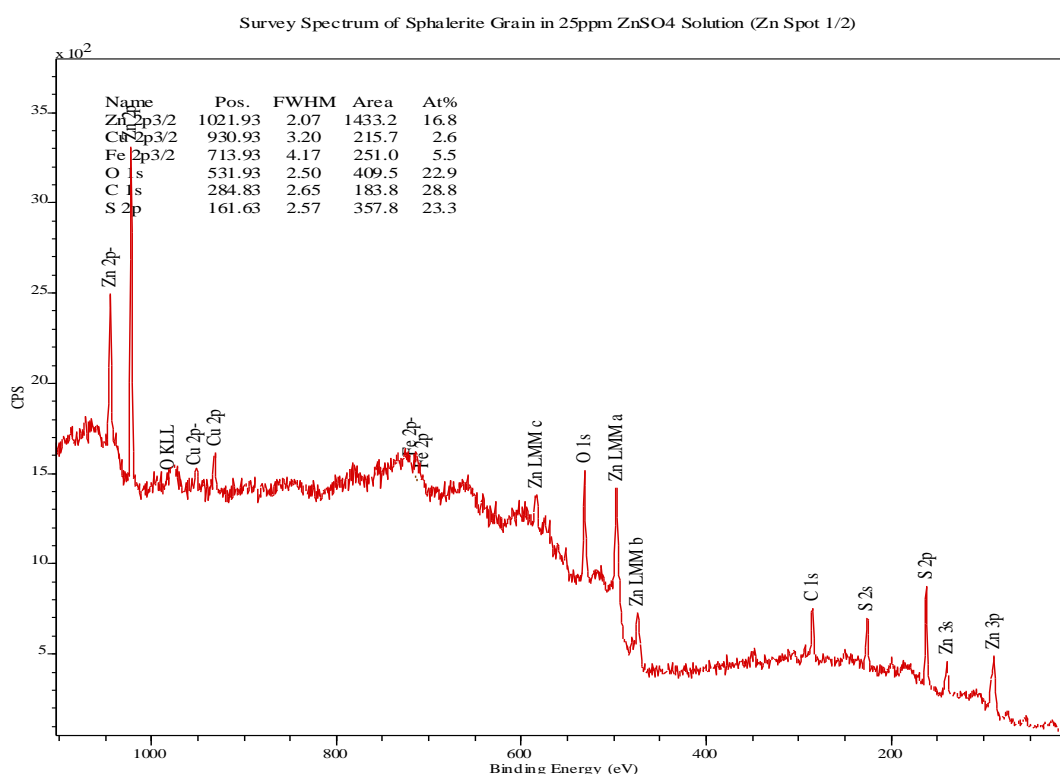
C-17 Survey spectrum of a sphalerite grain in 5ppm CuSO₄ solution



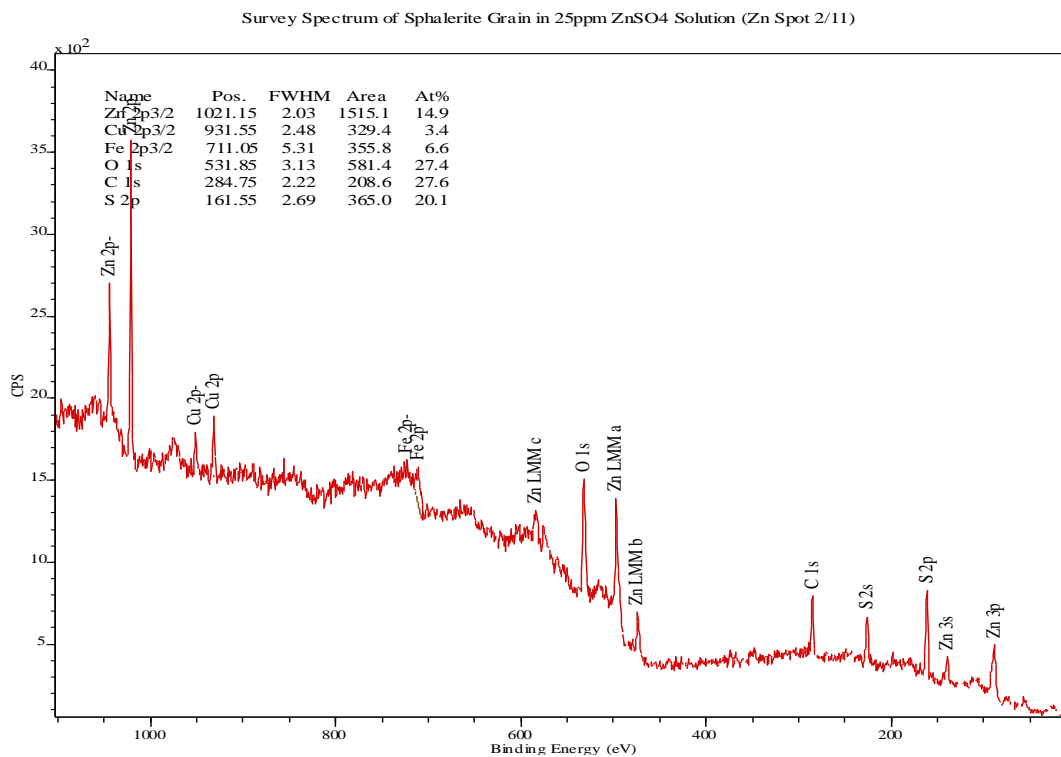
C-18 Survey spectrum of a sphalerite grain in 5ppm CuSO₄ solution



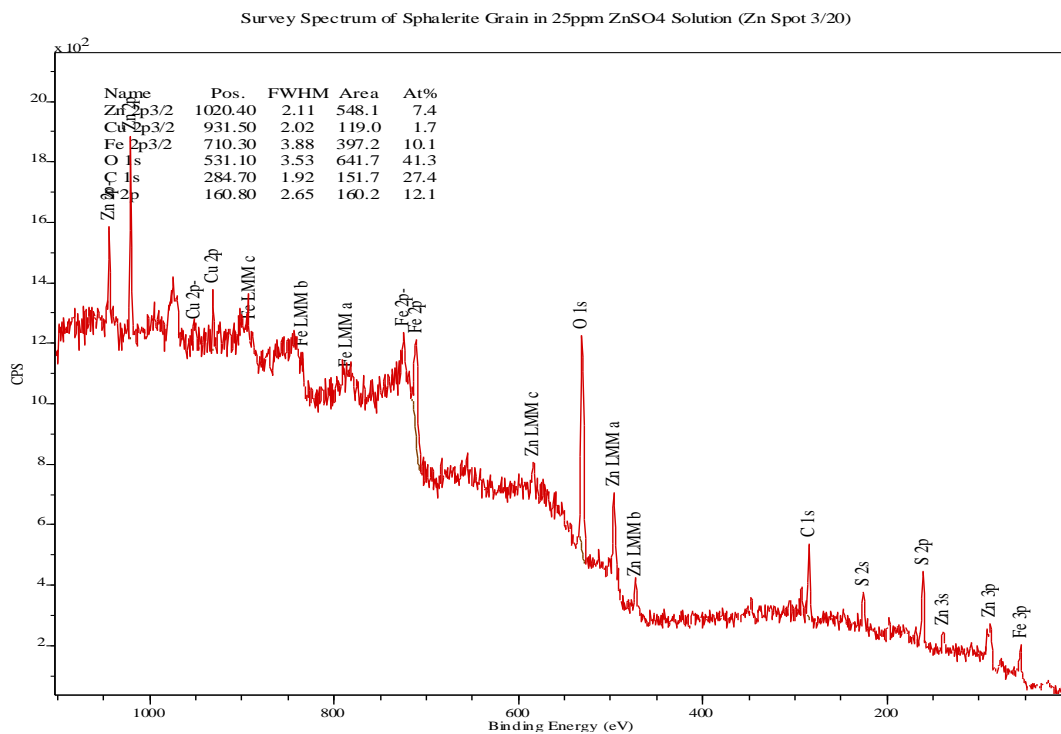
C-1 9 Survey spectrum of a sphalerite grain in 5ppm CuSO₄ solution



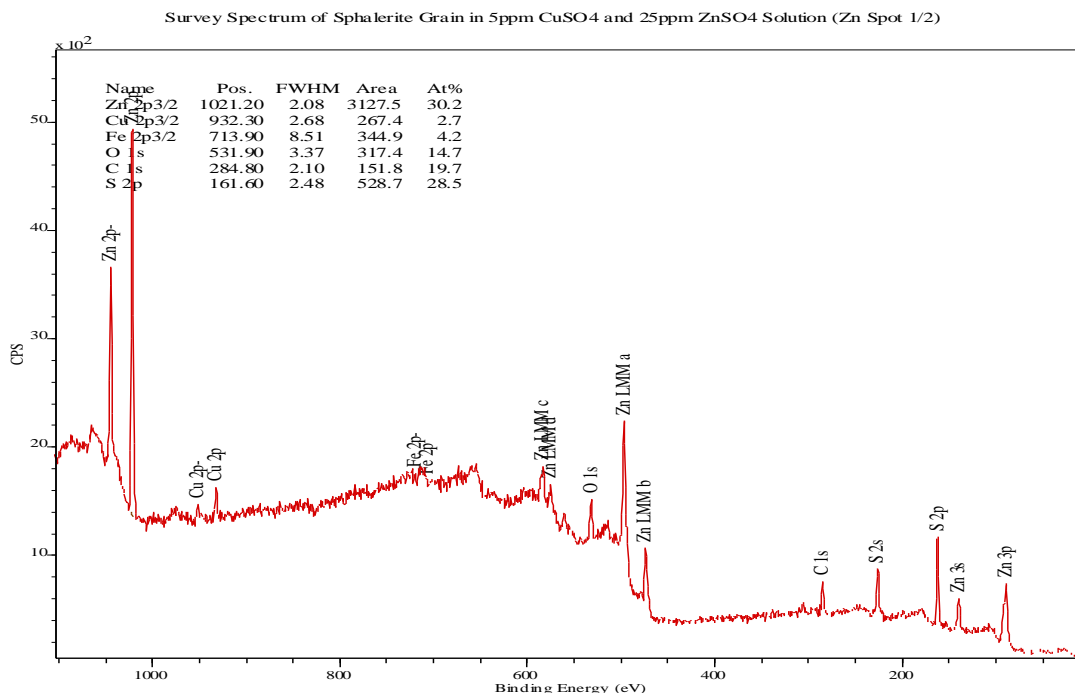
C-1 10 Survey spectrum of a sphalerite grain in 25ppm ZnSO₄ solution



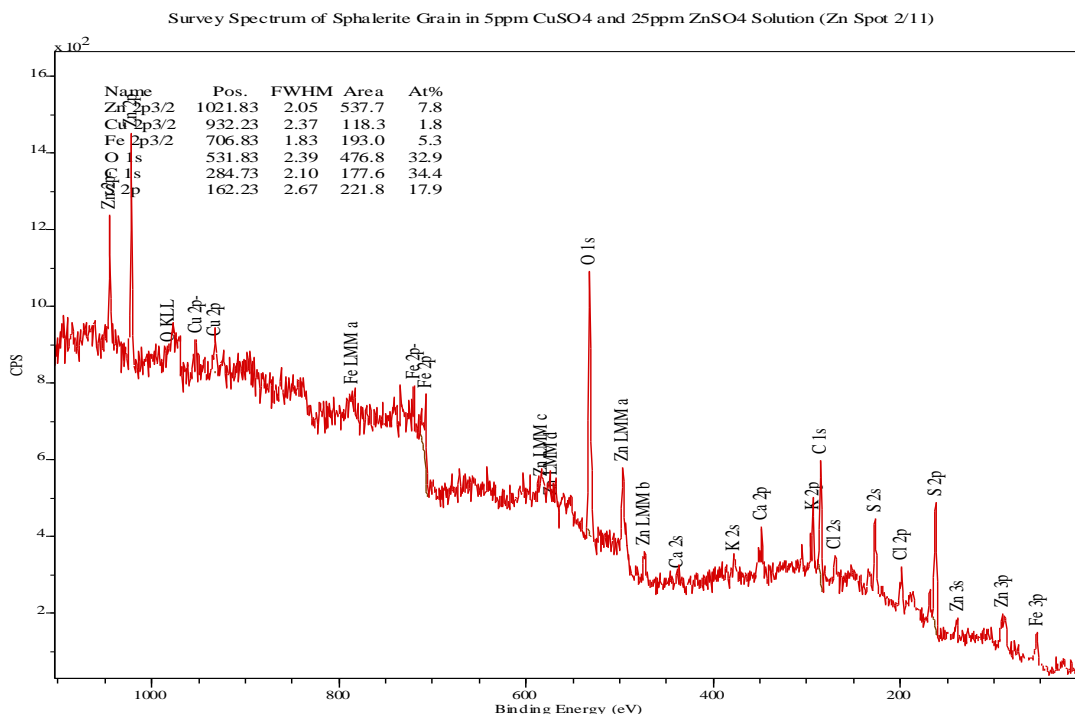
C-1 11 Survey spectrum of a sphalerite grain in 25ppm ZnSO₄ solution



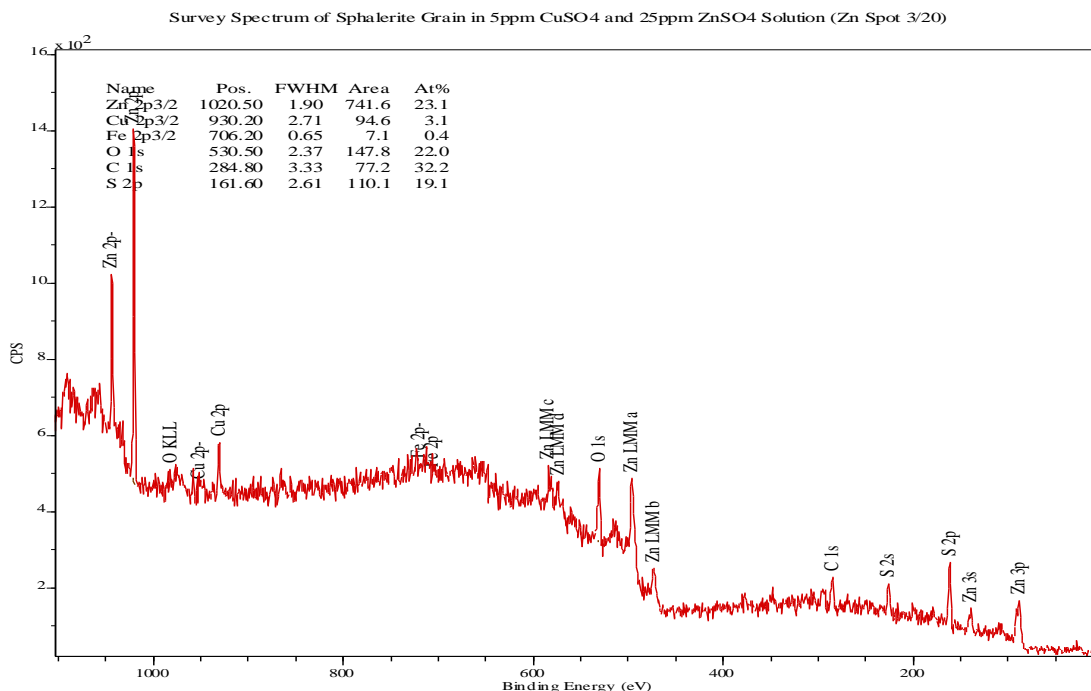
C-1 12 Survey spectrum of a sphalerite grain in 25ppm ZnSO₄ solution



C-1 13 Survey spectrum of a sphalerite grain in 5ppm CuSO₄ and 25ppm ZnSO₄ solution

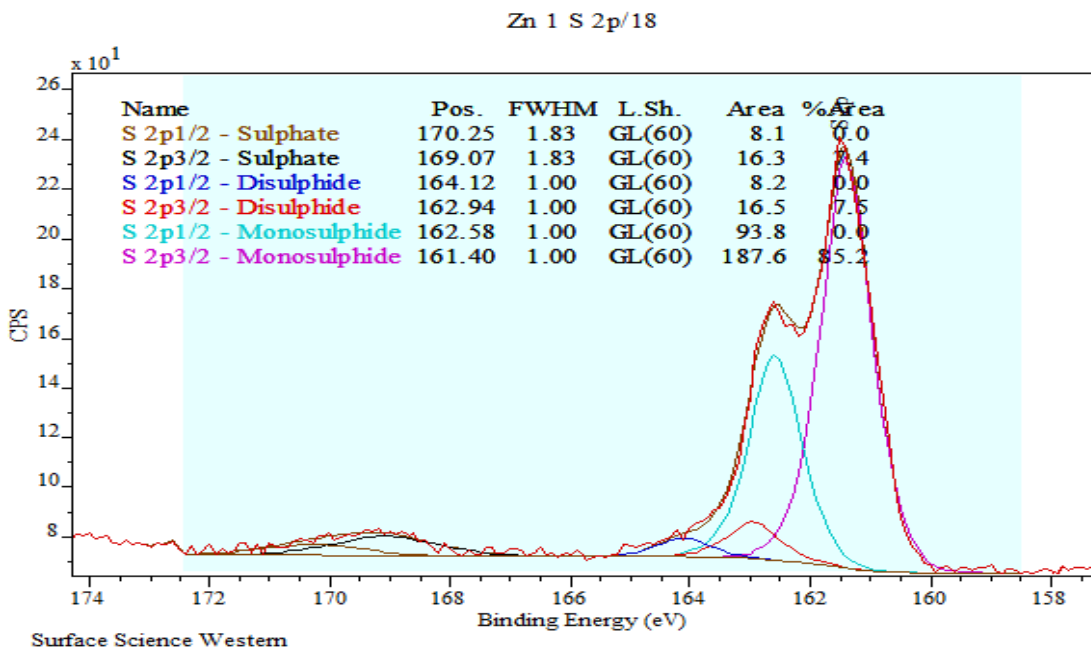


C-1 14 Survey spectrum of a sphalerite grain in 5ppm CuSO₄ and 25ppm ZnSO₄ solution

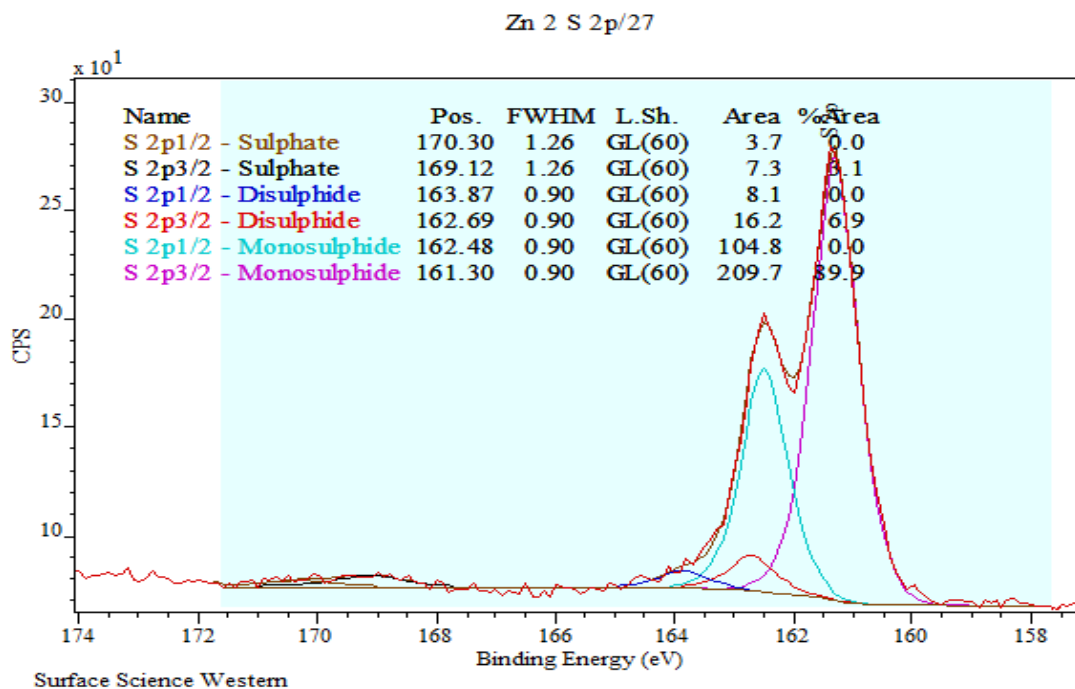


C-1 15 Survey spectrum of a sphalerite grain in 5ppm CuSO₄ and 25ppm ZnSO₄ solution

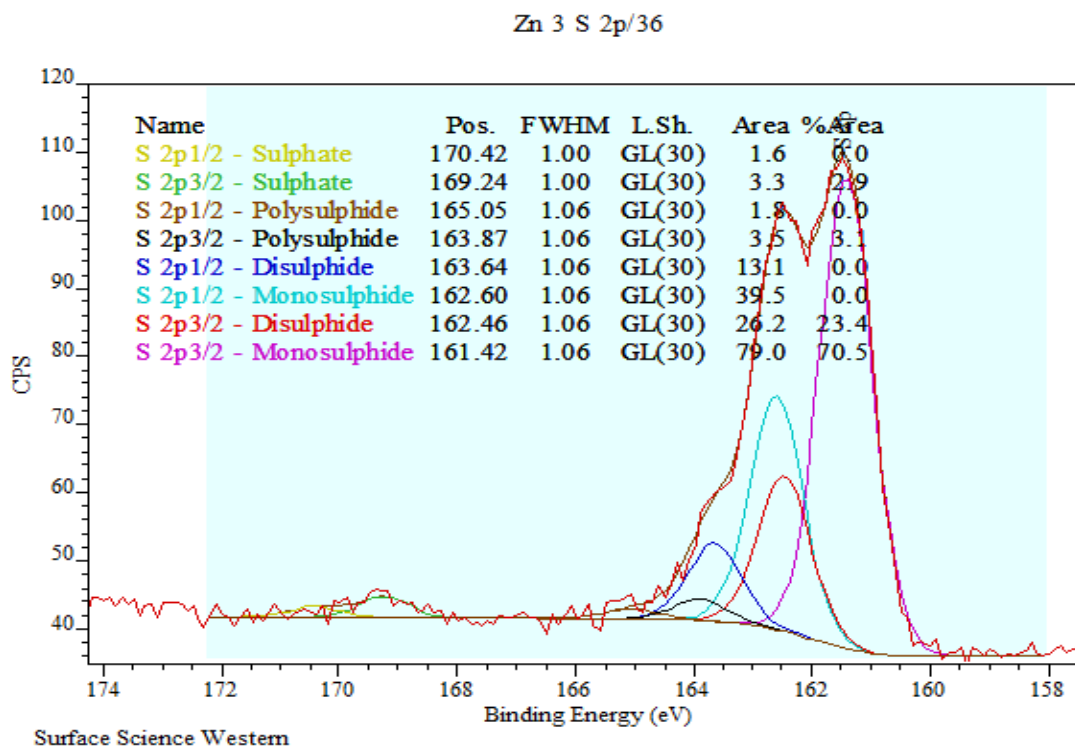
3.2 XPS High Resolution Spectra



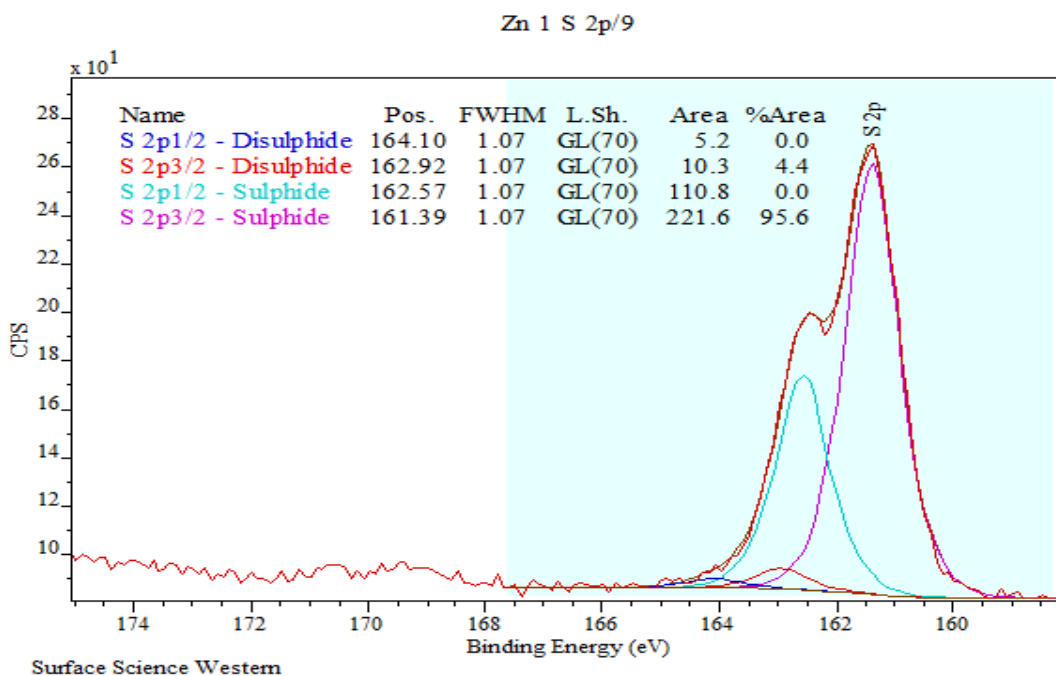
C-2 1 High Resolution Spectra of S 2p Peaks on Sphalerite in De-ionized Water



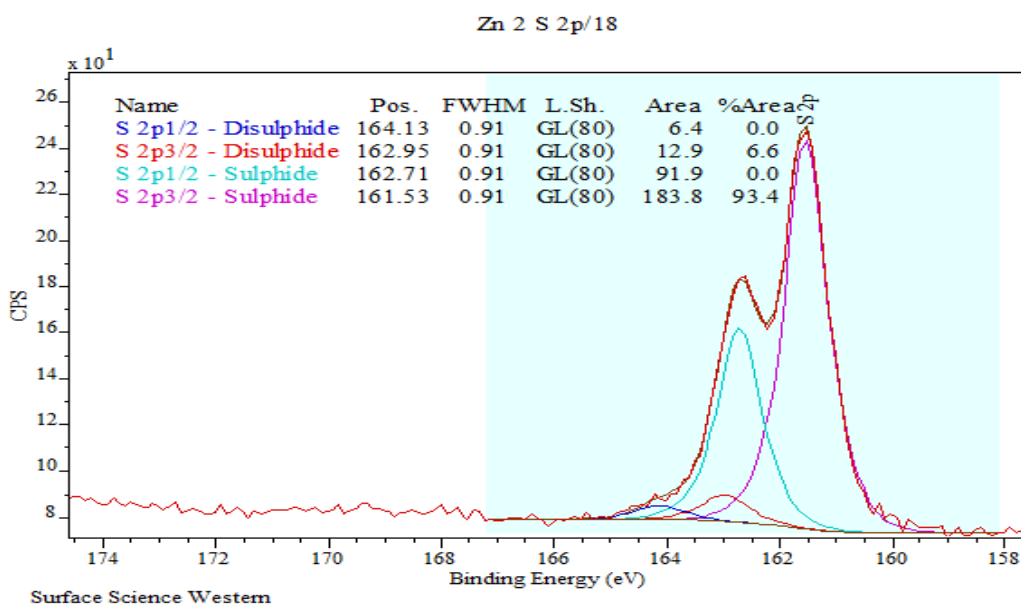
C-2 2 High Resolution Spectra of S 2p Peaks on Sphalerite in De-ionized Water



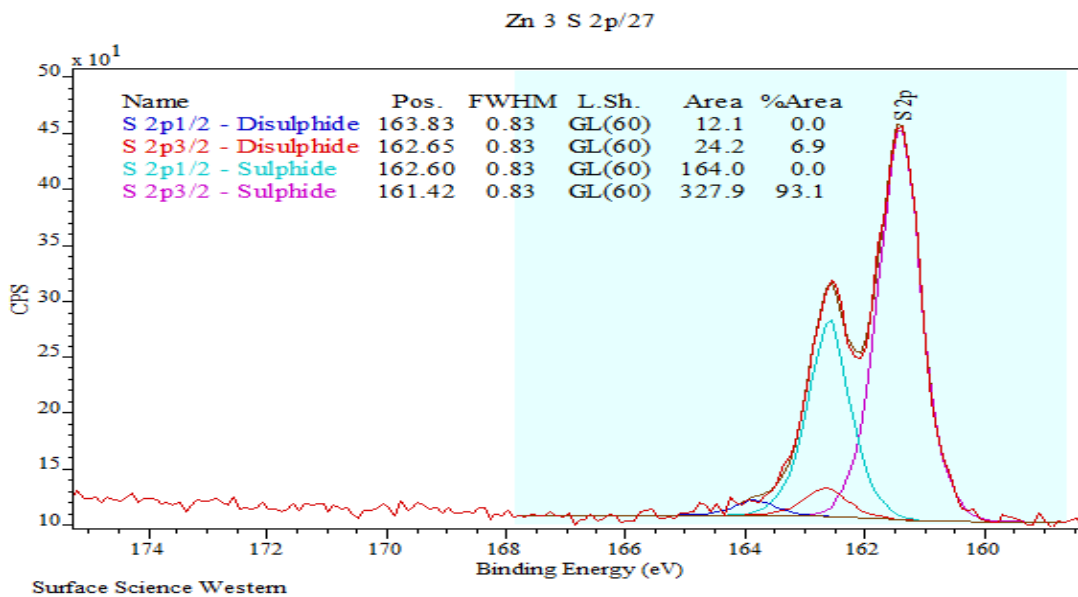
C-2 3 High Resolution Spectra of S 2p Peaks on Sphalerite in De-ionized Water



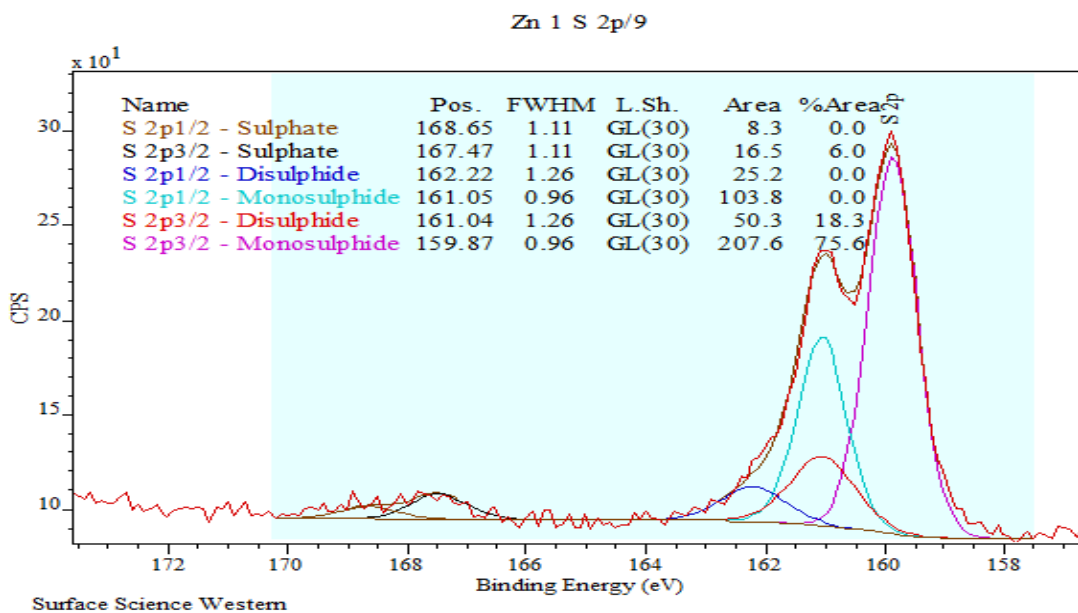
C-2 4 High Resolution Spectra of S 2p Spectra on Sphalerite in 5ppm CuSO₄ Solution



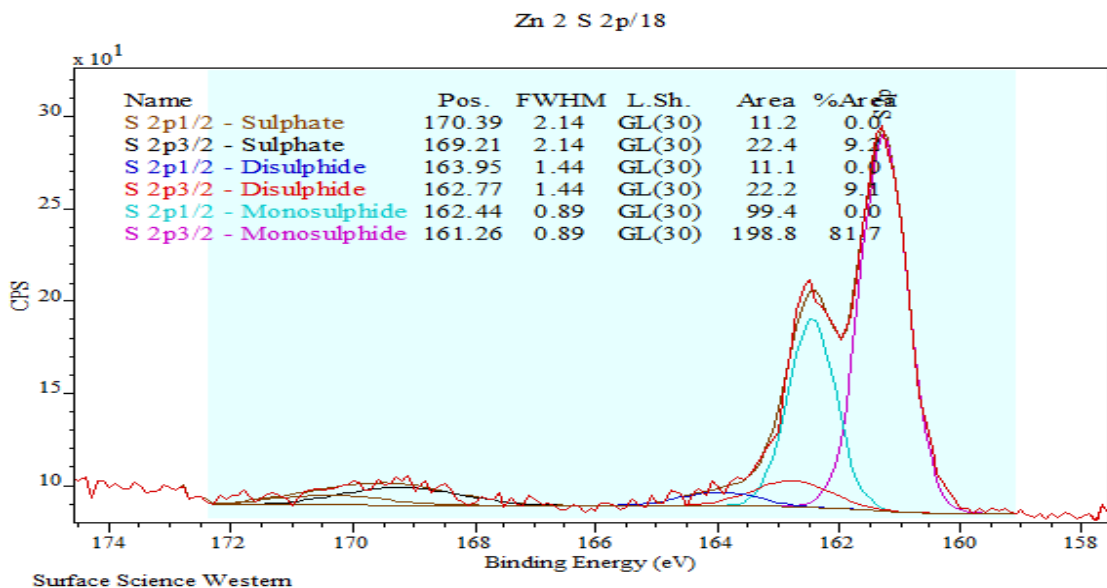
C-2 5 High Resolution Spectra of S 2p Spectra on Sphalerite in 5ppm CuSO₄ Solution



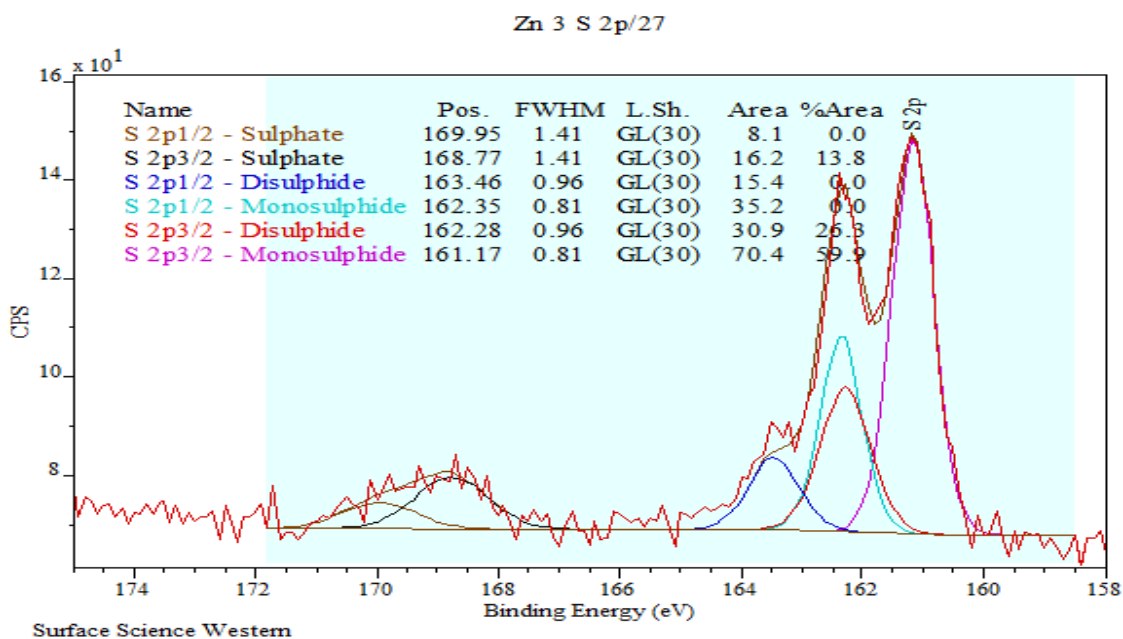
C-2 6 High Resolution Spectra of S 2p Spectra on Sphalerite in 5ppm CuSO₄ Solution



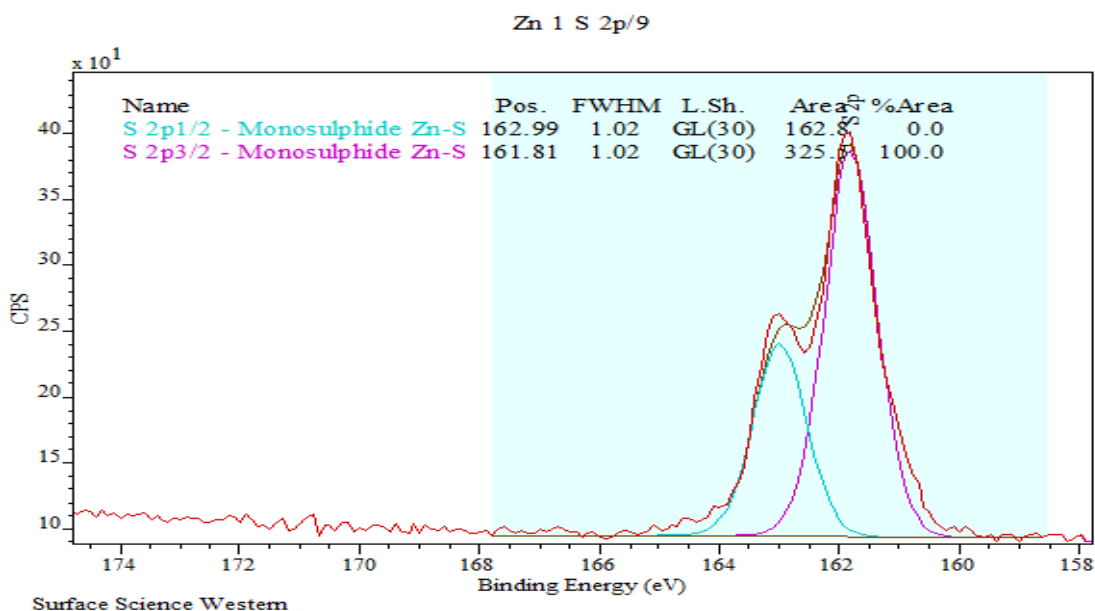
C-2 7 High Resolution Spectra of S 2p Peaks on Sphalerite in 25ppm ZnSO₄ Solution



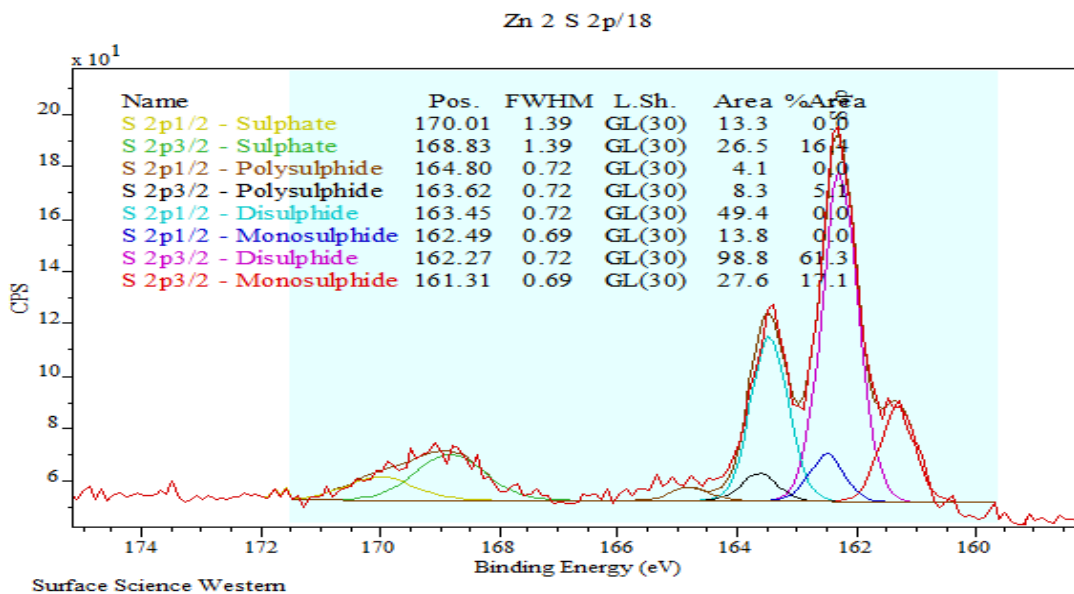
C-2 8 High Resolution Spectra of S 2p Peaks on Sphalerite in 25ppm ZnSO₄ Solution



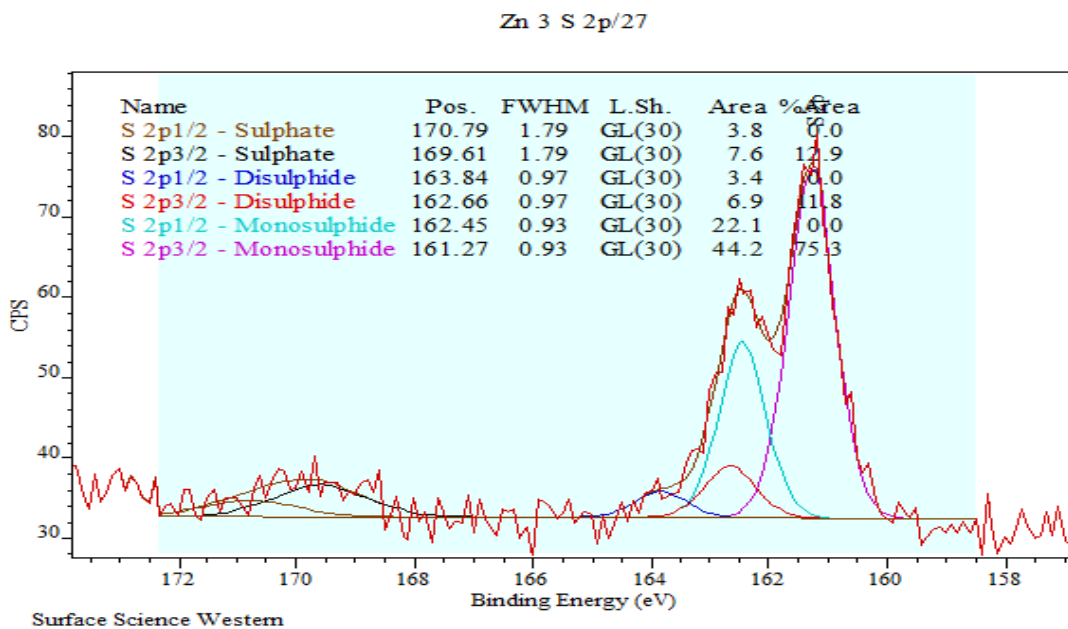
C-2 9 High Resolution Spectra of S 2p Peaks on Sphalerite in 25ppm ZnSO₄ Solution



C-2 10 High Resolution Spectra of S 2p Peaks on Sphalerite in 25ppm ZnSO₄ and 5ppm CuSO₄ Solution



C-2 11 High Resolution Spectra of S 2p Peaks on Sphalerite in 25ppm ZnSO₄ and 5ppm CuSO₄ Solution



C-2 12 High Resolution Spectra of S 2p Peaks on Sphalerite in 25ppm ZnSO₄ and 5ppm CuSO₄ Solution

4 Curriculum Vitae

Name: Mike Laliberty

Post-secondary Education and Degrees: The University of Western Ontario
London, Ontario, Canada
1987-1991 B.Sc. (Biology)

The University of Western Ontario
London, Ontario, Canada
2006-2009 HB.Sc. Geology

The University of Western Ontario
London, Ontario, Canada
2010-2014 M.Sc.

Honours and Awards: Natural Science and Research Council of Canada Industrial Undergraduate Student Research Award (NSERC-USRA)
2009

Related Work Experience Exploration Geologist,
West Kirkland Mining (2011-2012)
Queenston Mining/Osisko Mining (2012-present)

Publications:

Olsen, C., Makni, S., Hart, B., Laliberty, M., Pratt, A., Blatter, P. and Lanouette, M. (2012). The successful application of a laboratory-developed test protocol utilizing electrochemical and surface chemical analysis to the industrial flotation process of a complex sulphide (Cu-Pb-Zn-Au-Ag) ore. *XXVI International Mineral Processing Congress (IMPC 12)*. September 24-28, 2012, New Delhi, Paper 771.